STATISTICAL MODELING OF SIMULATION ERRORS AND THEIR REDUCTION VIA RESPONSE SURFACE TECHNIQUES

By

Hongman Kim

A DISSERTATION SUBMITTED TO THE FACULTY OF THE
VIRGINIA POLYTECHNIC INSTITUTE AND STATE UNIVERSITY
IN PARTIAL FULFILLMENT OF THE REQUIREMENTS FOR THE DEGREE OF
DOCTOR OF PHILOSOPHY
IN
AEROSPACE ENGINEERING

William H. Mason, Chairman

Raphael T. Haftka

Layne T. Watson

Bernard Grossman

Eugene M. Cliff

June 18, 2001

Blacksburg, Virginia

Keywords: discretization error, convergence error, response surface technique, Weibull distribution, *M*-estimation

STATISTICAL MODELING OF SIMULATION ERRORS AND THEIR REDUCTION VIA RESPONSE SURFACE TECHNIQUES

By

Hongman Kim

Committee Chairman: William H. Mason

Aerospace Engineering

(ABSTRACT)

Errors of computational simulations in design of a high-speed civil transport (HSCT) are investigated. First, discretization error from a supersonic panel code, WINGDES, is considered. Second, convergence error from a structural optimization procedure using GENESIS is considered along with the Rosenbrock test problem.

A grid converge study is performed to estimate the order of the discretization error in the lift coefficient (C_L) of the HSCT calculated from WINGDES. A response surface (RS) model using several mesh sizes is applied to reduce the noise magnification problem associated with the Richardson extrapolation. The RS model is shown to be more efficient than Richardson extrapolation via careful use of design of experiments.

A programming error caused inaccurate optimization results for the Rosenbrock test function, while inadequate convergence criteria of the structural optimization produced error in wing structural weight of the HSCT. The Weibull distribution is successfully fit to the optimization errors of both problems. The probabilistic model enables us to estimate average errors without performing very accurate optimization runs that can be expensive, by using differences between two sets of results with different optimization control parameters such as initial design points or convergence criteria.

Optimization results with large errors, outliers, produced inaccurate RS approximations. A robust regression technique, *M*-estimation implemented by iteratively reweighted least squares (IRLS), is used to identify the outliers, which are then repaired by higher fidelity optimizations.

The IRLS procedure is applied to the results of the Rosenbrock test problem, and wing structural weight from the structural optimization of the HSCT. A nonsymmetric IRLS (NIRLS), utilizing one-sidedness of optimization errors, is more effective than IRLS in identifying outliers. Detection and repair of the outliers improve accuracy of the RS approximations. Finally, configuration optimizations of the HSCT are performed using the improved wing bending material weight RS models.

Acknowledgements

During the last four years, the MDO research group at Virginia Tech has provided me with a unique educational environment. Close cooperation with devoted professors and many talented students helped me broaden academic and professional perspectives.

I spent a lot of time in the office of Dr. William Mason, my adviser, to discuss many challenging problems we faced in the research. I remember that his office was a busy place because there were always many students who wanted to ask him questions. His passion and expertise in aircraft design have been a real treat to me and I'm deeply grateful for his continuous support and encouragements.

I would like to express my deepest thanks to Dr. Raphael Haftka at the University of Florida for his enormous help and encouragements. The geographical distance was not a match to his passion for research and teaching. The weekly teleconferences, numerous email correspondences, and chances of face-to-face talk with him always provided me with new perspectives on the subject. I'm very grateful to Dr. Bernard Grossman for his support and encouragements. He offered fresh suggestions to my work and it was a pleasure to work with him. Dr. Layne Watson helped me a lot by sharing his expertise in mathematics and statistics. Many chances of discussion with him were valuable assets to me. Dr. Eugene Cliff offered very insightful discussions, and I appreciate his efforts in the committee.

I would like to express special thanks to Dr. Jeffrey Birch in the Department of Statistics at Virginia Tech, who introduced me to the world of applied statistics. I really enjoyed his classes, where I learned many ideas used in this work. Dr. Chris Roy at Sandia National Laboratory offered valuable comments on the issues of discretization error, and his contributions are appreciated.

It was a great pleasure to work with many gentlemen, my colleague graduate students in Virginia Tech and the University of Florida. In particular, contributions from Chuck Baker and Melih Papila are appreciated. Close presence of Sangmook Shin and Yongwook Kim was always a great help to me. I received a lot from brothers and sisters of the Korean Baptist Church of Blacksburg, and I would like to give special thanks to the single bible study group for our fellowship in Jesus Christ.

I could not be here without love and support of my family. Very special love goes to my grandmother. She was my first friend. Thanks from my heart goes to my sister and brother's family, who were together in pleasant and difficult times of life. I would like to express my deepest love to my father, who showed me endless support and love. Finally, I would like to share the joy of this small achievement with my mother who rests in heaven with the Lord.

Table of Contents

List of Tables

List of Figures

Nomenclature

ANOVA	analysis of variance
b	wing span
$\boldsymbol{b}$	vector of artificial coefficients for parameterized Rosenbrock function
b_k	artificial coefficients of the parameterized Rosenbrock function
b_k^*	b_k to minimize f_o from the parameterized Rosenbrock function
B	tuning constant of the biweight weighting function
BC	boundary condition
c_{root}	wing root chord
c_{tip}	wing tip chord
CDF	cumulative distribution function
CFD	computational fluid dynamics
C_L	wing lift coefficient
C_p	pressure coefficient
DOE	design of experiments
e	optimization error
$\bar{e}$	average of the optimization error of sample data
$e(\ )$	function to be minimized in M-estimation
e_a	approximate error of W_s from structural optimization of HSCT
e_t	estimated error of W_s from structural optimization of HSCT
$\boldsymbol{e_r}$	vector of residual error
ECDF	empirical cumulative distribution function
$f(x; b)$	probability density function of x depending on a parameter b
$\underline{f}$	approximation of the objective function in GENESIS structural optimization
f_o	Optimum of the parameterized Rosenbrock function for a given $\boldsymbol{b}$
F	cumulative distribution function
FCCC	face centered central composite design
FE, FEA	finite element, finite element analysis

FF	full factorial experimental design
F_n	empirical cumulative distribution function
$\underline{g}$	approximation of the objective function in GENESIS structural optimization
h	mesh step size
H	tuning constant of the Huber's weighting function
H.O.T	higher order terms
HSCT	high-speed civil transport
IL	inlier
IRLS	iteratively reweighted least squares
l	number of levels in an experimental design
$l(\ )$	likelihood function
L	chordwise distance from the front-most leading edge and the rear-most trailing edge of the wing planform
LE	leading edge
m	number of independent design variables in a response surface model
M	Mach number
$M_{¥}$	free stream Mach number
MDO	multidisciplinary design optimization
MLE	maximum likelihood estimate
MMFD	modified method of feasible direction
n	number of data points of a sample or an experimental design
n_x	number of chordwise panels for WINGDES analysis
n_y	number of spanwise panels in the wing half span for WINGDES analysis
NIRLS	nonsymmetric IRLS
OL	outlier
p	number of regression coefficients in a response surface model
PDF	probability density function
q	order of the accuracy of a discretized computation
$\boldsymbol{r}$	vector of scaled residual in M-estimation
r_i	scaled residual in M-estimation
R^2	coefficient of the multiple determination of least squares fit

RE	Richardson extrapolation
RMSE	root mean squares error of a response surface fit
RS, RSM	response surface, response surface methodology
RSRE	response surface fit to Richardson extrapolation results
s	estimate of standard deviation of the random error in M-estimation
SLP	sequential linear programming
SQP	sequential quadratic programming
SS_{model}	Sum of squares of regression model
$SS_{residual}$	Sum of squares of residual error
SS_{total}	Total sum of squares of the response variable
t/c	thickness to chord ratio of airfoil
TE	trailing edge
VCM	variable-complexity modeling
v_i	configuration design variables of the five variable HSCT problem
$W(\boldsymbol{r})$	diagonal matrix of IRLS weighting
W_b	wing bending material weight
W_{fuel}	fuel weight
W_s	optimal wing structural weight (objective function of the structural optimization of the HSCT)
W_{TOGW}	takeoff gross weight
$x_{(i)}$	i-th entity of a sample sorted in increasing order
$\boldsymbol{x_0}$	initial point for optimization
x_i	i-th entity of a sample
x_{ji}	j-th independent variable of the i-th observation
X	Gram matrix in the model equation of least squares fit
y	continuum solution
$\boldsymbol{y}$	vector of observations of a response variable
$\hat{\boldsymbol{y}}$	vector of fits of the response variable
y_h	discretized solution for the current value of h
$y_{h/2}$, $y_{h/4}$	discretized solution for refined meshes
$y_h^{(2)}$, $y_{h/2}^{(2)}$	Richardson extrapolation formulas

$y_{(h/8)}^{(2)}$	Richardson extrapolation formula for finitely refined mesh of $h/8$
y_i	i-th observation of a response variable
z_c	camber distribution of a wing
a_1	coefficient of the leading term of the discretization error expanded in h
b	$\sqrt{M_\infty^{\ 2} - 1}$
b_0, b_j, b_{jk}	regression coefficients of a response surface model
b	vector of the regression coefficients of a response surface model
$\hat{b}$	vector of estimates of the regression coefficients
c^2	test statistic of the c^2 goodness-of-fit test
e_i	random error in a response surface model
e	vector of random errors in a response surface model
f	perturbation velocity potential of the linearized potential equation
$f(t)$	failure rate of distribution function
r	function of the scaled residual in M-estimation
s	standard deviation of a random variable
$\hat{s}$	estimate of standard deviation of a random variable
s^2	variance of a random variable
$\hat{s}^{\,2}$	estimate of variance of a random variable
$\hat{s}_{data}$	estimate of standard deviation of the optimization error from a sample data
$\hat{s}_{fit}$	estimate of standard deviation of the optimization error from a fitted distribution
L_{ILE}	inboard leading edge sweep angle
m	mean of a random variable
$\hat{m}_{data}$	estimate of mean of the optimization error from a sample data
$\hat{m}_{fit}$	estimate of mean of the optimization error from a fitted distribution
y	y function in M-estimation

Chapter 1 Introduction

1.1 Motivation

Computational simulations have become essential elements in engineering. Recent advances in computational simulations have been supported by improvements in computational modeling and numerical algorithms, which were made affordable by growing computer power and software technology [1]. Effective utilization of computational simulation in place of expensive and time-consuming experimental tests enables engineers to achieve better designs with reduced cost and design cycle time. Since most important decisions are made in the early phases of the design process when much of the key information is uncertain, it is important to reduce the lack of information at the early design phase [2]. So, there are increasing needs to use high-fidelity analyses in the very early stages of the design process.

In multidisciplinary design optimization (MDO) [3], the design task is approached as an optimization problem by considering various disciplines simultaneously. It is a systematic approach to exploit the interactions between different disciplines in the early design phases. Efforts to use higher fidelity tools, such as computational fluid dynamics (CFD) and finite element analysis (FEA), in MDO are being actively pursued. For example, Knill *et al.* [4] used CFD for drag calculations in the conceptual design of a high-speed civil transport (HSCT). Raveh *et al*. used CFD analysis for aeroelastic analysis and design of an aircraft wing [5]. Sobieszczanski-Sobieski *et al.* [6] performed, with the help of parallel computing, optimization of a car body using a finite element model of 390,000 degrees of freedom. Balabanov *et al.* [7], [8], used FEA-based structural optimization to improve the prediction of the wing weight of an HSCT over weight equations based on historical data.

Although capabilities of computational simulations have been increased to simulate real world phenomena more accurately, there remain many possible sources of error. In particular, discretization errors are fundamental for all methods where discretized models are used to replace continuum mathematical models [9]. In many cases, discretization errors show some systematic behavior. On the other hand, computational simulations often produce high frequency noise due to incomplete convergence, discretization error, or round-off error accumulation [8],

[9], [10], [11]. Even when the magnitude of the noise error is small from a perspective of single analysis, the high frequency error may cause trouble for gradient-based optimization methods. Furthermore, the errors may result in *outliers*, simulation results lying outside of the trend of other nearby results, and countermeasures are required.

Because of the importance of using accurate simulation results in the design process, there are growing needs to verify computational simulations [9], [12]. It is very difficult to determine the accuracy of simulation results or to detect any erroneous results when the simulation procedures are complicated and computationally expensive. Nonetheless, if computational simulation is to be considered seriously for use in real design tools, as current engineering environments require, the uncertainties of computational simulations should be estimated and controlled to be within a reasonable level.

1.2 Review of the Literature

Traditional engineering design approaches are deterministic. Idealized models and input parameters are assumed to be accurate. Afterwards, safety factors can be introduced to address the unavoidable uncertainties in the model and environments. Also, in the traditional design optimization, engineers try to single out the best design point, *i.e.*, a search for *the global optimum*. Afterwards, post optimality analysis may provide sensitivity information with respect to design changes.

In reality, the knowledge that engineers have about the design problem is imperfect and incomplete. Uncertainty is ubiquitous in measurement data, simulation models, design parameters, and the operational environment of the product. Robust design techniques [2], [13], have emerged as a new design paradigm. In MDO, the robust design concept becomes an essential element when economic or manufacturing factors are to be included in design decisions [14], [15].

In the framework of robust design, effects of uncertainties are incorporated into the evaluation of candidate designs, which provide additional information to aid the engineer's decision. First, the uncertainty sources are identified. In engineering applications the identified uncertainties are often modeled via probability distributions [16] or fuzzy sets [17]. Probabilistic

models and fuzzy set models describe different aspects of uncertainty [18]; probabilistic models mainly describe random variability in parameters such as material property variations, while fuzzy set models are used to describe mainly vagueness, such as uncertainty in choosing among alternatives.

There are mainly two approaches to estimation of uncertainty of a system: *the extreme condition approach* and *the statistical approach*. The extreme condition approach seeks the bounds of system output: the anti-optimization technique [19] and interval analysis [20] are two examples. The statistical approach finds the probability of failure/success of the system and frequently requires data sampling to construct a cumulative distribution function of the output through uncertainty propagation. Monte Carlo [21] simulation is a brute force technique using random sampling that might be prohibitively expensive. To reduce the cost of Monte Carlo simulation, surrogate models for the expensive analysis have often been used, such as response surface approximations [16]. More efficient sampling techniques have been developed such as Latin hypercube sampling [22] and Taguchi's orthogonal array [23]. Also, fast probability integration techniques have been developed [24],[25].

Simulation errors are one of the major uncertainty sources in the robust design framework. However, limited work has been done to address design uncertainties due to errors of computational simulations. It appears that the error estimation of computational simulations has been treated as a different issue than design uncertainty [26], [27]. A serious problem is that there is no standard terminology for uncertainties. 'Uncertainty' appears in many different contexts in the literature, mixed with several related words like variability, imprecision, vagueness, or error [28], [29], [30]. In experimental measurements, error usually means *the difference of the measurement from the true value*, while uncertainty can be defined as *an estimate of the error* [31]. In computational simulation fields, it seems that error and uncertainty are used interchangeably, and the choice between error and uncertainty depends on the author's preference. This confusion in the terminology is partly because idealized computational models are used in place of physical experiments.

Gu *et al.* [32] classified simulation errors as *bias error* and *precision error*. Bias error is usually deterministic and consists of *approximation error* in the analytical model and *algorithmic error* in the numerical model. The precision error means the variability of input

parameters and is probabilistic. The definitions are helpful in identifying error sources, but they are not intended for a complete taxonomy of simulation uncertainty.

Recently, Oberkampf *et al.* [33], [34] suggested a comprehensive framework for uncertainties in computational simulations. Their work was to identify uncertainty sources in each stage of modeling and simulation. They used three categories for the sources of the *total uncertainty*: *variability*, *uncertainty*, and *error*. *Variability* is the inherent variation associated with the system or environment, which is irreducible. *Uncertainty* is defined as the potential deficiency in any phase or activity of the modeling process that is due to 'lack of knowledge'. Uncertainty can be reduced when more information is obtained. For example, in the range calculation of an aircraft, if we know only approximately the specific fuel consumption of the engine, because it is under development, it causes uncertainty in the predicted range of the aircraft. Once the exact specification of the engine is known, the uncertainty is reduced or removed. *Error* is defined as a recognizable deficiency in any phase or activity of modeling and simulation that is *not* due to lack of knowledge; error can be recognized upon examination. Error includes spatial and temporal convergence error, round-off error accumulation, and iterative convergence error. Variability, uncertainty, and error, identified in each stage of modeling and simulation, constitute the total uncertainty and propagate into the system, resulting in uncertainties of the system output. Batill *et al.* [35] applied the framework to characterize the uncertainties in MDO.

Oberkampf *et al.*'s framework is useful in two aspects. First, it provides a well-defined terminology for uncertainty sources organized into detailed classification. Second, it is a comprehensive framework including each phase of modeling and simulation. They define six phases: conceptual modeling, mathematical modeling, programming activities, discretization and algorithm selection, numerical solution, and solution representation. In the current work, we will focus on simulation *error* according to the above framework. For application problems, we will consider errors from an aerodynamics simulation and a structural optimization procedure. It is important to note that error is a part of the total uncertainty according to the framework, and may have random properties.

Once the uncertainty sources are identified and their effects are estimated, it is possible that different measures are taken according to variability, uncertainty, or error, to reduce the total uncertainty. Only a few studies have been done on design uncertainty analysis regarding

simulation errors. For discretization error, Richardson extrapolation has been widely used [9], [36], [26]. Recently, there have been efforts to use response surface models to reduce the effects of discretization error on the robust design of a finite element bar [37], [38]. For modeling error, DeLaurentis and Mavris [39] used the beta distribution to model the error of low-fidelity stability derivative calculations, and performed robust design optimization of a supersonic transport with airplane stability considerations. Surrogate models of computational simulations may cause error in design optimization due to their modeling deficiencies. Papila and Haftka [40] analyzed response surface models to identify regions where large modeling errors of lower order polynomial models are expected.

Response surface techniques [41] build an approximation to output response via least squares fit based on experimental or simulation data at carefully selected design points. In MDO research it has become a popular surrogate model for higher fidelity analyses [4], [6], because with some initial investment to construct a database, expensive analysis can be replaced by a simple algebraic equation that is very inexpensive to evaluate. Another advantage of the response surface approximation is that it filters noise error typical of higher fidelity simulations [10], which may be troublesome to optimization. Researchers at Virginia Tech and the University of Florida have applied the response surface approximation to noisy data from structural optimization of a high-speed civil transport [8].

Simulation results with large errors are of particular concern because they increase the total uncertainty in modeling and simulation. When many simulation results are available, response surface techniques can be used to identify erroneous simulations as bad data points, statistical outliers [42], and further investigation of those bad results may lead to identifying the causes of the errors. The standard least squares method used in response surface fitting is not robust to outliers; response surface fits may be greatly affected by a few bad data points. Robust regression techniques provide response surface fits with protection against outliers [43], [44]. Researchers at Virginia Tech and the University of Florida have applied robust regression techniques to data from structural optimization [45], [46], [47]. The structural optimization data contained bad optima due to convergence difficulties with the structural optimization. Robust response surface techniques successfully identified those bad results as outliers, and the accuracy of the response surface approximation was improved by repairing them.

1.3 Objective

A high-speed civil transport (HSCT) design code [48], [49] has been developed by the Multidisciplinary Analysis and Design (MAD) Center for Advanced Vehicles of Virginia Tech. The HSCT is a good test bed for MDO research because successful designs of such a concept require close interaction between traditional disciplines. Most of the disciplinary modules of the code have the capability of variable-complexity modeling (VCM) [49], [50], [4], [8], where low, high, and possibly mid fidelity analysis are combined to reduce the cost of higher fidelity simulations. For example, low fidelity weight analysis uses weight equations of FLOPS [51] based on historical data. For more accurate estimation of wing structural weight, GENESIS [52] structural optimization based on finite element analysis is performed as a high-fidelity analysis.

The objective of the present work is to estimate simulation errors in the HSCT design codes and develop countermeasures to reduce them. In most situations, error is difficult to determine because the true values are not known except for a few special cases of verification. To determine error, more accurate simulations or experiments are required, which can be very time consuming and expensive to perform. In modeling and simulation, estimation of error becomes more complicated because error can be caused at any phase of modeling and simulation [34]. Dealing with all of the error sources is beyond the scope of the present work, and we will focus on simulation errors associated with 1) the discretization and algorithm selection phase and 2) the numerical solution phase.

First, the simulation error of a supersonic panel code, WINGDES [53], [54], will be investigated. WINGDES is a wing analysis and design code based on linearized potential theory and the leading edge thrust concept. HSCT codes use WINGDES to calculated optimal wing camber distribution for structural optimization [55] to provide the aerodynamic load distribution. The supersonic panel method is also a basis for a refined analysis for the drag due to lift of the HSCT wing [56]. Because rectangular non-body fitted panels are used to model the wing planform, the panel solutions tend to be noisy. This is the reason we selected WINGDES for a study of simulation errors. A grid convergence study showed that discretization error is a major error component in WINGDES. Richardson extrapolation ([57], pp. 180-186) may be used to estimate the discretization error. Instead a response surface approach will be used to model the

discretization error following Alvin [37] and Kammer *et al.* [38]. The response surface approach can be also computationally cheap, because a carefully designed experimental design may allow one to do fewer simulation runs than required for Richardson extrapolation. In addition, the noise filtering capability of a response surface fit may have an advantage over Richardson extrapolation for the noisy data from WINGDES. We will compare the response surface approach and Richardson extrapolation in predicting C_L on refined panels.

Second, errors from optimization failures will be studied. Sub-optimization problems are often solved to optimize substructure of a system and used as a computational simulation within a system level optimization. Optimization may produce incorrect results due to algorithmic weaknesses, local optima, or even user's programming error. Many engineering optimization problems require iterative algorithms that may be difficult to converge to high precision due to computational cost. Errors from the Rosenbrock [58] test problem and structural optimization of the HSCT are investigated. Optimization errors appear as high frequency noise, and it is possible that they can be treated as random variables [59]. We will show that a probabilistic model enables us to estimate the magnitude of noisy errors from optimization problems.

Outliers should be given close attention when surrogate models are constructed from computational simulations. The standard least squares fit for response surface approximation is not robust against outliers, although the response surface fit may filter out small amplitude and high frequency noise. Outliers may cause a poor response surface approximation. If an inaccurate response surface approximation is used as a surrogate model in system level simulation or design optimization, it increases the total uncertainty of the simulation and design. Therefore, it is important to identify the outliers in the data and repair them if possible [43], [45], [46], [47]. We will apply robust regression techniques to deal with the outlier problems of the Rosenbrock test problem and the structural optimization of the HSCT.

1.4 Methodology

To determine the error or quality of a single simulation is a difficult task. However, when many simulation results are available, such as when building a response surface model from *a priori* simulation runs, statistical tools can be used to estimate errors. Design of experiments

(DOE) [60] is a technique to choose sample points to be used to study the effects of independent variables on the response variables. It is well known that the characteristics of simulation error are different from those of experimental noise. For example, repeated numerical simulations for the same data normally give the same results, while repeated physical experiments do not. So, the use of duplicate points, which is common in experimental research, is avoided with numerical simulations.

Discretization error is fundamental when discretized models of the system are solved. Discretization errors may involve systematic and noise components as well. Richardson extrapolation, which generates higher accuracy results from lower order results, tends to amplify the noise error. Response surface techniques can be used to model the discretization error by incorporating the mesh size. It was suggested that response surface models might be an efficient way to reduce discretization errors by using a carefully selected experimental design [37], [38]. In addition, the noise filtering capability of the response surface model can be useful when noise error is present as well as systematic discretization error.

It was suggested that it could be useful to use probabilistic models for high frequency simulation errors [59]. For example, it was found that the noise from the HSCT structural optimization is not systematic error. If we perform structural optimization for two slightly different HSCT configurations, the magnitude of error for one configuration does not enable us to predict the optimization error of the other configuration, because of the unexpected variation of the error. This is in contrast to systematic error such as modeling error, where the error usually varies continuously along design changes. Therefore, we may fit model probability distributions to error data via maximum likelihood estimates (MLE) [61]. In MLE, we seek the parameters of the distribution function to maximize the probability of the observed sample. The distribution fit has been widely used in simulation and modeling theory [62]. Several model distribution functions [62], [63], like Gaussian, exponential and Weibull, are considered. The fitted error distributions can be used to estimate the magnitudes of the simulation errors [59].

The computational simulations in the current work are intended to construct response surface approximations of the simulation codes. Response surface fits naturally filter out small amplitude high frequency noise error that might cause trouble with a gradient based optimizer. It should be noted that the mean square error of the response surface fit may be a good measure of

noise error in ideal situations, where the polynomial model is correct and the errors have zero mean with constant variance.

Standard least squares fits for response surface approximations can be greatly affected by outliers, data points with large simulation errors. A robust statistical technique, known as *M*-estimator [64], [65], can be used instead of the least squares. The *M*-estimation implemented by iteratively reweighted least squares (IRLS) [44], [66] gives robust fits resistant to outliers by downweighting and removing them from the fit. The small weighting values are indicators of outliers and the detected outliers might be repaired by more accurate simulation efforts. Repairing only the outliers can be computationally cheaper than performing more accurate, yet expensive, simulations for all of the data.

In addition, optimization error tends to be one-sided [47], [59]. Optimization is typically an iterative process, and is rarely allowed to converge to high precision due to computational cost considerations. If optimization error occurs due to incomplete convergence, the calculated optimum will be greater than the true optimum in a minimization problem provided that the calculated optimum is feasible. If so, the error is expected to be positive. This implies that the mean of the error cannot be zero, and the symmetric weighting function used in the IRLS procedure can be improved by taking into account skewness of the error. We will demonstrate the approach of using a nonsymmetric weighting function [47] in IRLS procedures, which is denoted as NIRLS (nonsymmetric IRLS), for detecting outliers in structural optimization of HSCT design.

1.5 Outline

The design research group of the MAD Center at Virginia Tech has been developing multidisciplinary analysis and optimization programs for aerospace vehicles. Simulation errors associated with the design of a high-speed civil transport (HSCT) will be studied.

In Chapter 2, a general description of the configuration optimization of an HSCT design will be presented along with a discussion of the analysis modules used in variable-complexity modeling. A simplified five variable problem is described which was used in the present research. Chapter 3 presents examples of simulation errors in the HSCT design problem. First,

the discretization error from a supersonic panel method is described. Then, the noise error from wing structural weight calculations using structural optimizations is presented.

Statistical techniques used in the study are presented in Chapter 4 through Chapter 6. An overview of response surface techniques is presented in Chapter 4. Noise filtering capabilities of response surface models are discussed. Probabilistic models for noisy simulation errors will be presented in Chapter 5. Several candidate model distributions will be introduced for the noise error. The MLE to fit the model distributions to the data will be explained. The c^2 goodness-of-fit test will be introduced as a formal test to check the agreements between the fit and data. Normally, estimation of the convergence error requires simulation using tightened convergence parameters, which can be expensive. A novel approach to estimating simulation errors without more accurate simulations is discussed, using the differences of two noisy simulation data from two different settings of program control parameters. In Chapter 6, a robust regression technique known as *M*-estimation is introduced. Iteratively reweighted least squares (IRLS) will be discussed along with various weighting functions. To make use of the one-sidedness of optimization error, a nonsymmetric weighting function is devised.

In Chapter 7, errors from a supersonic panel code, WINGDES, are studied. Results of a grid (panel) convergence study are presented. Richardson extrapolation formulas of higher order accuracy are derived for finitely refined meshes. The response surface technique is used to model the discretization error and the results are compared to the estimations by Richardson extrapolation.

Chapter 8 presents a test problem study of optimization error. Optimization failures of various optimization programs on the Rosenbrock function are discussed. The Weibull distribution is used for the probabilistic modeling of noise errors from optimization failures. The probabilistic models were used to estimate the magnitude of noise error. The IRLS techniques are used to identify optimization results with large errors. The improvements of the response surface model due to outlier repair are discussed.

Estimation and reduction of errors from structural optimization of an HSCT will be presented in Chapter 9 and Chapter 10. Estimation of the optimization error via a probabilistic model will be presented in Chapter 9. The effects of convergence criteria on the optimization error will be discussed, and the most influential convergence criterion is identified. The distribution of error will be found by fitting the Weibull model to the convergence error via

MLE. The usefulness of the probabilistic model will be demonstrated via an indirect distribution fit using differences of two simulation results. In Chapter 10, outlier detection results via IRLS techniques will be presented. To utilize the one-sidedness in the optimization error, a nonsymmetric weighting function is proposed over symmetric weighting functions. The results show that the nonsymmetric IRLS (NIRLS) is more effective in pinpointing outliers than regular IRLS. The outliers are repaired via more accurate optimization runs, and effects of outlier repair on the accuracy of response surface approximation are discussed. HSCT configuration optimizations are performed to see the effects of the improvements of response surface models on the optimum designs. Finally, conclusions of this research are presented in Chapter 11.

Chapter 2 HSCT Configuration Design Optimization Problem

2.1 Formulation of the Problem

Researchers at the Multidisciplinary Analysis and Design (MAD) Center for Advanced Vehicles at Virginia Tech have developed a high-speed civil transport (HSCT) design procedure [4], [8], [49]. The HSCT is designed to carry 250 passengers at a cruise Mach number of 2.4 for a range of 5500 nautical miles. The idealized mission profile is composed of take-off, subsonic climb, supersonic cruise/climb, and landing segments. The HSCT is a good test bed for multidisciplinary design optimization (MDO) research because this type of aircraft requires close interaction among traditional disciplines to meet the challenging requirements. The takeoff gross weight (W_{TOGW}) is selected as the objective function to be minimized, which is a combined figure of merit of the aircraft. Since the takeoff gross weight can be expressed as a sum of fuel weight and dry weight, the aerodynamic drag is reflected by the fuel weight and the structural efficiency is indicated by the dry weight. Also, the takeoff gross weight can be correlated to the life cycle cost of the aircraft in that the dry weight indicates the acquisition cost while the fuel weight reflects the operational cost.

The general HSCT model [8], [67] is parameterized by 29 design variables (Table 2.1). Of these, 26 describe the geometry, two the mission, and one the thrust. This provides a realistic description of the complex geometry with a relatively small number of design variables and allows us to investigate a wide variety of aircraft configurations. The geometry variables consist of nine for the wing planform, five for the airfoil shape, and eight for the fuselage geometry. See Figure 2.1 for the configuration variables to define the geometry of the airplane. The starting cruise altitude and the cruise climb rate are the two mission variables. The optimization has up to sixty-eight inequality constraints (Table 2.2), including geometry, performance, and aerodynamics related constraints.

In the current study we used a simplified version of the HSCT problem, following Knill *et al.* [4], with five design variables. The five design variable case includes fuel weight, W_{fuel},

and four wing shape parameters: root chord, c_{root}, tip chord, c_{tip}, inboard leading edge sweep angle, L_{ILE}, and the thickness to chord ratio for the airfoil, t/c (see Figure 2.2). Note that traditional variables such as leading edge sweep angle are used instead of the coordinate of the leading edge break point to enable a compact definition. In the five variable case, fuselage, vertical tail, mission and thrust related parameters are kept unchanged at the baseline values. Table 2.3 shows the values and ranges of the five design variable problem along with other variables fixed at the baseline values. In the simplified problem, the stability derivative related constraints are dropped because the tail size is kept unchanged at the baseline value. The list of constraints used in the simplified problem is marked out of the 68 constraints in Table 2.2. The primary reason for the simplification was to avoid an excessive amount of computation when building response surface models for high dimensional problems. In addition, using the simplified problem reduced the problem of modeling deficiency of lower order polynomials. However, the simplification does not necessarily mean that the current study of the simulation error is restricted to low dimensional problems.

2.2 Analysis Methods and Tools

2.2.1 Aerodynamic Analysis

Variable complexity modeling (VCM) [49], [50], [56] combines lower and higher fidelity analysis codes to alleviate the computational burden of using high-fidelity codes exclusively in design optimization. The HSCT code adopted the VCM approach; there are a series of analysis codes of different fidelity levels intended for the same job. For example, three methods are available for supersonic wave drag calculation: a modified version of Eminton's code of low fidelity [68], Harris's wave drag code of mid-fidelity [69], and Euler CFD analysis of high-fidelity [4]. For the drag due to lift calculation, the analytic method by Cohen and Friedman [70] of low fidelity, and a supersonic panel program ([56], pp. 41-49) of mid-fidelity based on Carlson's Mach box method with attainable leading edge thrust concept [53], [54], are available. For supersonic skin friction drag, an algebraic method was used [71], [72].

2.2.2 Weight and Structural Analysis

The takeoff gross weight of the HSCT is estimated using weight equations from the Flight Optimization System (FLOPS) program based on historical data. However, a study by Huang [73] found that the FLOPS weight equations are inaccurate for HSCT type aircraft, for which few historical data are available, particularly in estimating the wing bending material weight (W_b) as a function of the wing planform shape. Consequently structural optimization was adopted to obtain more accurate W_b by Balabanov *et al.* [8]. GENESIS [52] structural optimization software by VR&D was used with a finite element (FE) model. The structural optimization is a sub-optimization for the system level configuration design. In practice, the structural optimizations are performed *a priori* for many aircraft configurations and a response surface model of W_b was constructed as a function of the configuration design variables.

Table 2.1: Twenty-nine configuration design variables for HSCT.

Number	Name of design variables
Planform Variables	
1	Wing root chord, c_{root}
2	LE break point, *x*, *LEbx*
3	LE break point, *y*, *LEby*
4	TE break point, *x*, *TEbx*
5	TE break point, *y*, *TEby*
6	LE wing tip, *x*, *LEtx*
7	Wing tip chord, c_{tip}
8	Wing semi span, *b/2*
Airfoil Variables	
9	Location of max. thickness, $(x/c)_{max\text{-}t}$
10	LE radius, R_{LE}
11	Thickness to chord ratio at root, $(t/c)_{root}$
12	Thickness to chord ratio LE break, $(t/c)_{break}$
13	Thickness to chord ratio at tip, $(t/c)_{tip}$
Fuselage Variables	
14	Fuselage restraint 1 location, x_{fus1}
15	Fuselage restraint 1 radius, r_{fus1}
16	Fuselage restraint 2 location, x_{fus2}
17	Fuselage restraint 2 radius, r_{fus2}
18	Fuselage restraint 3 location, x_{fus3}
19	Fuselage restraint 3 radius, r_{fus3}
20	Fuselage restraint 4 location, x_{fus4}
21	Fuselage restraint 4 radius, r_{fus4}
Nacelle, Mission, and Empennage Variables	
22	Inboard nacelle location, $y_{nacelle}$
23	Distance between nacelles, $Dy_{nacelle}$
24	Fuel weight, W_{fuel}
25	Starting cruise altitude
26	Cruise climb rate
27	Vertical tail area
28	Horizontal tail area
29	Engine thrust

Table 2.2: Constraints for the HSCT design.

Number	Constraint Description	Used in the five variable problem
1	Range ≥ 5500 n.mile	√
2	Required C_L at landing speed ≤ 1	√
3-20	Section $C_l \leq 2$	√
21	Landing angle of attack ≤ 12°	
22	Fuel volume ≤ half of wing volume	√
23	Spike prevention	√
24-41	Wing chord ≥ 7.0 *ft.*	√
42-43	No engine scrape at landing a	
44-45	No engine scrape at landing a, with 5° roll	
46	No wing tip scrape at landing	
47	Rudder deflection for crosswind landing ≤ 22.5°	
48	Bank angle for crosswind landing ≤ 5°	
49	Takeoff rotation to occur ≤ 5 *sec*	
50	Tail deflection for approach trim ≤ 22.5°	
51	Wing root T.E. ≤ horizontal tail L.E.	
52	Balanced field length ≤ 11000 *ft.*	
53	TE break scrape at landing with 5° roll	
54	LE break ≤ semi span	√
55	TE break ≤ semi span	
56-58	$(t/c)_{root}$, $(t/c)_{break}$, and $(t/c)_{tip} \geq 1.5\%$	
59	$X_{fus1} \geq 5$ *ft.*	
60	$X_{fus2} - X_{fus1} \geq 10$ *ft.*	
61	$X_{fus3} - X_{fus2} \geq 10$ *ft.*	
62	$X_{fus4} - X_{fus3} \geq 10$ *ft.*	
63	300 *ft* - $X_{fus4} \geq 10$ *ft.*	
64	$Y_{nacelle}$ ≥ side of fuselage	
65	$DY_{nacelle} \geq 0$	
66	Engine-out limit	
67-68	Maximum thrust required ≤ available thrust	

Table 2.3: The simplified version of the HSCT design with five configuration variables.

HSCT configuration design variable (Total 29 variables)	Values and Ranges for the five variable problem	Used for the five variable problem
Planform Variables		
Root chord, c_{root}	150-190 *ft.*	v_1
Tip chord, c_{tip}	7-13 *ft.*	v_2
Wing semi span, *b/2*	74 *ft.*	
Length of inboard LE, s_{ILE}	132 *ft.*	
Inboard LE sweep, L_{ILE}	67^o– 76^o	v_3
Outboard le sweep, L_{OLE}	25^o	
Length of inboard TE, s_{ITE}	Straight TE	
Inboard TE sweep, L_{ITE}	Straight TE	
Airfoil Variables		
Location of max. thickness, $(x/c)_{max\text{-}t}$	40%	
LE radius, R_{LE}	2.5	
Thickness to chord ratio at root, $(t/c)_{root}$	1.5-2.7%	v_4
Thickness to chord ratio LE break, $(t/c)_{break}$	$(t/c)_{break} = (t/c)_{root}$	
Thickness to chord ratio at tip, $(t/c)_{tip}$	$(t/c)_{tip} = (t/c)_{root}$	
Fuselage Variables		
Fuselage restraint 1 location, x_{fus1}	50 *ft.*	
Fuselage restraint 1 radius, r_{fus1}	5.2 *ft.*	
Fuselage restraint 2 location, x_{fus2}	100 *ft.*	
Fuselage restraint 2 radius, r_{fus2}	5.7 *ft.*	
Fuselage restraint 3 location, x_{fus3}	200 *ft.*	
Fuselage restraint 3 radius, r_{fus3}	5.9 *ft.*	
Fuselage restraint 4 location, x_{fus4}	250 *ft.*	
Fuselage restraint 4 radius, r_{fus4}	5.5 *ft.*	
Nacelle, Mission, and Empennage Variables		
Inboard nacelle location, $y_{nacelle}$	20 *ft.*	
Distance between nacelles, $Dy_{nacelle}$	6 *ft.*	
Fuel weight, W_{fuel}	350000-450000 *lb.*	v_5
Starting cruise altitude	65000 *ft.*	
Cruise climb rate	100 *ft./min.*	
Vertical tail area	548 $ft.^2$	
Horizontal tail area	800 $ft.^2$	
Engine thrust	39000 *lb.*	

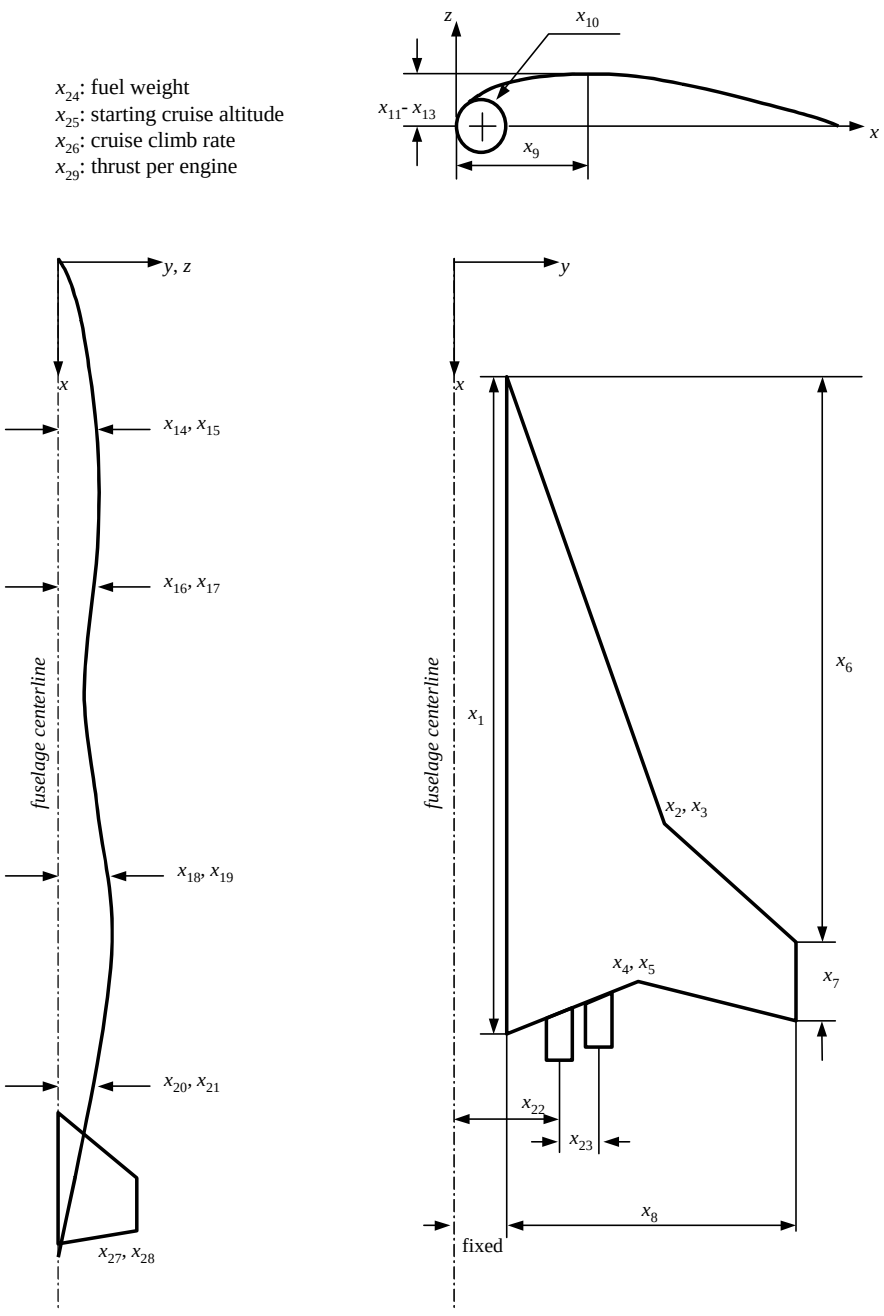

Figure 2.1: Design variables of the 29 variable HSCT design.

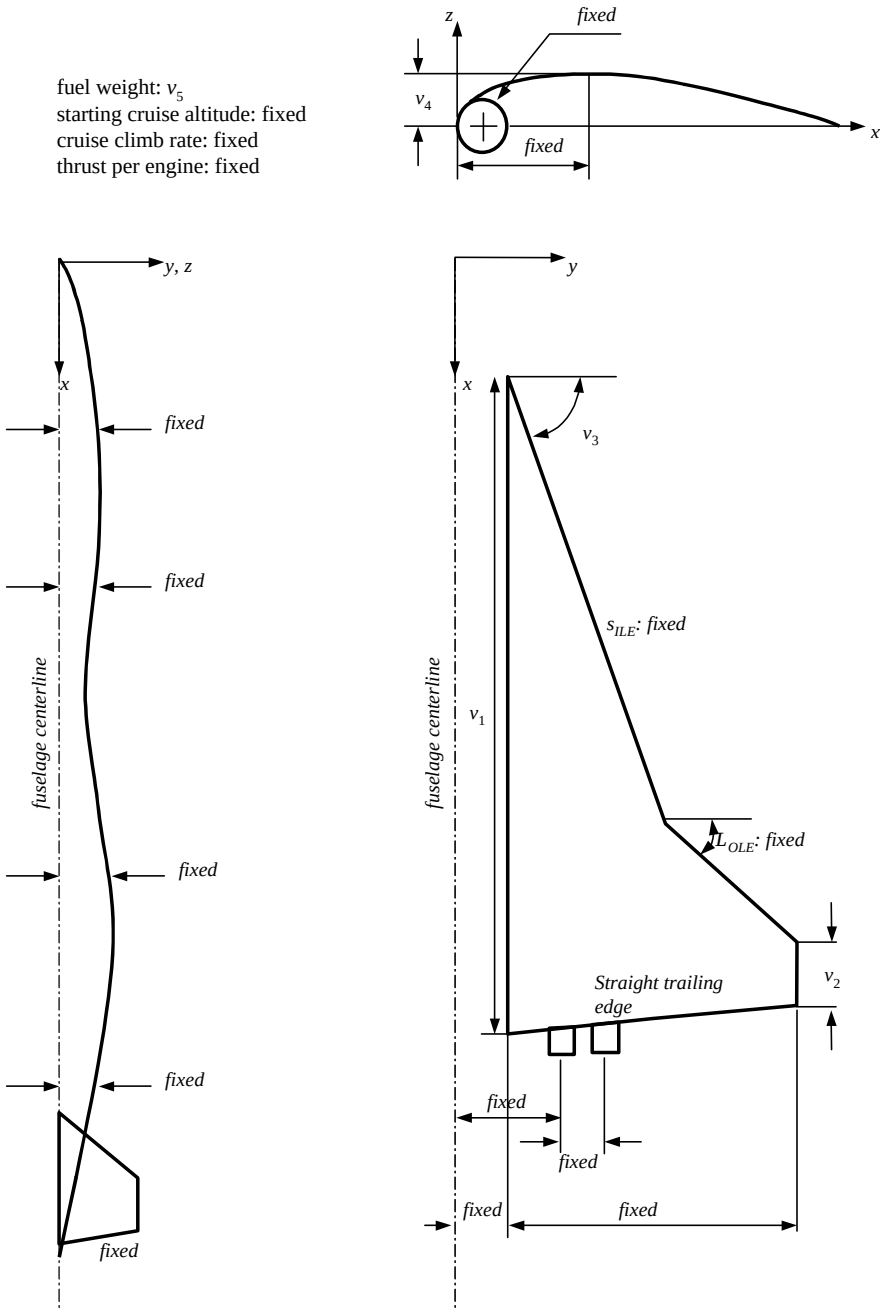

Figure 2.2: Design variables of the five variable HSCT design.

Chapter 3 Examples of Simulation Errors in HSCT Design

Errors can occur in many different phases in computational simulations. Oberkampf *et al.* [33], [34] defined six phases of computational simulations to categorize many error sources: conceptual modeling, mathematical modeling, programming activities, discretization and algorithm selection, numerical solution, and solution presentation. In the current study, we will focus on discretization error and numerical solution error. In this chapter, two computational simulations, supersonic aerodynamics and structural optimization, in the HSCT code will be presented along with description of their error characteristics.

3.1 Supersonic Aerodynamic Analysis Using WINGDES

A supersonic panel method [54] known as a Mach box method is used in the HSCT code. WINGDES [53] is a subsonic/supersonic wing analysis and design code based on linearized potential theory and the attainable leading edge suction concept. WINGDES is used to calculate optimal camber distribution for the structural optimization of HSCT. For a thin wing lying in the plane of $z = 0$, the linearized potential equation is written as

$$
\begin{aligned}
& b f_{xx} - f_{yy} - f_{zz} = 0, \\
\text{BCs}: \quad & f_z = U_\infty \frac{\partial z_c}{\partial x} \text{ on the plane of } z = 0 \text{ occupied by the wing,} \\
& f_x = 0 \text{ on the plane of } z = 0 \text{ except for the region occupied by the wing,} \\
& f \to 0 \text{ far from the wing,}
\end{aligned}
\tag{3.1}
$$

where f is the perturbation velocity potential, $b = \sqrt{M_\infty^{\ 2} - 1}$, and z_c is the z coordinate of the camber line including the angle of attack. The solution of Eq. 3.1 is given in [74] as

$$
\Delta C_p(x, y) = -\frac{4}{b} \frac{\partial z_c}{\partial x}(x, y) + \frac{1}{bp} \iint_t \frac{(x - x)\Delta C_p(x, h) dx dh}{(y - h)^2 \sqrt{(x - x)^2 - b^2 (y - h)^2}}, \tag{3.2}
$$

where the integral region t is the area included by the forward Mach cone from (x, y). Note that the Cauchy principal value theorem is used for singular points (see Ref. [75]) in the area integral.

To replace Eq. 3.2 by a numerical summation, a rectangular grid system is used as shown in Figure 3.1, taken from Ref. [54]. The panel size is decided by the number of spanwise panels in the wing half span, n_y, because the number of chordwise panels, n_x, is proportional to n_y since the aspect ratio of the panels is fixed such that $Dx = bDy$, or

$$n_x \approx \frac{L}{b}\frac{n_y}{b/2}, \tag{3.3}$$

where L is the chordwise distance from the front-most leading edge and the rear-most trailing edge of the wing planform, and b is the wing span. In practice, more panels are used than illustrated in Figure 3.1, and n_y is 40 by default in the HSCT code.

The integral region for point (x, y) is shown as the shaded region in Figure 3.1. Because the solution at (x, y) depends on only the upstream region, DC_p can be calculated sequentially from the apex of the wing leading edge. When mesh halving is used by doubling n_y, the number of panels for WINGDES is increased by four times (= 2^2). Because DC_p is calculated for each of the panels by considering the effect of the panels in the zone of dependence, the computational time is expected to increase by 16 (= 2^4) times. Table 3.1 lists CPU times per WINGDES run on a SGI Origin 2000 workstation. For the default panel system with n_y = 40, the computational cost is negligible. However, the cost increased rapidly, and the CPU time was increased by 12.0, 15.3, and 18.0 times by successive mesh halving, and takes more than 16 minutes for n_y = 320.

It was reported that the results of the Mach box method are noisy with respect to the wing planform change of an HSCT [67], because the non-body fitted rectangular grid system caused non-smooth changes of the analysis panel model. WINGDES was used to calculate the lift coefficient (C_L) of the HSCT by considering only the wing. Figure 3.2 shows the calculated C_L at M = 2.4 with an angle of attack of 0.04 radian (≈ 2.292 deg.), as the wing tip chord (v_2 of the five variable problem) changes from 7 through 13 *ft*. with other variables being fixed at the reference values. Due to the computational cost, only 21 data points are used for n_y = 320 in Figure 3.2,

while we computed 101 data points for n_y = 40, 80, 160. Here, C_L is from the pure panel solution without considering the effects of leading edge thrust. That is because we are interested in the error of the panel solution itself, while the leading edge thrust calculation in WINGDES uses only the leading edge region of the panel solution and involves several empirical smoothing routines.

For the default panel of n_y = 40, systematic discretization error was substantial while noise error was also present. Due to the systematic discretization error, C_L was increased by about 0.001 (1.5%) from n_y = 40 to n_y = 320. The noise error was rapidly reduced when the panel system was refined by mesh halving such as n_y = 80, 160, and 320. Compared to the noise error that is about 0.0001 (0.15%), the systematic discretization error is the main concern. From Figure 3.2, both types of error are seen to decrease, as the panels are refined, although the convergence of the systematic error is slow.

3.2 Structural Optimization

A structural optimization procedure based on a finite element (FE) model is used to calculate the wing structural weight of the HSCT. The FE model developed by Balabanov [7], [8] used 40 design variables (see Figure 3.3), including 26 variables to control skin panel thickness, 12 variables to control spar cap areas, and two for the rib cap areas. Five load cases are considered for the structural optimization (Table 3.2). The loads applied to the structural FE model are composed of the aerodynamic and inertia forces. Inertia loads represent the combined effects of non-structural and structural weight. The HSCT code calculates aerodynamic loads for each of the load cases. A mesh generator by Balabanov [55] calculates the applied load at the structural nodes, and creates the input for GENESIS. The structural optimization is performed for each aircraft configuration. The objective function is the total wing structural weight (W_s) and wing bending material weight (W_b) is assumed to be 70% of W_s. In previous papers [45], [47], we calculated W_b by considering the skin elements that are not at minimum gauge. However, this procedure caused an additional noise error besides the error due to incomplete optimization,

which is our main concern in the paper. So, in this work we used the objective function itself, W_s instead of W_b, to characterize the error.

The main concern of this study is the error of the structural optimization. W_s from the structural optimization contained substantial noise. Figure 3.4 shows W_s results for 21 HSCT configurations generated by linear interpolation between two extreme points in the HSCT design space. Design 1 corresponds to (1, –1, 1, –1, 1) and design 21 corresponds to (-1, 1, -1, 1, -1) in a coded form of the HSCT configuration variables. The original results are noisy and two data points lie well outside the trend. They are called statistical outliers. There were efforts [7] to reduce the noise error by changing the optimization algorithm or by improving the calculation of the optimal airfoil camber from WINGDES [7], [55]. However, substantial noise error still remained and the response surface technique was used to smooth the noise in the structural optimization data. When a standard least squares fit is used, a few outliers such as those in Figure 3.4 may have a large effect on the response surface approximations. We found that incomplete convergence of the optimization procedure was the main source of the noise [59]. Redoing the optimization runs using tightened convergence criteria successfully repaired the noisy results as seen in Figure 3.4. The details of this process will be discussed in Chapter 9.

Table 3.1: Computational time for supersonic aerodynamic analysis of HSCT using WINGDES according to panel step sizes.

Number of spanwise panels in half span, n_y	CPU time per WINGDES run on a SGI Origin 2000, (seconds)
40	0.3
80	3.6
160	55.0
320	989.2

Table 3.2: Load cases for the structural optimization of HSCT.

Load Case	Mach number	Load factor	Altitude (*ft.*)	Fuel
High speed cruise	2.4	1.0	63175	50%
Transonic climb	1.2	1.0	29670	90%
Low-speed pull-up	0.6	2.5	10000	95%
High-speed pull-up	2.4	2.5	56949	80%
Taxiing	0.0	1.5	0	100%

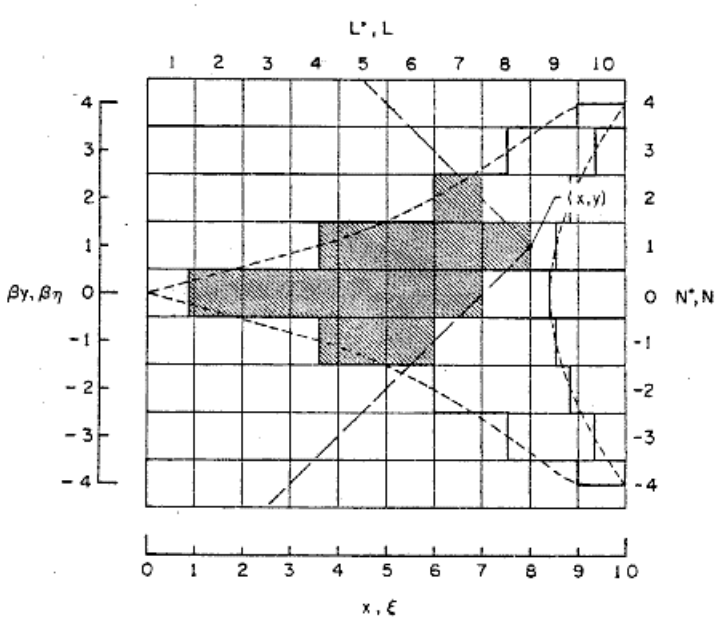

Figure 3.1: Panel system of WINGDES (from Ref. [54]).

In this illustration, the number of spanwise panels in half span, n_y, is 4, and the number of chordwise panel, n_x, is 10. The aspect ratio of the panels is fixed for supersonic calculations because $Dx = bDy$.

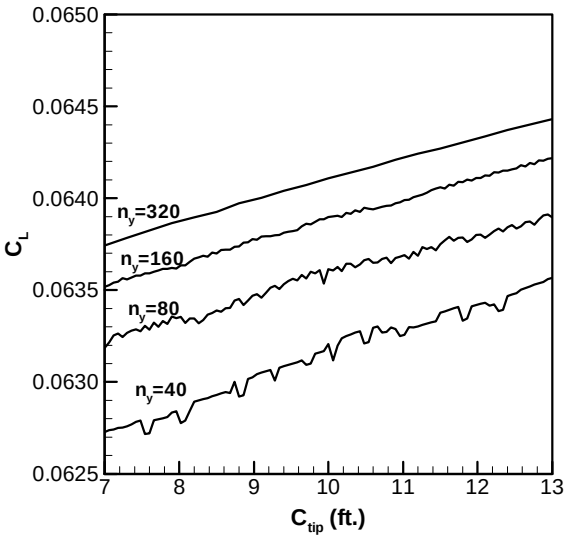

Figure 3.2: Variation of lift coefficient, C_L, with wing tip chord for various panel sizes (M = 2.4, a = 2.292°).

The panels are refined both in spanwise and chordwise directions (see Eq. 3.3). It is clear that the numerical noise decays rapidly with increased number of panels. The systematic discretization error is substantially larger than the noise error.

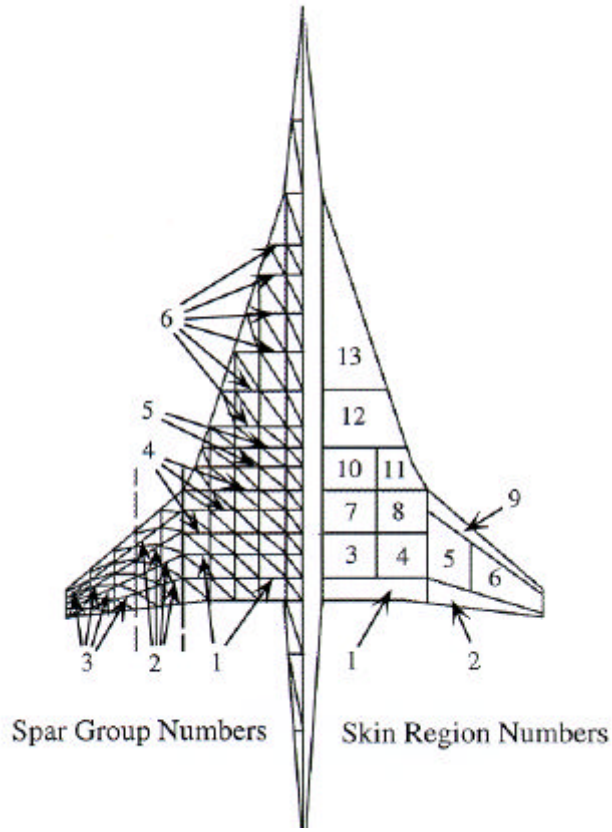

Figure 3.3: Typical FE mesh for the structural optimizations.
It shows six spar groups and thirteen skin groups for the upper surface. Each group is controlled by a design variable of the structural optimization.

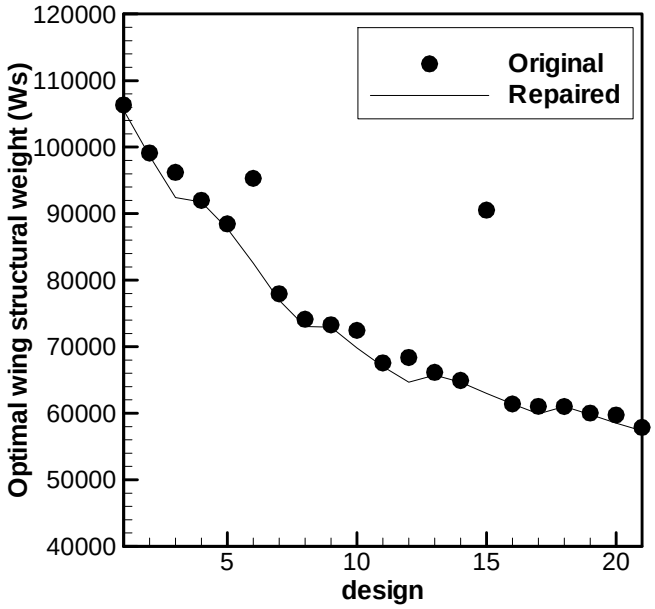

Figure 3.4: Noisy results from HSCT structural optimization and repaired results using tightened convergence criteria.

Structural optimizations are performed for 21 HSCT configurations generated by linear interpolation between two extreme points in the five variable HSCT problem. Design 1 corresponds to (1, –1, 1, –1, 1) and design 21 corresponds to (-1, 1, -1, 1, -1) in a coded form of the HSCT configuration variables.

Chapter 4 Response Surface Methodology

Response surface methodology (RSM) [41] is a branch of statistics used to study the effects of independent variables on a dependent variable, called the response. Design of experiments (DOE), analysis of variance (ANOVA), and regression analysis are the main elements of RSM. Typically, the independent variables are assumed to be non-random and under control of the experimenter, while the response is a random variable.

Response surface (RS) techniques have gained popularity in the application of multidisciplinary design optimization due to their multiple merits. First, the disciplinary analysis code is run *a priori* to build a database, and can be separated from the optimizer. Thus, code integration problems due to proprietary codes are avoided by using RS approximations. Second, the database building process is well suited for use in a parallel computing environment. Third, the RS fit replaces the analysis code by a simple algebraic expression. Low order polynomials of the RS fit take very little computation time compared to analysis programs such as FEA and CFD. The RS surrogate models can be used very effectively in optimization or evaluation of design uncertainty. Lastly, the RS fit naturally filters out the high frequency noise typical with high-fidelity simulations.

4.1 Design of Experiments

Design of experiments (DOE) provides methods to select the combinations of independent variables for which experiments will be performed to build a database ([41], pp.79-133). The experimenter wants to find an experimental design that is not only effective in that it captures all important relationships between the independent and response variables, but also efficient in that it requires a minimal number of experiments. In design optimization studies, the response variable may be the objective function or one of the constraints, and the response variable is modeled as a function of the design variables. The design variables are the independent variables in the DOE and have lower and upper bounds that constitute a hypercube

in which the optimum design is sought. Typically, each design variable is scaled such that it has the range of [–1, +1] in standard DOE software to avoid numerical error in the calculation.

One natural choice for the experimental design is to use all the vertices of the hypercube to cover all of the *m*-dimensional design space (*m* is the number of independent design variables). It is called the full factorial design (FF) of level two (-1 and +1), to which usually a linear polynomial model is fit. To use higher order polynomial models, the level of the experimental design is increased. If the midpoint of each variable is added to the lower and upper level, we have a full factorial design of level three to which a quadratic polynomial model can be fit. One problem associated with the full factorial design is that the number of experiments (computational simulations) increases rapidly as the number of design variables increases. In general, the full factorial design of level *l* requires l^m data points, or experiments. For example, three level full factorial design for a 10 variable problem requires $3^{10} = 59049$ experiments. This is prohibitively large unless experiments take very little time and cost. This problem is known as the *curse of dimensionality*. There are alternatives to the full factorial design that require a smaller number of points, such as face centered central composite design (FCCC) and *D*-optimal design. See Appendix A for a description of the experimental designs.

Originally RS techniques have been developed to fit experimental data from agricultural research. During the last decade, the RS techniques have gained popularity as surrogate models for computational simulations. Certain modifications are desirable in DOE for computational simulations. For example, use of replicates of design points is common in experimental studies, while it is not recommended in computational simulation where the results are deterministic in that the output (response) is the same with respect to the same input (independent variables). However, numerical simulations can be very sensitive to nominal changes of input or may produce different results depending on computer platforms. Therefore, it would be valid to say that computer simulations are not perfectly deterministic.

4.2 Least Squares Fit

Least squares (LS) fit is the standard way to fit a RS model equation to the data generated by the DOE approach. In engineering applications a quadratic model is often used for the RS fit. With *n* data points, the quadratic model for *m* independent variables is written as

$$y_i = b_0 + \sum_{1 \le j \le m} b_j x_{ji} + \sum_{1 \le j \le k \le m} b_{jk} x_{ji} x_{ki} + e_i, \qquad i = 1, \ldots, n, \tag{4.1}$$

where y_i is the i-th observation of the response variable, x_{ji} is the j-th independent variable of the i-th observation, b's are the model coefficients to be estimated, and e_i is the random error assumed to have zero mean and constant variance s^2. In a matrix form, the linear regression model is

$$\boldsymbol{y} = Xb + e \tag{4.2}$$

where $\boldsymbol{y} = \begin{bmatrix} y_1 \\ y_2 \\ \vdots \\ y_i \\ \vdots \\ y_n \end{bmatrix}$, $X = \begin{bmatrix} 1 & x_{11} & x_{21} & \cdots & x_{m1} & x_{11}x_{11} & x_{11}x_{21} & \cdots & x_{11}x_{m1} & x_{21}x_{21} & x_{21}x_{31} & \cdots & x_{m1}x_{m1} \\ 1 & x_{12} & x_{22} & \cdots & x_{m2} & x_{12}x_{12} & x_{12}x_{22} & \cdots & x_{12}x_{m2} & x_{22}x_{22} & x_{22}x_{32} & \cdots & x_{m2}x_{m2} \\ \vdots & \vdots & \vdots & \vdots & \vdots & \vdots & \vdots & \vdots & \vdots & \vdots & \vdots & \vdots & \vdots \\ 1 & x_{1i} & x_{2i} & \cdots & x_{mi} & x_{1i}x_{1i} & x_{1i}x_{2i} & \cdots & x_{1i}x_{mi} & x_{2i}x_{2i} & x_{2i}x_{3i} & \cdots & x_{mi}x_{mi} \\ \vdots & \vdots & \vdots & \vdots & \vdots & \vdots & \vdots & \vdots & \vdots & \vdots & \vdots & \vdots & \vdots \\ 1 & x_{1n} & x_{2n} & \cdots & x_{mn} & x_{1n}x_{1n} & x_{1n}x_{2n} & \cdots & x_{1n}x_{mn} & x_{2n}x_{2n} & x_{2n}x_{3n} & \cdots & x_{mn}x_{mn} \end{bmatrix}$, $e = \begin{bmatrix} e_1 \\ e_2 \\ \vdots \\ e_i \\ \vdots \\ e_n \end{bmatrix}$,

and $b = \begin{bmatrix} b_0 & b_1 & b_2 & \cdots & b_m & b_{11} & b_{12} & \cdots & b_{1m} & b_{22} & b_{23} & \cdots & b_{mm} \end{bmatrix}^T$.

Note that for the quadratic model, there are $p = (m+1)(m+2)/2$ parameters. X is an $n \times p$ matrix of the shape functions (monomials from the quadratic model) called the design matrix, e is an n-vector of noise error, and b is a p-vector of regression coefficients. For standard least squares, estimates of the expected value of y are calculated as

$$\hat{\boldsymbol{y}} = X\hat{b} = X(X^T X)^{-1} X^T \boldsymbol{y}, \tag{4.3}$$

and the residual error $\boldsymbol{e_r}$ is the difference between the actual data and the fit,

$$\boldsymbol{e_r} = \boldsymbol{y} - \hat{\boldsymbol{y}}. \tag{4.4}$$

The root mean square error (RMSE), the unbiased estimate of s, is

$$\hat{s} = \sqrt{\frac{\boldsymbol{e}_r^T \boldsymbol{e}_r}{n-p}}. \tag{4.5}$$

4.3 Analysis of Variance

Techniques of analysis of variance (ANOVA) ([41], pp. 28-32) are similar to the sensitivity study of the response variables with respect to the independent variables. Many of the statistical procedures in response surface methodology depend on the relationship between the total and regression (model) sums of squares ([76], pp. 22-23). The relationship is

$$\sum_{i=1}^{n}(y_i - \bar{y})^2 = \sum_{i=1}^{n}(\hat{y}_i - \bar{y})^2 + \sum_{i=1}^{n}(y_i - \hat{y}_i)^2 , \tag{4.6}$$

i.e.,

$$SS_{\text{total}} = SS_{\text{model}} + SS_{\text{residual}} . \tag{4.7}$$

Equation 4.7 represents the following conceptual identity,

$$\begin{pmatrix}\text{Total variability}\\ \text{in response}\end{pmatrix} = \begin{pmatrix}\text{Variability explained}\\ \text{by model}\end{pmatrix} + \begin{pmatrix}\text{Variability}\\ \text{unexplained}\end{pmatrix}. \tag{4.8}$$

In this way, the usefulness of the regression model can be examined. The coefficient of the multiple determination R^2 is defined as

$$R^2 = \frac{SS_{\text{model}}}{SS_{\text{total}}} = \frac{\sum_{i=1}^{n}(\hat{y}_i - \bar{y})^2}{\sum_{i=1}^{n}(y_i - \bar{y})^2} . \tag{4.9}$$

R^2 represents the proportion of variation in the response data that is explained by the model. From Eq. 4.6, we see that $0 \le R^2 \le 1$. One would expect a large value of R^2 for a good RS model. However, a large value of R^2 does not necessarily imply the regression model is a good one because adding variables to the RS model always increases R^2 ([41], pp. 30-31). In addition, an acceptable R^2 value may depend on the nature of the sample data such as accuracy or randomness ([76], pp. 37-39).

ANOVA is also the basis of the variable selection scheme. Influential variables may be identified by analyzing the portion of the systematic variability of the response due to the change of each independent variable. Conversely, weak variables may be identified and removed from further analysis. A measure of the uncertainty of the regression coefficients is the partial *t*-test,

$$t = \frac{\hat{b}_j}{\hat{s}\sqrt{(X^T X)^{-1}_{jj}}}. \tag{4.10}$$

The *t*-statistic is essentially the ratio of the estimated coefficient to its standard error. Hence, coefficients with small *t* were not accurately estimated, and they are candidates to be removed from the model.

4.4 Noise of Simulation Data and RS Fit

Most computer simulations are deterministic unless pseudo random numbers are used. In terms of the response surface model of Eq. 4.2, it corresponds to that the data has a negligible random variability, *i.e.*, $e \approx \mathbf{0}$. However, many computational simulation programs result in noisy results due to discretization of continuums, truncation error, round-off error, or incomplete convergence of iterative methods.

When the simulation data is noisy, the response surface fit is expected to smooth out the noise and to find the true response. If the regression model (Eq. 4.2) is true, the residual error is due to random noise error. As a result, the root mean squares error, $\hat{s}$, is a good estimate of the magnitude of the noise from the simulation. When the response surface model in Eq. 4.2 is not perfect as in many applications, RMSE is a sum of the noise error and the modeling error of the polynomial model.

Chapter 5 Probabilistic Modeling of Simulation Errors

Practices of robust design classify the design variables into control variables and random variables [16]. The control variables are assumed to be under control of the engineers and non-random, while the random variables have intrinsic variability. Usually the random variables are modeled via probability distributions, and the robust design approach seeks the set of control variables to minimize the risk due to variations of the random variables.

Sometimes simulation errors are modeled as probability distributions for deterministic computer simulations. Probabilistic modeling of simulation errors may be based on the typical magnitude of errors of the computational simulation [77]. It might be justified by the fact that when one picks a design point randomly in the design space, the error is randomized due to the random sampling. However, the probabilistic model is often used without any justification of the model based on data, by simply assuming that the error is following a distribution such as uniform, Gaussian, *etc*. For a better model of the simulation error, systematic examination of the error characteristics is necessary.

5.1 Overview of Probabilistic Modeling of Errors

Probabilistic models are more realistic for noise error than systematic error. Once the distribution of the simulation error is found, detailed information on the error can be obtained. Simulation and modeling theory [61], [62] provides techniques to find the distribution of simulation error from sample data. Our goal is to model the simulation error via probability distribution functions. The procedure can be summarized in four steps.

Step 1: Examine the sample data

Do an exploratory examination of the sample data. Simple graphical tools such as a histogram or box plot can be useful [78] to observe the characteristics of the error. Possible questions are: 1) Is the error discrete or continuous? 2) Is the error systematic or noisy? 3) Is the error symmetric about the mean? 4) What is the typical magnitude of error? 5) Is the error homogeneous over the design space? 6) Are there any unusual data points of extremely large error? 7) Is the Gaussian model reasonable?

Step 2: Select candidate model distributions

According to the examination of Step 1, select a few candidate distributions that seem to fit the sample data well. In some cases, theories behind the sample data may suggest a certain model distribution.

Step 3: Fit the model distribution to the sample data

Usually a model distribution has one or more parameters to be estimated to fix the specific distribution from a distribution family. The model distribution is fitted to the sample data by finding the parameters that fit the data best.

Step 4: Check how good the fit is

The fitted distribution should be compared with the data to check the quality of fit. A few goodness-of-fit tests are available.

5.2 Model Distribution Functions

Simulation and modeling theory provides various model distribution functions to be used as candidates for simulation errors [61], [62], [63]. Table 5.1 describes three distributions we have considered: Gaussian, exponential, and Weibull distributions. The Gaussian distribution is a symmetric bell shaped distribution that is very often used to model random variability. It is the distribution behind linear theory of statistics and has many appealing theoretical properties. The exponential and Weibull distributions are defined for nonnegative random variables and therefore are one-sided. For certain cases, the simulation error is expected to be nonnegative, and the one-sided model distributions are expected to work better than symmetric ones.

Model distribution functions usually have a few parameters that define the distribution. For example, the Gaussian distribution has mean m and standard deviation s as parameters. Figure 5.1 shows the probability density function (PDF) of the Gaussian distribution for different standard deviations s. The exponential distribution has only one free parameter b. The Weibull distribution has two parameters, the shape parameter a, and the scale parameter b. Figure 5.2 shows the PDF of the Weibull distribution for various shape parameters a. Note that the Weibull distribution reduces to the exponential distribution when $a = 1$. One common application of the exponential and Weibull models is for modeling of time to failure [62]. See Appendix B for the interpretation of the Weibull distribution based on the concept of failure rate.

5.3 Maximum Likelihood Estimate of Model Distribution

We use maximum likelihood estimation (MLE) ([61], pp. 188-192) to fit the distribution to optimization error data. Let x be a random variable whose probability density function (PDF) $f(x; b)$ is characterized by a single parameter b. Assuming that the sampled data x_i ($i = 1,\ldots, n$) are independently and identically distributed, the probability that the sample of size n consists of values in the small intervals, $x_i \le x \le x_i+Dx$, is given by the product

$$f(x_1;b)\Delta x f(x_2;b)\Delta x \cdots f(x_n;b)\Delta x = l(b)(\Delta x)^n. \tag{5.1}$$

The x_i 's are fixed at the sample values, and $l(b)$ is called the likelihood function:

$$l(b) = \prod_{i=1}^{n} f(x_i;b). \tag{5.2}$$

For example, when $f(x; b)$ is the exponential distribution function,

$$l(b) = \prod_{i=1}^{n} \frac{1}{b} \exp(-\frac{x_i}{b}). \tag{5.3}$$

MLE seeks the parameter *ß* that maximizes the likelihood function, or equivalently its logarithm. For example, the log likelihood function of the exponential distribution is

$$\log(l) = -n\log(b) - \frac{1}{b}\sum_{i=1}^{n} x_i. \tag{5.4}$$

From $\partial(\log(l))/\partial(b) = 0$, the MLE solution can be shown to be the mean of the data. However, for more general distributions MLE may require the solution of a system of nonlinear equations.

5.4 c^2 Goodness-of-Fit Test

Once we get the MLE of the parameters, we check whether the data is consistent with our trial distribution with the c^2 (Chi-square) goodness-of-fit test ([61], pp. 192-198). To compute the c^2 test statistic, we subdivide the entire range of the fitted distribution into k adjacent intervals. For sample size n, the test statistic is calculated as

$$c^2 = \sum_{j=1}^{k} \frac{(N_j - np_j)^2}{np_j}, \tag{5.5}$$

where N_j is the observed frequency in the j-th interval. p_j is the expected probability of the j-th interval from the fitted distribution, and then np_j is the expected frequency in the j-th interval. If the fit is good, (N_j - np_j) will be small, and the test statistic c^2 will also be small. Therefore, a large value of the c^2statistic indicates that the data is inconsistent with the fitted distribution. The largeness of the test statistic is usually measured by comparing it to the c^2distribution with (k-1-m) degrees of freedom (m is the number of parameters in the distribution) to which it will belong as n goes to infinity. This comparison is given in terms of a p-value, which is defined as the probability that the test statistic is greater than the calculated value when the fitted distribution is true. A p-value near one implies a good fit and a small chance that the data is inconsistent with the distribution. Conversely, a small p-value implies a poor fit and a high chance that the data is inconsistent with the distribution.

5.5 Probability Plot

For a sample of size n, x_i (i = 1, …, n), an approximate cumulative distribution function can be constructed. First, the sample data is sorted in ascending order and $x_{(i)}$ denotes the i-th smallest data. Since the cumulative distribution function (CDF) $F(x_{(i)})$ is defined as Prob(x ≤ $x_{(i)}$), the empirical cumulative distribution function (ECDF) ([61], pp.181-183) is expressed as

$$F_n(x_{(i)}) = i/n. \tag{5.6}$$

Obviously, i/n is an estimate of Prob(x ≤ $x_{(i)}$) from the sample data. It is known that $F_n(x_{(i)})$ converges to the CDF $F(x)$ from which the x_i's are taken as the sample size increases to infinity. In practice, a slight modification is done for Eq. 5.6 to avoid the problem of making F_n = 1 for a finite $x_{(n)}$,

$$F_n(x_{(i)}) = (i\text{-}0.5)/n. \tag{5.7}$$

The probability plot ([61], pp. 181-188) compares the ECDF of a sample with the CDF of an assumed distribution. There are several kinds of probability plots. Here we discuss only one type, called a Quantile-Quantile plot (Q-Q plot). A quantile of order q is defined as $F^{-1}(q)$, where F^{-1} is the inverse function of CDF $F(x)$; it is the value of x for which the cumulative density of x is q. For a Q-Q plot, the following n points are plotted,

$$(F^{-1}((i\text{-}0.5)/n), x_{(i)}) \quad (i = 1,\ldots,n), \tag{5.8}$$

which are pairs of the quantile of CDF and the corresponding quantile ECDF. If the assumed CDF is true, we expect that the pairs of the quantiles are the same for a large sample. Therefore, when we compare the sample data and the fitted distribution via MLE, we expect that the Q-Q plot will be close to a straight line of unit slope passing the origin if the fit is good. Any systematic deviation from the reference line indicates that the fit is not good.

5.6 Indirect Fit of Error Distribution using Differences of Simulation Results

Our objective is to find a probability distribution of error from a lower fidelity simulation. When MLE (see Section 5.3) is used to fit the error distribution, it is usually necessary to run higher fidelity runs to estimate the error of the lower fidelity runs. However, the high-fidelity method may be too expensive computationally, or sometimes high-fidelity simulations are not available. In these situations, we may be able to find the error distributions by fitting the differences between two results from different sets of program control parameters. Examples of program control parameters can be convergence criteria of iterative methods or initial design points in optimization.

Assume that we have simulation results with two different sets of program control parameters. We denote the simulation results by y_1 and y_2 according to the program control settings used. The unknown true solution is common for y_1 and y_2, and will be denoted by y_t.

Then the simulation errors with control parameters setting #1 and setting # 2 can be represented as random variables, *s* and *t*, respectively:

$$\begin{aligned} s &= y_1 - y_t, \\ t &= y_2 - y_t. \end{aligned} \tag{5.9}$$

For example, if the error data follows the exponential distribution, *s* and *t* have the following probability distribution functions

$$\begin{aligned} g(s) &= \frac{1}{b_1}\exp(-\frac{s}{b_1}), \\ h(t) &= \frac{1}{b_2}\exp(-\frac{t}{b_2}). \end{aligned} \tag{5.10}$$

The difference between the pair of y_1 and y_2 is equal to the difference between the errors, because the true solution y_t is the same. That is,

$$x = s - t = (y_1 - y_t) - (y_2 - y_t) = y_1 - y_2. \tag{5.11}$$

The probability density of the differences of simulation results (in short, simulation differences) can be obtained as a convolution of the joint distribution [79] of $g(s)$ and $h(t)$, provided that *s* and *t* are independent each other:

$$f(x; b_1, b_2) = \begin{cases} \int_0^\infty g(s)h(s-x)ds = \dfrac{1}{b_1 + b_2}\exp(\dfrac{x}{b_2}) & \text{if } x < 0 \\ \int_x^\infty g(s)h(s-x)ds = \dfrac{1}{b_1 + b_2}\exp(-\dfrac{x}{b_1}) & \text{if } x \geq 0 \end{cases}. \tag{5.12}$$

This is a continuous distribution of the simulation difference $x \in (-\infty, \infty)$. Now we can fit the simulation difference, *x*, to the model function Eq. 5.12 via MLE. In the maximum likelihood approach we find parameters b_1 and b_2 that maximize the likelihood function

$$l(b_1, b_2) = \prod_{i=1}^{n} f(x_i; b_1, b_2), \tag{5.13}$$

where f is defined in Eq. 5.12. This is an unconstrained optimization problem in two variables. Equivalently we can maximize the log likelihood function,

$$\log l(b_1, b_2) = \sum_{i=1}^{n} \log f(x_i; b_1, b_2). \tag{5.14}$$

Table 5.1: Examples of model functions for continuous distribution.

	Gaussian	Exponential	Weibull
Density $f(x)$	$\frac{1}{\sqrt{2ps^2}}\exp\left(\frac{-(x-m)^2}{2s^2}\right)$	$\begin{cases}\frac{1}{b}\exp\left(-\frac{x}{b}\right) & \text{if } x \geq 0 \\ 0 & \text{otherwise}\end{cases}$	$\begin{cases}ab^{-a}x^{a-1}\exp\left(-\left(\frac{x}{b}\right)^a\right) & \text{if } x \geq 0 \\ 0 & \text{otherwise}\end{cases}$
Parameters	Location parameter m Scale parameter s	Scale parameter b	Shape parameter a Scale parameter b
Mean	m	b	$\frac{b}{a}\Gamma\left(\frac{1}{a}\right)$
Variance	s^2	b^2	$\frac{b^2}{a}\left\{2\Gamma\left(\frac{2}{a}\right)-\frac{1}{a}\left[\Gamma\left(\frac{1}{a}\right)\right]^2\right\}$

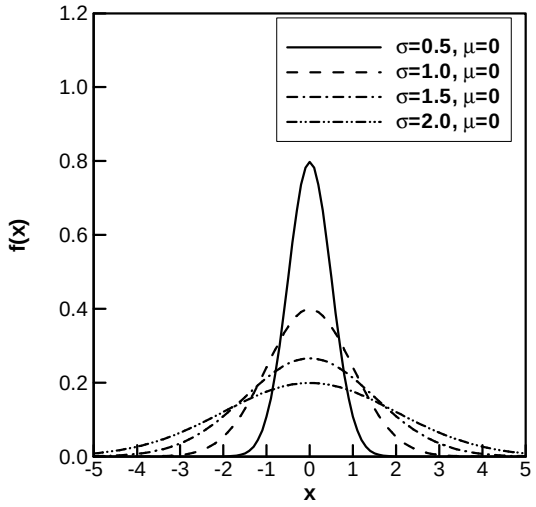

Figure 5.1: Probability density functions for Gaussian with $m = 0$ and various s.

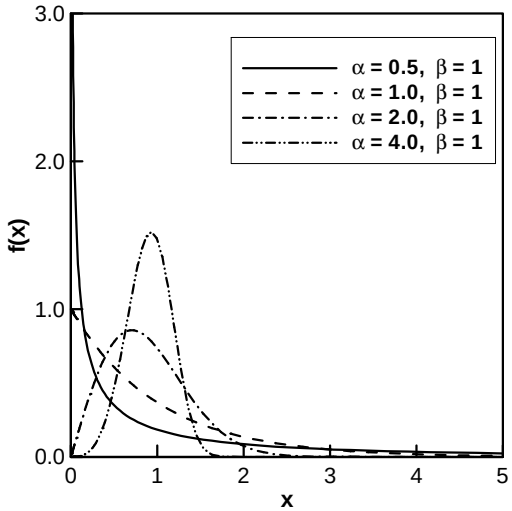

Figure 5.2: Probability density functions for Weibull with $b = 1$ and various a.

Chapter 6 Robust Regression Techniques and Outlier Detection

The least squares fit in standard response surface methodology is not robust. If the database for the response surface fit contains simulation results with large errors, the least squares fit can be greatly affected by the bad data points. The objective of robust statistics [64], [65] is to provide alternative estimation techniques when standard assumptions for the model are not valid. For example, in multiple linear regression, the random error is assumed to have a constant variance with zero mean. Robust regression techniques are designed to give a reasonable fit when the error distribution is not homogeneous, and give estimates as good as the least squares fit when the error distribution is ideal. Also, robust regression techniques provide protection against outliers [43], [65], data points out of the main trend. It gives a robust fit for the data contaminated with outliers (bad simulation results) and enables us to identify those outliers, which may lead to further investigation of the cause of the error.

6.1 Iteratively Reweighted Least Squares

Among several robust regression methods we will discuss the *M*-estimator (maximum likelihood type) [64], [65]. It can be shown that the MLE is an *M*-estimator. For a more robust estimate of $\boldsymbol{ß}$, we minimize a measure of the residuals r_i:

$$e(\hat{b}) = \sum_{i=1}^{n} r(r_i), \quad \text{where} \quad r_i = \frac{(\boldsymbol{y} - X\hat{b})_i}{s}. \tag{6.1}$$

Here, r is a function of the residual scaled by s, a known estimate of the standard deviation of e. For example, in the case of the familiar least squares method, $r(x) = x^2/2$. A necessary condition for a minimum is

$$\nabla e(\hat{b}) = 0. \tag{6.2}$$

The y function is defined as the derivative of r

$$y(x) = \frac{dr(x)}{dx}. \tag{6.3}$$

Then, a necessary condition for a minimum becomes

$$X^T y = 0, \text{ where } y = (y_1, y_2, ..., y_n)^T = (y(r_1), y(r_2), ..., y(r_n))^T. \tag{6.4}$$

To write Eq. 6.4 in a form of weighted least squares, we define the weighting function as

$$w(x) = \frac{y(x)}{x}. \tag{6.5}$$

Now, with $\boldsymbol{r} = (r_1, \ldots, r_n)^T$, Eq. 6.4 becomes

$$X^T W(\boldsymbol{r})\boldsymbol{r} = 0, \quad \text{where} \quad W(\boldsymbol{r}) = diag(w(r_1), w(r_2), ..., w(r_n)). \tag{6.6}$$

Note that for ordinary least squares $y(x) = x$ and $w(x) = 1$.

For ordinary least squares, Eq. 6.6 is a linear equation for the coefficient vector $\hat{b}$ through the scaled residual $\boldsymbol{r}$. However, in general Eq. 6.6 is a system of nonlinear equations, and iterative methods are required to obtain the solution. The most popular approach is iteratively reweighted least squares (IRLS), which is attributed to Beaton and Tukey [66]. Using the definition of residual in Eq. 6.1, the necessary condition of Eq. 6.6 is written as

$$X^T W(\boldsymbol{r}) X\hat{b} = X^T W(\boldsymbol{r})\boldsymbol{y}, \tag{6.7}$$

which can be expressed as an iterative formula

$$\hat{b}^{(i+1)} = \left[X^T W\left(\frac{\boldsymbol{y} - X\hat{b}^{(i)}}{s} \right) X \right]^{-1} X^T W\left(\frac{\boldsymbol{y} - X\hat{b}^{(i)}}{s} \right) \boldsymbol{y}, \tag{6.8}$$

or

$$\hat{b}^{(i+1)} = \hat{b}^{(i)} + \left[X^T W\left(\frac{\boldsymbol{y} - X\hat{b}^{(i)}}{s} \right) X \right]^{-1} X^T W\left(\frac{\boldsymbol{y} - X\hat{b}^{(i)}}{s} \right) (\boldsymbol{y} - X\hat{b}^{(i)}). \tag{6.9}$$

Several possible weighting functions summarized in Table 6.1 and Figure 6.1, were considered here. We preferred Beaton and Tukey's biweight function [66] to Huber's minimax [80] because it gives zero weighting to the outliers and thus the outliers are distinctly identified (see Figure 6.1). s is calculated as $1.5 \underset{i}{median} \, | (\boldsymbol{y} - X\hat{b})_i |$ as recommended by Myers [76]. The other function in Table 6.1, labeled as NIRLS, will be discussed later in Section 6.2. B in Table 6.1 is a tuning constant depending on the characteristics of the error distribution. Myers [76] suggested limiting the tuning constant to a range of one to three. The shape of the weighting functions in Figure 6.1 clearly shows that they penalize outliers with zero or low weighting while giving a weighting of one or near one to inliers.

Equation 6.9 is not guaranteed to converge to the global minimum of $e(\hat{b})$. Because the IRLS results depend on the initial guess for the regressor coefficients, $\hat{b}$, we need a good initial guess of $\hat{b}$. With a non-redescending y function (Figure 6.2) like Huber's minimax, Birch [81] proved that Eq. 6.9 is globally convergent to a unique solution, the global minimum of $e(\hat{b})$. Therefore, to get the initial estimates of the regressor coefficients $\hat{b}$, we adopted Huber's minimax function. Then the IRLS procedure using the biweight function was continued using these initial coefficients. The IRLS procedure with Huber's minimax function converged faster; it took about 20 iterations for convergence while using the biweight required about 100 iterations for the data from structural optimization of the HSCT.

The IRLS procedure is demonstrated for a one-dimensional example in Figure 6.3. The eleven data points were generated by adding some artificial errors to the true response of $y = 0.8 - 0.7x + 0.25x^2$. Two data points at $x = 0.5$ and 0.9 have particularly large errors and may be

called outliers. The least squares fit is distracted by the outliers and over-predicts the response. Robust regression techniques are expected to give a better fit than the least squares fit. The IRLS procedure using the biweight function is applied. The IRLS fit is seen to give a better prediction by giving zero weighting and effectively excluding the outliers from the fit. Note that outliers are identified by the IRLS procedure. In practice, we may want to investigate the cause of the outliers and efforts to repair them may be desirable.

6.2 Nonsymmetric IRLS (NIRLS)

Now we consider the NIRLS entry in Table 6.1. The usual IRLS procedure assumes symmetry of the error with zero mean error. However, for optimization data, the scaled residual r_i is mostly positive for outliers (see Eq. 6.1), because they are caused by the failure of the optimization while seeking a minimum. For unconstrained optimization, any failure of optimization procedure will produce an optimum with one-sided error. Also, some of constrained optimization algorithms seek the optimum in feasible region, and premature convergence of optimization will produce one-sided error except that the optimizer cannot find a feasible design.

To account for the skewed error in the outliers, we devised a nonsymmetric weighting function by combining the biweight and Huber's weighting function, and labeled it as the NIRLS (nonsymmetric IRLS) weighting function. For the NIRLS weighting function shown in Figure 6.1, data points with negative residuals are down-weighted according to Huber's function, whereas points with positive residuals are down-weighted by the biweight function. In this way, NIRLS down-weights points with positive residual error more severely. NIRLS has been successfully applied to noisy data from structural optimization of the HSCT [47], and to low fidelity optimization data of cracked composite panels [82]. We will demonstrate the advantage of the nonsymmetric weighting function on the Rosenbrock test problem in Chapter 8 and structural optimization of the HSCT in Chapter 10.

IRLS/NIRLS techniques effectively remove outliers from the fit by downweighting them. However, when only a few data points are used in a response surface fit due to consideration of computational cost, excluding outliers may be undesirable because it may lead to poor predictions where the outliers are located. Therefore, a better strategy is to repair the detected outliers by performing higher fidelity simulation runs if practical [46]. If the high-fidelity runs

are much more expensive than the lower fidelity runs, repairing only the outliers detected by IRLS/NIRLS may have a computational advantage over performing high-fidelity runs for all the runs. The general IRLS/NIRLS procedure described in this section is summarized in Figure 6.4.

Table 6.1: Weighting functions of *M*-estimator.

Name	$W(r)$	Range	Tuning Constant
Huber's minimax [80]	1 $H\lvert r\rvert^{-1}$	$\lvert r\rvert \le H$ $\lvert r\rvert > H$	$H = 1.0$
Beaton and Tukey's biweight [66]	$(1-(r/B)^2)^2$ 0	$\lvert r\rvert \le B$ $\lvert r\rvert > B$	$B = 1.0$ or 1.9
NIRLS	$H\lvert r\rvert^{-1}$ 1 $(1-(r/B)^2)^2$ 0	$r \le -H$ $-H < r \le 0$ $0 < r \le B$ $r > B$	$H = 1.0$ $B = 1.0$ or 1.9

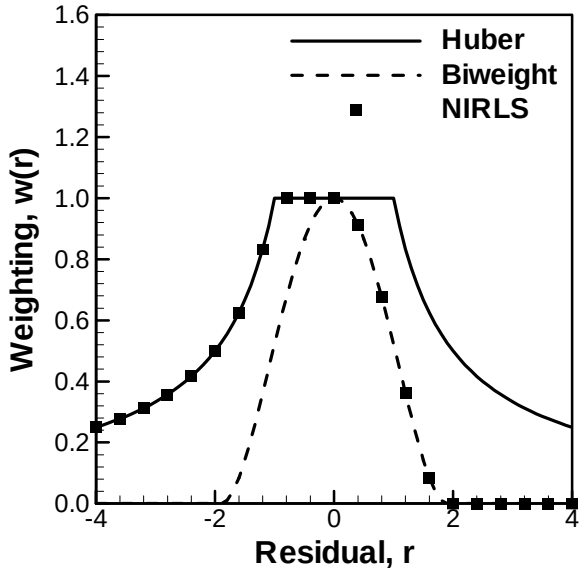

Figure 6.1: Various weighting functions of the *M*-estimator.

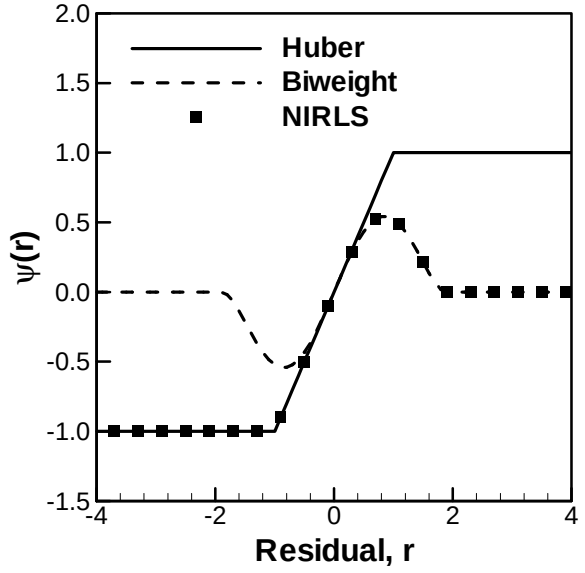

Figure 6.2: The corresponding y functions of the *M*-estimator.

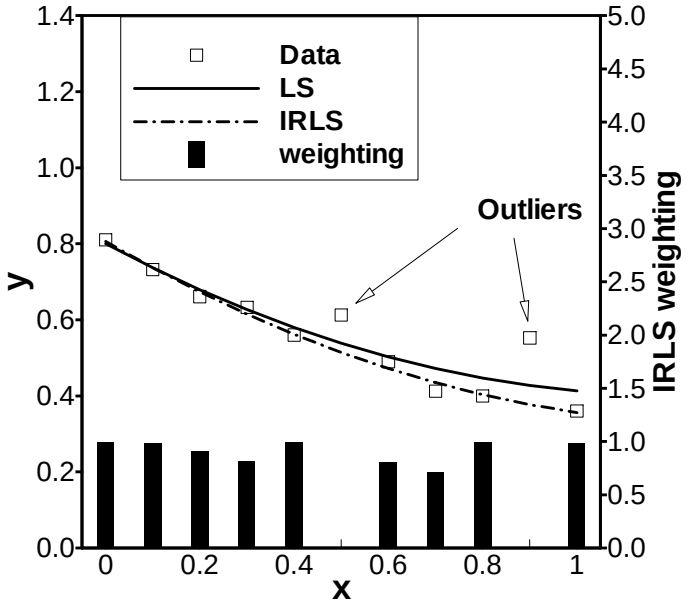

Figure 6.3: One-dimensional example of outlier detection by IRLS.

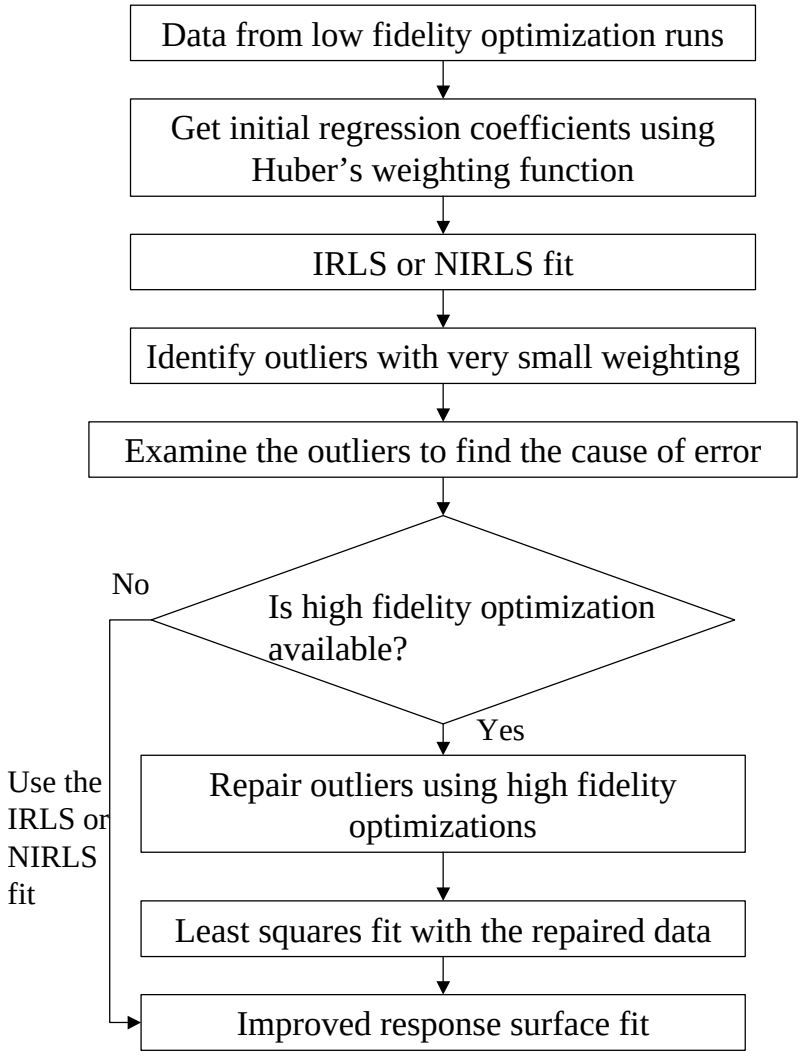

Figure 6.4: Flow chart of the IRLS/NIRLS procedure for low fidelity optimization data.

Chapter 7 RS Modeling of Errors from Supersonic Aerodynamic Simulation

Discretization error is fundamental to all simulations using a discretized representation of a continuum. In Section 3.1, we observed that the C_L calculation from WINGDES had a systematic discretization error and low amplitude noise as well. It was seen that the noise error was small compared to the discretization error. Traditionally, Richardson extrapolation is used to get accurate estimates of the continuum solution from results on relatively coarse meshes. One important aspect of Richardson extrapolation is that it applies not only to solution values at mesh points, but also to a solution functional such as C_L. However, Richardson extrapolation tends to magnify noise errors such as machine round-off errors and incomplete iteration errors (Ref. [9], p. 109-112).

Alvin [37] applied response surface (RS) techniques to model the discretization error by incorporating mesh size, *h*, into the RS model. He showed that the RS approach effectively reduced discretization error in a finite element analysis of a one-dimensional bar, and it was noted that the RS model had computational advantage via careful use of design of experiments. Kammer *et al*. [38] used a rational polynomial function as a RS model to improve extrapolation results when coarser mesh results are used. We utilize their RS approaches to model the discretization error from WINGDES, and the RS approach will be compared to Richardson extrapolation. The results demonstrate again the computational advantages of the RS model for discretization error. Besides, we address several new aspects of the RS approach. First, we perform a grid convergence study for WINGDES to estimate the order of the discretization error. Second, the noise filtering capability of a RS fit may have an additional advantage over Richardson extrapolation. Third, an approach of fitting a RS model to the Richardson extrapolation results will be compared to the RS approach in terms of accuracy and computational cost.

7.1 Grid Convergence Study of WINGDES

Figure 7.1 shows the grid convergence of C_L from WINGDES for the reference HSCT configuration in the five design variable problem. Originally, the number of spanwise panels in the half span, n_y, was 40. The reciprocal of n_y is a measure of the mesh step size, h. Here we changed panel sizes widely, from a very coarse panel system of $n_y = 10$, to 320 by increments of 10. The panels are refined in both spanwise and chordwise directions such that the number of chordwise panels, n_x, is proportional to n_y (see Eq. 3.3). The circle symbols in Figure 7.1 correspond to mesh halving cases, that is n_y = 10, 20, 40, 80, 160, and 320. It is seen that the discretization error would be no greater than 0.002 for $n_y = 40$, about 3% of C_L. Because the theoretical convergence property of the supersonic panel method is not known, the order of error convergence should be estimated from the simulation results. In Richardson extrapolation, the discretized simulation is assumed to have error terms expressed in a polynomial of a step size h,

$$y_h = y + ah^q + O(h^{q+1}), \tag{7.1}$$

where y_h is the discretized solution for the current value of h, y is the continuum solution, a is an unknown coefficient, and q is the order of the method [38]. Asymptotic error convergence is achieved when the higher order error term, $O(h^{q+1})$, is small enough compared to the leading error term, ah^q, and a does not change with h.

If the error of y_h is first order, *i.e.*, q = 1, the response of y_h according to step size, h, should be linear. Figure 7.1 indicates that the order of error convergence q is lower than one for C_L from WINGDES because the slope of the grid convergence curve gets steeper as the mesh step size decreases. It is not unusual that low order panel methods show slow error convergence [83], [84]. If simulation results from three different step sizes are available, the order of convergence q can be estimated (Ref. [9], p. 131). If the mesh is refined by reducing the mesh size by half, using Eq. 7.1

$$r = \frac{y_h - y_{h/2}}{y_{h/2} - y_{h/4}} = \frac{h^q - (h/2)^q}{(h/2)^q - (h/4)^q} = 2^q. \tag{7.2}$$

Therefore,

$$q = \log(r) / \log(2) . \tag{7.3}$$

Table 7.1 shows estimates of q using three WINGDES results of mesh halving. It appears that asymptotic convergence is achieved after $n_y = 40$ with $q \approx 0.5$, and the error converges like $h^{0.5}$.

7.2 Higher Order Formulas using Richardson Extrapolation

7.2.1 Extrapolation for $h = 0$

Richardson extrapolation generates higher order formulas from a series of relatively coarse mesh results (Ref. [57], pp. 180-186). Numerical results of $O(h^q)$ can be expressed as,

$$y_h = y + a_1 h^q + H.O.T., \tag{7.4}$$

where *H.O.T.* represents higher order terms than h^q. Note that the second leading error term is not necessarily h^{q+1} for C_L from WINGDES because q is a non-integral number. If the mesh is refined by reducing the step size by half, *i.e.*, mesh-halving,

$$y_{h/2} = y + a_1 (h/2)^q + H.O.T., \tag{7.5}$$

$$y_{h/4} = y + a_1 (h/4)^q + H.O.T.. \tag{7.6}$$

A higher order formula is obtained by eliminating the leading error term, $a_1 h^q$. By subtracting 2^q times Eq. 7.5 from Eq. 7.4,

$$y_h^{(2)} = \frac{2^q y_{h/2} - y_h}{2^q - 1}, \tag{7.7}$$

where the superscript number in the parenthesis indicates that the order of the formula is higher than h^q. By the same token, from Eq. 7.5 and Eq. 7.6,

$$y_{h/2}^{(2)} = \frac{2^q y_{h/4} - y_{h/2}}{2^q - 1}. \tag{7.8}$$

Richardson extrapolation assumes that the errors are in the asymptotic convergence range. Caution should be taken because Richardson extrapolation will be inaccurate if the mesh step size is not small enough for the error to reach asymptotic convergence. Moreover, noise in data, typical in numerical simulations on discretized models, tends to be magnified by extrapolation (Ref. [9], p. 109-112).

7.2.2 Extrapolation for Finite Mesh Sizes

Richardson extrapolation is designed to extrapolate for y, the continuum solution. In practice, the continuum solutions are not known or are not calculable due to excessive computational cost. That makes it difficult to compare the accuracy of the extrapolation. For quantitative comparison of accuracy of extrapolation, Richardson extrapolation may be reformulated to predict results for finer, but still finite meshes.

By solving Eq. 7.4 and Eq. 7.5 for y and a_1, and substituting them into Eq. 7.6, we obtain a higher order formula for $h/4$,

$$y_{(h/4)}^{(2)} = \frac{y_h + y_{h/2}}{2} + \frac{y_h - y_{h/2}}{1 - 1/2^q}\left[\frac{1}{2^{2q}} - \frac{1}{2}\left(1 + \frac{1}{2^q}\right)\right]. \tag{7.9}$$

Note that a parenthesis is used in the subscript of $y_{(h/4)}^{(2)}$ to indicate an extrapolation for a finitely refined mesh. To get an extrapolation for $h/8$, we need

$$y_{h/8} = y + a_1 (h/8)^q + H.O.T.. \tag{7.10}$$

By solving Eq. 7.5 and Eq. 7.6 for y and a_1, and substituting them into Eq. 7.10, a higher order formula similar to Eq. 7.9 is obtained,

$$y_{(h/8)}^{(2)}(h/2,h/4)=\frac{y_{h/2}+y_{h/4}}{2}+\frac{y_{h/2}-y_{h/4}}{1-1/2^q}\left[\frac{1}{2^{2q}}-\frac{1}{2}\left(1+\frac{1}{2^q}\right)\right], \tag{7.11}$$

where (h/2, h/4) in the left hand side indicates that it is a higher order formula using solutions at h/2 and h/4. To get a higher order formula for h/8 using solutions at h and h/2, Eqs. 7.4, 7.5, and 7.10 are combined,

$$y_{(h/8)}^{(2)}(h,h/2)=\frac{y_h+y_{h/2}}{2}+\frac{y_h-y_{h/2}}{1-1/2^q}\left[\frac{1}{2^{3q}}-\frac{1}{2}\left(1+\frac{1}{2^q}\right)\right]. \tag{7.12}$$

7.3 RS Modeling of Discretization Error

A RS model is built for pre-defined ranges of design variables, forming the design box. Typically, the design box encloses regions of interest, and the RS model is used to predict the response within the design box. On the other hand, prediction outside of the design box is not recommended because such extrapolation using a RS model may have a large error. Richardson extrapolation is used to predict the continuum solution because of the unaffordable cost of the discretized solution for very fine meshes. To apply Richardson extrapolation, asymptotic convergence of the error needs to be achieved, and the order of error should be known. If similar conditions are met, RS models can be used to extrapolate for the continuum solution.

Experiments are performed on a few different mesh sizes, h, which are incorporated into a RS model. One possible advantage of the RS approach lies in its flexibility in selection of data points. A carefully designed experiment may use solutions of refined meshes only sparingly, while Richardson extrapolation requires a series of solutions at different mesh sizes for every design point.

7.3.1 Incorporating Discretization Error into the RS Model

The RS approach is applied to a one-dimensional problem: C_L from WINGDES for different wing tip chords (c_{tip}). Following Ref. [38], a polynomial model, quadratic in x and order q in h, is proposed,

$$y_h = b_0 + b_1 x + b_2 x^2 + a_1 h^q + a_2 x h^q + a_3 x^2 h^q + e, \tag{7.13}$$

where y_h is the discretized solution of C_L, e is a random error, and the a's and b's are coefficients to be estimated. Linear interaction terms between h and x are included and the order of error estimated in Section 7.1, q = 0.5, was used in the model. Note that the continuum solution may be obtained by setting h = 0,

$$y = y_{h=0} = b_0 + b_1 x + b_2 x^2. \tag{7.14}$$

7.3.2 Comparison between Richardson Extrapolation and RS Approach

Richardson extrapolation (RE) was used to predict continuum solutions of C_L. Two cases of mesh fineness were tried as follows.

- RE1: Richardson extrapolation from h, h/2 (n_y = 40, 80) using Eq. 7.7
- RE2: Richardson extrapolation from h/2, h/4 (n_y = 80, 160) using Eq. 7.8

For each case, RE is applied to C_L for six HSCT designs of different c_{tip}. Since a coarser mesh result and a finer mesh result are required to perform a Richardson extrapolation, there are twelve WINGDES runs for each case, six on coarser mesh and six on finer mesh (see Figure 7.2). Next, the RS model (Eq. 7.13) was fit to each of the two experimental designs with the twelve data points used in RE approach. In addition, two experimental designs of less number of refined mesh results were tried to show computational advantages of the RS approach.

- RS1.12: RS fit to six points at h (n_y = 40) and six points at h/2 (n_y = 80)
- RS2.12: RS fit to six points at h/2 (n_y = 80) and six points at h/4 (n_y = 160)
- RS1.9: RS fit to six points at h (n_y = 40) and three points at h/2 (n_y = 80)
- RS2.9: RS fit to six points at h/2 (n_y = 80) and three points at h/4 (n_y = 160)

Figure 7.2 compares the results of the RE and the RS model. RE results show artificial noise for RE1 (Figure 7.2(a)), while the results of RS1.12 are smooth and look more reasonable. The poor results of RE1 are due to the noise in the data, particularly for n_y = 40. As the panels were refined, the noise in the data was reduced. That may explain the relatively smooth results of Case RE2 (Figure 7.2(b)), using only refined panels of n_y = 80 and 160. Except for some minor noise, predictions of C_L by RE2 appear to be comparable to RS2.12. The results demonstrate the advantages of the RS model over Richardson extrapolation when simulation data is noisy. To fit the RS model, we don't need all of the twelve data points used in RS1.12 or RS2.12. For the Cases RS1.9 and RS2.9 in Figures 7.2(c) and (d), even though three of the refined mesh results were dropped from the fit, RS fits still give reasonable predictions. Because a WINGDES run on the refined mesh via mesh halving is about sixteen times more expensive than on the coarse mesh, almost half of the computational time would be saved for RS1.9 compared to RS1.12, or RS2.9 compared to RS2.12. Although a quantitative comparison was not performed because continuum solutions were not known, it is seen that the RS model is useful to reduce the noise problem associated with RE, and may be computationally more efficient by carefully selecting simulation cases to be computed via design of experiments.

To compare the accuracy of the methods quantitatively, RE and RS model were used to predict C_L at a finitely refined mesh of n_y = 320. The same combinations of mesh sizes used for prediction for h = 0 were used. New formulas have been derived for RE in Section 7.2.2, and Eqs. 7.12 and 7.11 were used for Cases RE1 and RE2, respectively. The RS models used to extrapolate the C_L at h = 0, can be reused by simply setting h according to the mesh sizes. Figures 7.3(a) and (b) show that the RS prediction of C_L is good, while RE magnified the noise for Case RE1. The magnification of noise got more serious with the RE prediction for h = 0 as seen in Figure 7.2 (a). When only three runs on finer meshes are used in the fit, the RS model still gave reasonable predictions of C_L as seen in Figures 7.3(c) and (d). The values of C_L at n_y =

320 from WINGDES are listed in Table 7.2 along with the errors of RE, defined as C_L (predicted by RE) – C_L (data from WINGDES). RE1 had an average error of 5.052×10^{-5} due to the noise, while the average error of RE2 was only 1.555×10^{-5}.

Table 7.3 shows the errors in C_L predictions by the RS model. The average error of RS1.12, 3.178×10^{-5}, is substantially lower than that of RE1, 5.052×10^{-5}. Note that the average error of RS1.9, 4.854×10^{-5}, was lower than that of RE1, although only nine data points were used in the RS fit; the RS approach was better than RE in terms of both accuracy and efficiency, when the noisy data of $n_y = 40$ was used in calculation. When the data is less noisy, RE and RS showed comparable average errors: 1.555×10^{-5} for RE2 and 1.532×10^{-5} for RS2.12. With fewer data points used in the fit, RS2.9 showed a higher average error of 2.543×10^{-5} than RE2. However, the loss of accuracy of the RS fits due to removing a few runs on finer meshes, is small in terms of the magnitude of the discretization errors seen in Figure 7.3.

7.3.3 RS Fit to the Data from Richardson Extrapolation

There might be a question concerning the RS approach; is the RS model of Eq. 7.13 necessary? Alternatively, a simpler RS model may be fit to the Richardson extrapolation results,

$$y_{h/8} = b_0 + b_1 x + b_2 x^2 + e \ . \tag{7.15}$$

This *posterior* RS approach will be denoted RSRE, and it is applied to the results of RE1 and RE2.

- RSRE1: RS fit to RE results for $h/8$ ($n_y = 320$) from h, $h/2$ ($n_y = 40$, 80)
- RSRE2: RS fit to RE results for $h/8$ ($n_y = 320$) from $h/2$, $h/4$ ($n_y = 80$, 160)

Figure 7.4 compares the results of RS and RSRE. From Figures 7.4(a) and (b), we observe that RSRE1 and RSRE2 give almost the same results as RS1.12 and RS2.12, respectively. It is seen that the mean errors of RS1.12 and RS2.12 in Table 7.3 are the same as those of RSRE in Table 7.4, up to four significant figures. This is a little bit surprising for

RS1.12 where RS produced a smooth response in contrast to the noise in the RE results. That should be attributed to the fact that only two levels of h were used in the experimental designs. With only two levels of h, the RS fit does no noise filtering in h. In other words, the smooth RS results of RS1.12 were thanks to noise filtering in x, which can be fully achieved when fitting a RS model to RE data. If more levels of h are used in the fit, it is possible that the RS approach will have noise filtering in h, showing some advantage over RSRE. However, the RS approach still may have some computational advantage over the RSRE approach for which point-by-point RE should be performed beforehand. Figures 7.4(c) and (d) show that RS1.9 and RS2.9 give a reasonable C_L prediction comparable to the RSRE approach, although three of the finer mesh results were not used in the fit.

Table 7.1: Estimates of order of error convergence of C_L from WINGDES.

	r	q
n_y = 10, 20, 40	2.1459	1.102
n_y = 20, 40, 80	0.7097	-0.495
n_y = 40, 80, 160	1.4329	0.519
n_y = 80, 160, 320	1.3557	0.439

Table 7.2: Error in C_L (n_y = 320) prediction of the Richardson extrapolation. RE1 used Eq. 7.12 and RE2 used Eq. 7.11.

C_{tip} (*ft.*)	C_L (n_y = 320)	Error in C_L (n_y = 320) prediction	
		Case RE1 (Using n_y = 40, 80)	Case RE2 (Using n_y = 80, 160)
7.0	0.0637429	-5.610×10^{-6}	1.084×10^{-5}
8.2	0.0638953	-2.859×10^{-6}	7.292×10^{-6}
9.4	0.0640406	3.033×10^{-5}	-3.040×10^{-5}
10.6	0.0641707	-9.627×10^{-5}	-2.463×10^{-5}
11.8	0.0643036	2.947×10^{-5}	-4.712×10^{-6}
13.0	0.0644306	-1.386×10^{-4}	1.543×10^{-5}
Average error		5.052×10^{-5}	1.555×10^{-5}

Table 7.3: Error in C_L (n_y = 320) prediction of the RS model. RS model of Eq. 7.13 is used.

C_{tip} (*ft.*)	C_L (n_y = 320)	Error in C_L (n_y=320) prediction			
		Case RS1.12 (6 points in n_y = 40 and 6 points in n_y = 80)	Case RS1.9 (6 points in n_y = 40 and 3 points in n_y = 80)	Case RS2.12 (6 points in n_y = 80 and 6 points in n_y = 160)	Case RS2.9 (6 points in n_y = 80 and 3 points in n_y = 160)
7.0	0.0637429	-8.287×10^{-6}	-2.755×10^{-5}	1.842×10^{-5}	5.308×10^{-5}
8.2	0.0638953	3.560×10^{-6}	-2.205×10^{-5}	-9.580×10^{-6}	-9.128×10^{-7}
9.4	0.0640406	-1.021×10^{-6}	-2.782×10^{-5}	-2.427×10^{-5}	-3.195×10^{-5}
10.6	0.0641707	-1.395×10^{-5}	-3.680×10^{-5}	-1.757×10^{-5}	-3.195×10^{-5}
11.8	0.0643036	-5.340×10^{-5}	-6.712×10^{-5}	-7.639×10^{-6}	-1.908×10^{-5}
13.0	0.0644306	-1.104×10^{-4}	-1.099×10^{-4}	1.445×10^{-5}	1.560×10^{-5}
Average error		3.178×10^{-5}	4.854×10^{-5}	1.532×10^{-5}	2.543×10^{-5}

Table 7.4: Error in C_L (n_y = 320) prediction of the RS fit to the Richardson extrapolation results. RS model of Eq. 7.15 is used. RSRE1 is RS fit to RE1 of Eq. 7.12, and RSRE2 is RS fit to RE2 of Eq. 7.11.

C_{tip} (*ft.*)	C_L (n_y = 320)	Error in C_L (n_y = 320) prediction	
		Case RSRE1 (Using n_y = 40, 80)	Case RSRE2 (Using n_y = 80, 160)
7.0	0.0637429	8.275×10^{-6}	-1.838×10^{-5}
8.2	0.0638953	-3.598×10^{-6}	9.573×10^{-6}
9.4	0.0640406	1.011×10^{-6}	2.428×10^{-5}
10.6	0.0641707	1.400×10^{-5}	1.763×10^{-5}
11.8	0.0643036	5.338×10^{-5}	7.627×10^{-6}
13.0	0.0644306	1.104×10^{-4}	-1.442×10^{-5}
Average error		3.178×10^{-5}	1.532×10^{-5}

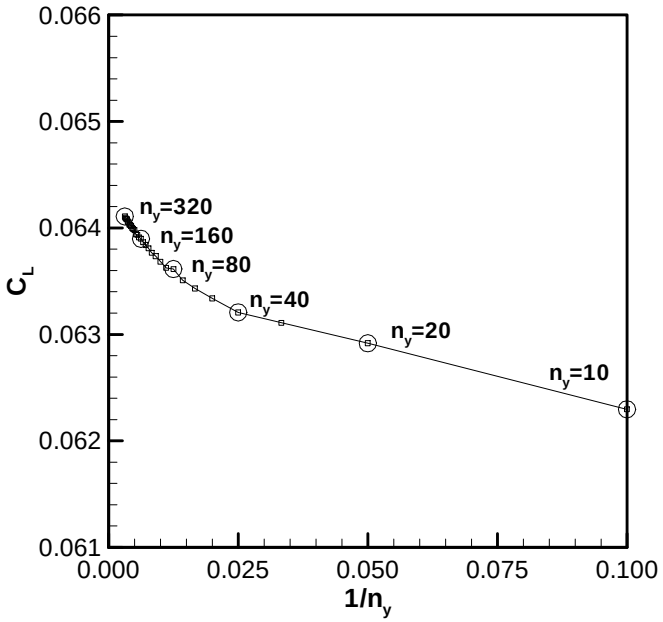

Figure 7.1: Grid convergence study of C_L from WINGDES (M = 2.4, a = 2.292°).
The panels are refined by increasing the number of spanwise panels in half span, n_y, from 10 through 320 by 10. The panels are refined in both spanwise and chordwise directions such that the number of chordwise panels, n_x, is proportional to n_y (see Eq. 3.3). Data points corresponding to mesh halving cases are circled. The reciprocal of n_y is a measure of the mesh step size, h. It is seen that the error convergence is lower than first order because the slope of the convergence curve gets steeper as the mesh step size decreases.

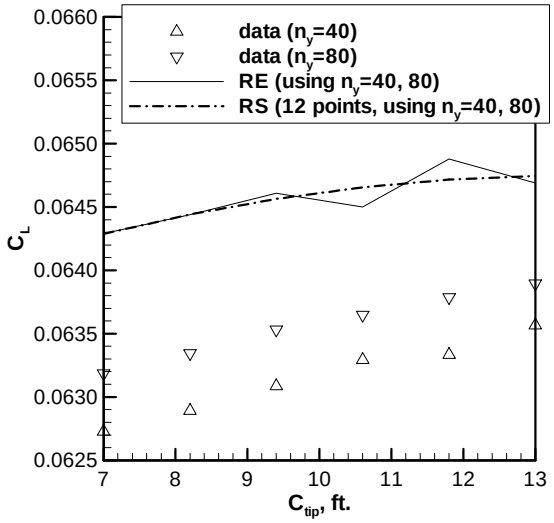

(a) Cases RE1 and RS1.12.

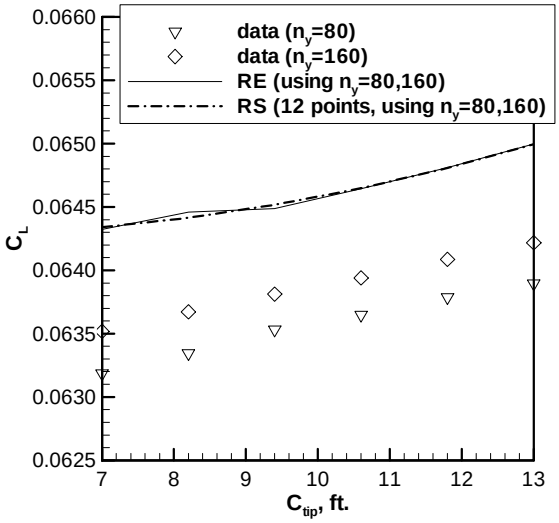

(b) Cases RE2 and RS2.12.

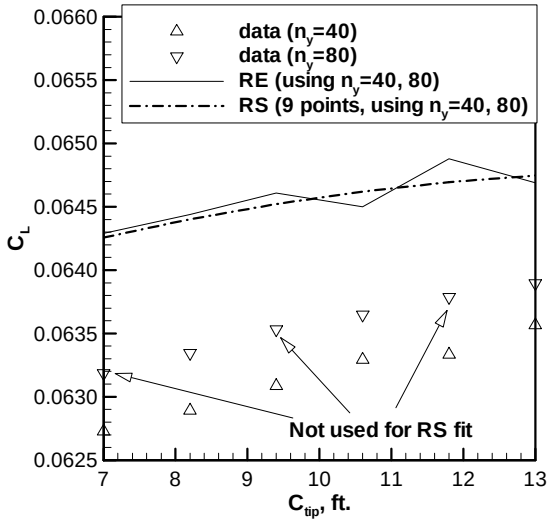

(c) Cases RE1 and RS1.9.

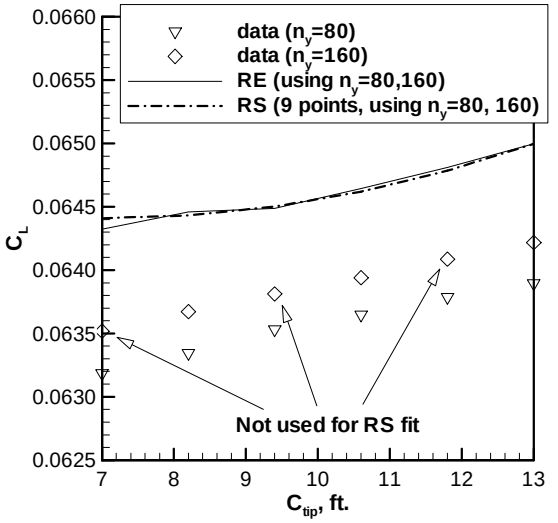

(d) Cases RE2 and RS2.9.

Figure 7.2: Comparison of C_L prediction for $h = 0$ between Richardson extrapolation (RE) and RS model.

RE1 and RE2 used Eq. 7.7 and Eq. 7.8, respectively. Eq. 7.13 was used for the RS model. For RS1.12, twelve points of C_L (six at $n_y = 40$ and six at $n_y = 80$) were used in the fit. For RS2.12, twelve points of C_L (six at $n_y = 80$ and six at $n_y = 160$) were used in the fit. For RS1.9, nine points of C_L (six at $n_y = 40$ and three at $n_y = 80$) were used in the fit. For RS2.9, nine points of C_L (six at $n_y = 80$ and three at $n_y = 160$) were used in the fit.

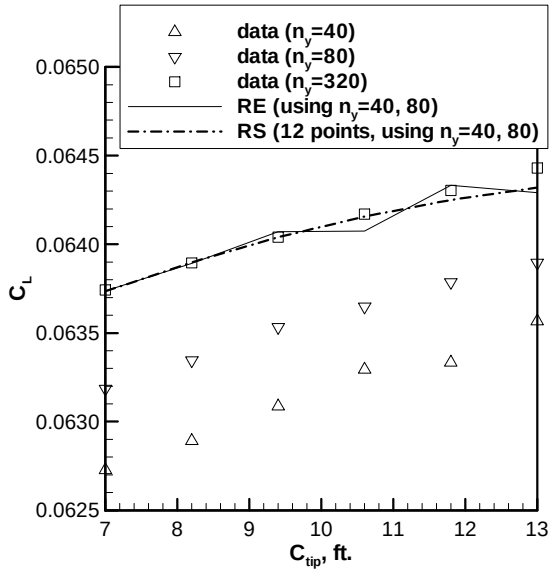

(a) Cases RE1 and RS1.12

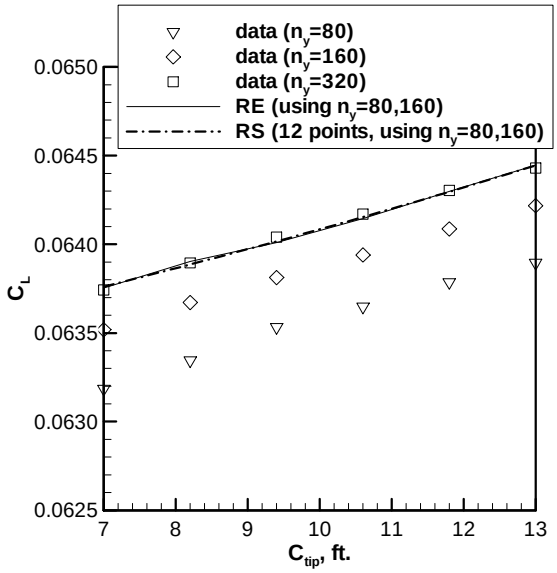

(b) Cases RE2 and RS2.12

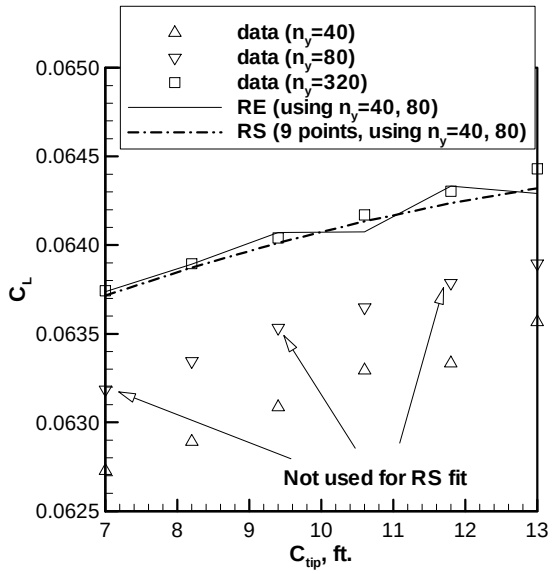

(c) Cases RE1 and RS1.9

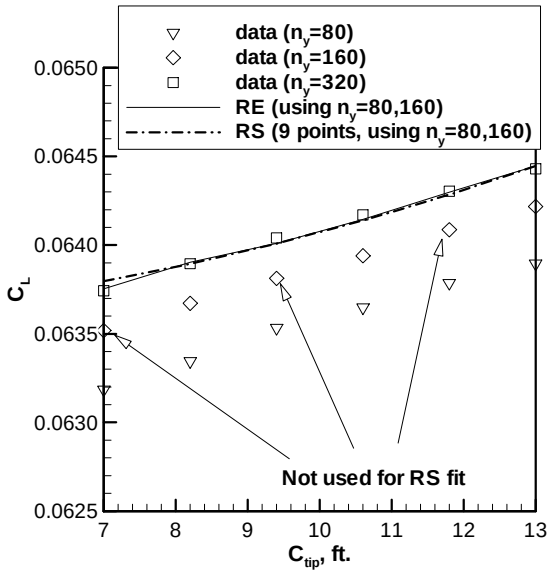

(d) Cases RE2 and RS2.9

Figure 7.3: Comparison of C_L prediction for $n_y = 320$ between Richardson extrapolation (RE) and RS model.

RE1 and RE2 used Eq. 7.12 and Eq. 7.11, respectively. Eq. 7.13 was used for the RS model. For RS1.12, twelve points of C_L (six at $n_y = 40$ and six at $n_y = 80$) were used in the fit. For RS2.12, twelve points of C_L (six at $n_y = 80$ and six at $n_y = 160$) were used in the fit. For RS1.9, nine points of C_L (six at $n_y = 40$ and three at $n_y = 80$) were used in the fit. For RS2.9, nine points of C_L (six at $n_y = 80$ and three at $n_y = 160$) were used in the fit.

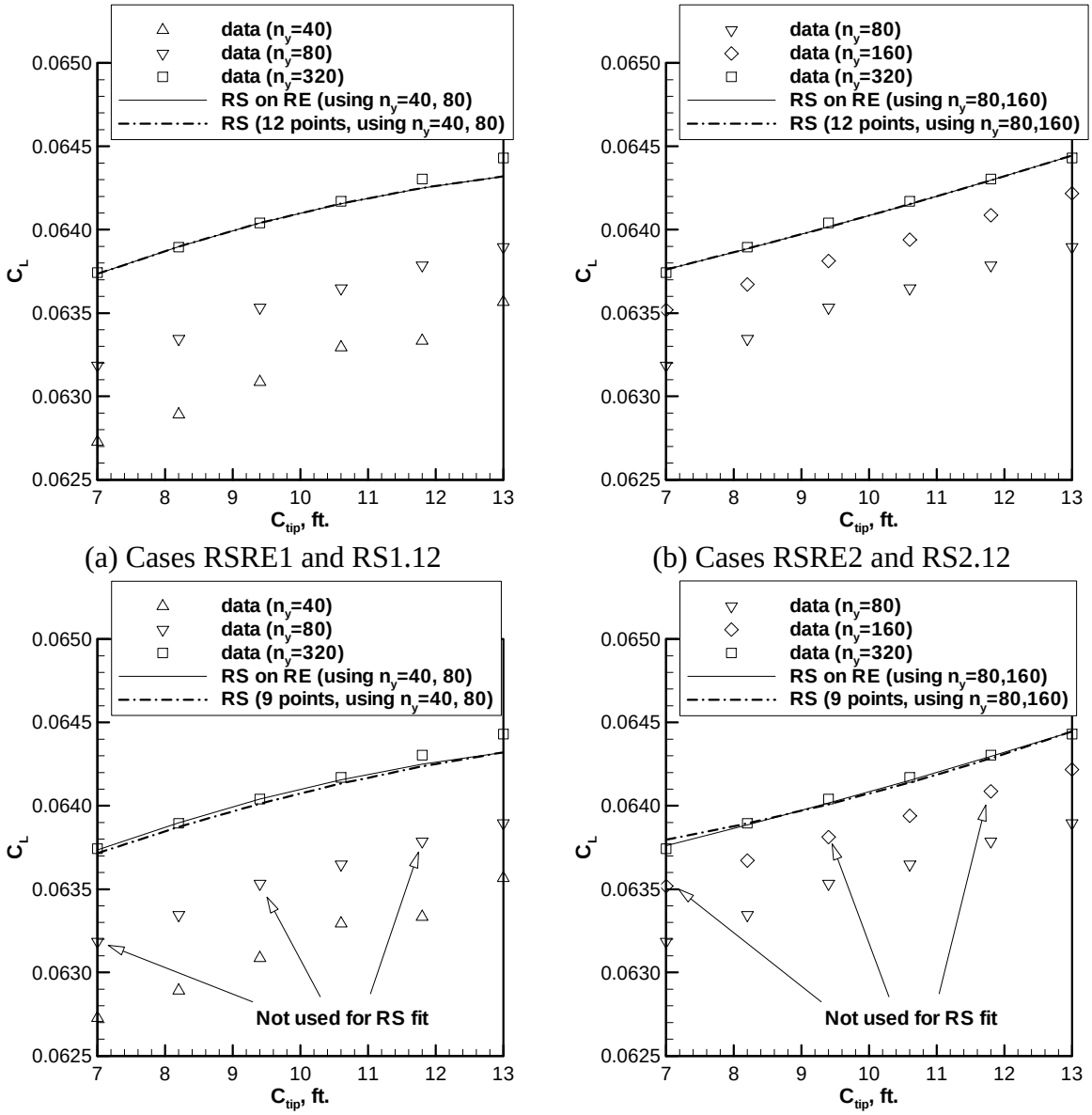

Figure 7.4: Comparison of C_L prediction for $n_y = 320$ between RS fit to the Richardson extrapolation results (RSRE) and RS model.

RSRE1 and RSRE2 fit Eq. 7.15 to the results of RE1 (Eq. 7.12) and RE2 (Eq. 7.11), respectively. Eq. 7.13 was used for the RS model. For RS1.12, twelve points of C_L (six at $n_y = 40$ and six at $n_y = 80$) were used in the fit. For RS2.12, twelve points of C_L (six at $n_y = 80$ and six at $n_y = 160$) were used in the fit. For RS1.9, nine points of C_L (six at $n_y = 40$ and three at $n_y = 80$) were used in the fit. For RS2.9, nine points of C_L (six at $n_y = 80$ and three at $n_y = 160$) were used in the fit.

Chapter 8 Test Problem Study of Errors from Optimization Failures

Most engineering optimization problems require iterative algorithms that may be difficult to converge to high precision due to computational cost. A sub-optimization problem is often solved within a system level optimization. For example, structural optimization was used to calculate optimal wing structural weight within the configuration optimization of the HSCT. Poor results from the nested sub-optimization may cause design uncertainties of the system. In this chapter, a simple test problem is used as an example of optimization errors. The statistical methods introduced in Chapters 5 and 6 will be used to estimate and reduce the optimization errors.

8.1 Errors of Various Optimization Methods on the Rosenbrock Function

Before addressing the HSCT problem, it is worthwhile to illustrate the convergence difficulties experienced by numerical optimization for a simple problem. Here we demonstrate the failure of some optimization algorithms for a simple unconstrained minimization problem, the generalized Rosenbrock function [58] in five dimensions:

$$f(\boldsymbol{x}) = \sum_{k=1}^{n-1} \left[100(x_{k+1} - x_k^{\,2})^2 + (1 - x_k)^2 \right], \quad (n = 5). \tag{8.1}$$

The unconstrained minimization problem has a unique optimum $\boldsymbol{x}^* = (1, 1, 1, 1, 1)$ at which $f^* = f(x^*) = 0$. We performed 500 runs from different initial points, which were randomly generated in the range of $[0, 2]^5$, to check for any optimization failures. As a criterion of failure, we used $f^* > 0.0001$ such that only runs with meaningful error, not due to finite convergence criteria of the optimization algorithm, are declared as failures. For the purpose of this

demonstration we used DOT [85], MATLAB [86], and the trust region routines from the PORT library [87], all with finite difference gradients. The results are summarized in Table 8.1. The *fminu* of MATLAB, an unconstrained minimization routine using the BFGS algorithm, failed to find the true optimum in seven out of 500 runs. DOT using a BFGS routine failed in 27 out of 500 runs. All failures occurred at essentially the same point, $\boldsymbol{x}$ = (-0.962, 0.936, 0.881, 0.778, 0.605). The condition number of the Hessian matrix at that point was about 2400, which is an indication of ill-conditioning of the design space. The trust region algorithm [88] in the PORT library is known to have robust convergence criteria, but the trust region routine *DMNF* with finite difference gradients failed in 488 out of the 500 cases, converging to a distinct point for each failure case. This unexpected failure was traced to a programming error on our part: the function calculating $f(\boldsymbol{x})$ was not declared as double precision, while the double precision PORT library was used. The programming error caused loss of significant figures in the variables passed to the objective function routine from the PORT library, and resulted in premature termination of the optimization procedure. When the programming error was corrected, PORT had no failures.

The Rosenbrock function example shows that optimization may produce a poor optimum due to algorithmic difficulties (*i.e.*, DOT and MATLAB) or user's programming errors (PORT), which is not an uncommon source of optimization error. In both cases, incomplete convergence produced one-sided optimization error with a bad result being always larger than the corrected result.

8.2 Parameterized Rosenbrock function

In the previous section, the Rosenbrock test function was used to demonstrate failures of optimization routines. Many optimization runs were performed using different initial points for the same Rosenbrock function. Often, a sub-optimization problem is solved within the system level optimization. For example, structural optimization is performed within the configuration optimization of the HSCT described in Chapter 2. To mimic the two levels optimization, we generalize the five dimensional Rosenbrock function by adding artificial parameters $\boldsymbol{b}$ to Eq. 8.1,

$$f(\boldsymbol{x};\boldsymbol{b}) = \sum_{k=1}^{4}\left[100(x_{k+1} - b_k x_k{}^2)^2 + (1-x_k)^2\right], \quad \text{where } \boldsymbol{b} = (b_1, b_2, b_3, b_4). \tag{8.2}$$

If we define

$$f_o(\boldsymbol{b}) \equiv \min_{\boldsymbol{x}} f(\boldsymbol{x};\boldsymbol{b}), \tag{8.3}$$

there are two levels of optimization; $\boldsymbol{b}^*$ is sought to minimize $f_o(\boldsymbol{b})$ in the upper level, and $\boldsymbol{x}^*$ is sought to minimize f for a given $\boldsymbol{b}$ to find $f_o(\boldsymbol{b})$ in the lower level. $\boldsymbol{b}$ corresponds to the configuration design variables of the HSCT in the system level and $\boldsymbol{x}$ corresponds to the design variables of the structural optimization, the sub-optimization. Assume that we want to find $\boldsymbol{b}$ that minimizes $f_o(\boldsymbol{b})$, and we may want to build a response surface approximation of $f_o(\boldsymbol{b})$ with respect to $\boldsymbol{b}$ as we do for the optimal wing structural weight of the HSCT.

We elected to change only b_1, b_2, and b_3, while keeping b_4 = 1, to make $f_o(\boldsymbol{b})$ have a unique minimum of zero at (b_1, b_2, b_3) = (1, 1, 1). The ranges of b_k's are chosen to be between 0.9 and 1.1. For a given set of b_k's, the parameterized Rosenbrock function is minimized from an initial design point $\boldsymbol{x}$ = (1.1, 0.9. 1.1, 0.9. 1.1). Figure 8.1 is a design line plot of f_o showing the noisy response of $f_o(b_1, b_2, b_3)$ when PORT with the programming error was used. It is a one-dimensional cut of the f_o response on eleven data points linearly interpolated between $\boldsymbol{b}$ = (0.9, 0.9, 0.9) and $\boldsymbol{b}$ = (1.1, 1.1, 1.1). The true response corresponds to results of PORT without the programming error. We can see that PORT with the programming error gave satisfactory results for only two out of the eleven runs. Define the optimization error

$$e = f_o{}^e - f_o{}^t, \tag{8.4}$$

where $f_o{}^e$ is the result of the erroneous PORT and $f_o{}^t$ is the result of the correct PORT. It is apparent that poor optimizations result in heavier designs and the optimization error is one-sided.

8.3 Estimation of the Optimization Error

We found that the user's programming mistake resulted in poor convergence in PORT optimization runs. The fact that optimization errors are noisy and one-sided leads us to use probabilistic modeling with appropriate candidate distributions. Once we find a probabilistic model of the error, it can be incorporated into a robust design study. Also, we will demonstrate that the probabilistic model is useful to estimate the average error of the optimization runs.

To measure the error of PORT on the parameterized Rosenbrock function, we need sample optimization runs. We used 125 (= 5×5×5) data points from a full factorial experimental design of five levels in $\boldsymbol{b}$. PORT with the programming error was performed to calculate f_o for each of the 125 variants of the parameterized Rosenbrock function. Two sets of 125 data points were generated by using two different initial $\boldsymbol{x}$'s: Case 1 using $\boldsymbol{x_0}$ = (1.1, 0.9, 1.1, 0.9, 1.1) and Case 2 using $\boldsymbol{x_0}$ = (0.9, 1.1, 0.9, 1.1, 0.9). Case 2 will be used to demonstrate the indirect approach of distribution fit in Section 8.3.3. Also, PORT without the programming error (denoted Case 0) was performed to calculate the error of Case 1 and Case 2 according to Eq. 8.4. The errors were large compared to the true f_o, whose average is 0.00399; the average error of Case 1 and Case 2 was 0.00658 (164.9%) and 0.00505 (126.6%), respectively. The low fidelity optimizations of Cases 1 and 2 cost as much computationally as the high-fidelity optimization of Case 0 (Table 8.2). The average number of function evaluations of Case 0 was 199, which is comparable to 209 of Case 1 or 187 of Case 2. Some of the function evaluations might have been wasted for Case 1 and Case 2, because the programming error of the low fidelity cases results in less accurate gradients.

8.3.1 Homogeneity of the Error Distribution

We selected the Weibull distribution as a model for the optimization error of PORT. It is defined for a nonnegative random variable and has great flexibility (see Figure 5.2). The parameters of the model function are found by the maximum likelihood estimate (MLE). A basic assumption of the MLE fit introduced in Section 5.3 is that the data is independently and

identically distributed. For the optimization data of the parameterized Rosenbrock function, the dependence of the data may not be a problem, since the sampling was done by an experimental design without replicates. To check whether the error distribution is the same at different points, the optimization error, e, is plotted against the true f_o in Figure 8.2(a) for Case 1 and Figure 8.2(b) for Case 2. Although there seems to be a few outliers, homogeneity of the error distribution appears to be a reasonable assumption. The correlation between e and the true f_o was low: 0.1635 for Case 1 and –0.0264 for Case 2.

8.3.2 Results of Direct Fit of PORT Optimization Error

A Weibull model was fit to the distribution of optimization errors of Case 1 and Case 2 using the *weibfit* routine of MATLAB [89], and the results are summarized in Table 8.3. The two parameters of the Weibull model, a shape parameter a, and a scale parameter b, were estimated via MLE. From the estimated parameters, $\hat{a}$ and $\hat{b}$, estimates of the mean ($\hat{m}_{fit}$) and standard deviation ($\hat{s}_{fit}$) of the error can be calculated using the formulas in Table 5.1. According to the p-values of the c^2 goodness-of-fit test, the fit to Case 1 was marginally rejected at the 0.05 significance level, while the fit to Case 2 was reasonable.

Recalling that the standard deviation is the same as the mean for the exponential distribution (when a = 1 in Weibull), $\hat{s}_{fit}$ greater than $\hat{m}_{fit}$ indicates that the optimization errors have greater scatter than the exponential model. The overall characteristics of the error can be identified using $\hat{m}_{fit}$ and $\hat{s}_{fit}$ from the MLE fit. On the other hand, the mean and standard deviation can be estimated directly from e by

$$\hat{m}_{data} = \bar{e}, \quad \hat{s}_{data} = \sqrt{\frac{\sum_{i=1}^{n}(e_i - \bar{e})^2}{n-1}}. \tag{8.5}$$

In Table 8.3, $\hat{m}_{fit}$ and $\hat{s}_{fit}$ were compared with $\hat{m}_{data}$ and $\hat{s}_{data}$. The agreement is good except for the standard deviation of Case 1, with 35.6% discrepancy.

The histograms in Figure 8.3 compare the shape of the error distribution to the Weibull fit. The optimization error is nonnegative, and the probability for large error decreases rapidly to

zero. Although the fit to Case 1 was marginally rejected by the c^2 test, the frequencies predicted by the direct fit show a reasonable match with the data in Figure 8.3(a). The fit to Case 2 in Figure 8.3(b) describes the data pretty well.

It should be noted that the above discussions about the results of c^2 tests and the corresponding *p*-values are not rigorous probability statements, because it is possible that the sample size n is not large enough for the asymptotic c^2 approximation to be accurate. Nevertheless, whether the true distribution is Weibull or not, the Weibull model does represent the data well and therefore may find usefulness in error modeling.

8.3.3 Results of Indirect Fit of PORT Optimization Error

The direct approach in Section 8.3.2 requires accurate optimization results to estimate the error. Sometimes, however, we do not have high-fidelity runs because we simply do not know how to improve the accuracy of the simulation. Assume that we do not know of the programming error that resulted in erroneous results from PORT. Then, we can use the pair of Cases 1 and 2 to estimate the error via the indirect fit (Section 5.6). Note that Case 2 uses a different initial $\boldsymbol{x}$ from Case 1. To reduce possible dependence of the errors between Case 1 and Case 2, the initial $\boldsymbol{x}$ of Case 2 was set such that each x_i was opposite to that of Case 1. The correlation between e_1 (error of Case 1) and e_2 (error of Case 2) was small, -0.0371.

The results of the difference fit using the Weibull model are shown in Table 8.4. Note that the distribution parameters a and b of Case 1 and Case 2 are simultaneously estimated. Because there is no closed form of the probability density of the difference for the Weibull model, Eq. 5.12 was numerically integrated using Gaussian quadrature (Ref. [57], pp. 222-228). See Appendix C for the details of the integration method. According to the c^2 test, the indirect fit was reasonable with a *p*-value of 0.4357.

From results of the indirect fit, we can estimate the mean and standard deviation of the optimization error of the two cases involved (Table 8.5), which can be compared to the estimates from data using Eq. 8.5. The estimates for Case 1 were reasonable with 2.7% discrepancy for the mean (m) and 6.1% discrepancy of the standard deviation (s). The estimates for Case 2 were in closer agreement with a 2.0% discrepancy for m and a 0.9% discrepancy for s. The results

demonstrate the usefulness of the probabilistic model for the optimization error. By incorporating the probability model into the indirect fit, we were able to estimate the error without obtaining accurate optimization results.

Compared to the results of the direct fit (Table 8.3), the indirect fit gave more accurate estimates of m and s for this particular example. For example, the direct fit had discrepancies of 5.2% and 35.6% for m and s, respectively in Case 1, while the discrepancies of the indirect fit were 2.7% and 6.1%, respectively. However, the result may not be generalized to other problems. In fact, we expect the direct fit to be as good as the indirect fit if the error data is accurately measured, because the sample size for the indirect approach is the same as that of the direct fit in MLE, while the number of parameters estimated is doubled.

8.4 Detection and Repair of Erroneous Optimization Runs

The robust regression techniques are demonstrated using SAS [90] statistical software to identify erroneous optimizations of PORT with the programming error. To construct a quadratic response surface approximation of $f_o(b_1, b_2, b_3)$, 27 variants of the Rosenbrock function are generated by using a three level full factorial design in b_k, (k = 1, 2, 3). Two different weighting functions from Table 6.1 are compared: the biweight function (denoted IRLS) and the nonsymmetric weighting function (denoted NIRLS). The identified outliers having IRLS/NIRLS weighting less that 0.01 are repaired using the correct PORT optimization.

Table 8.6 summarizes the results of outlier repair. Before outlier repair, the root mean square error (RMSE) of the quadratic response surface was 54.3% and the R^2 value was only 0.68. Because many data points suffered from poor optimization, an aggressive outlier search was performed using a lower value of the tuning constant B = 1.0. We defined big outliers as those showing 10% or greater error. 20 out of 27 data points satisfied this criterion. IRLS declared 9 points as outliers but only 7 of them were big outliers, while NIRLS detected 8 outliers and all of them were big outliers. Note that the mean repair on the outliers by NIRLS is 0.0213 while the mean repair on the outliers by IRLS is only 0.0124. By utilizing the one-sidedness of the error, NIRLS is more successful than the symmetric weighting function of IRLS. The data points not declared as outliers will be called *inliers*. The ratio of average repairs

between outliers and inliers can be considered as a measure of success of outlier detection. For NIRLS the ratio was 7.02 compared to 1.91 of IRLS. The response surface fit is improved via IRLS repair, and there is still substantial improvement by NIRLS repair over IRLS repair; the RMSE is 45.5% for IRLS repair and 29.7% for NIRLS repair. When all 27 points were repaired, the RMSE was only 4.3% and the R^2 was 0.9970.

8.5 Effects of Outlier Repair on the Quality of the Optimum of RS Approximation

The response surface approximations are compared in Figure 8.5 along the same design line used for Figure 8.1. Before outlier repair the response surface approximation over-predicts the true response because of the data points of positive error. With IRLS repair, the response surface prediction is improved but the trend of the response is not accurate. The response surface fit with NIRLS repair follows the true response closely. The response surface models are to be used to find the minimum of $f_o(b_1, b_2, b_3)$. It is clear from the figure that the response surface fit with NIRLS repair will find a more accurate optimum f_o^* than the response surface fit with IRLS repair. Table 8.7 summarizes the results of minimization of f_o according to the response surface models used. When using the response surface fit without repair, the optimum of f_o is located at the boundary of the design space of $\boldsymbol{b}$, which have ranges between 0.9 and 1.1. Considering that the true optimum is located at the center of the design box, the original response surface approximation completely failed to capture the trend of the true response. It is seen that f_o^* gets closer to the true optimum as more outliers are repaired. Comparing the accuracy at optima f_o^*, the response surface model with IRLS repair under-predicts the response by 0.00257 = 0.00082 - (-0.00175) while the error of NIRLS is only 0.00046 = 0.00028 - (-0.00018).

Table 8.1: Failure of various optimization programs for the five dimensional Rosenbrock function.

Software	MATLAB (*fminu*)	DOT	PORT (*DMNF*)	
Algorithm	BFGS	BFGS	Trust region	
Options	-	-	With programming error	Programming error corrected
Number of failures out of 500 runs	7	27	488	0

Table 8.2: Summary of PORT runs for 125 variants of the parameterized Rosenbrock function.

Cases	Case 0	Case 1	Case 2
Algorithm	Trust region	Trust region	Trust region
Description	Programming error corrected	With programming error, $\boldsymbol{x_0}$ = (1.1, 0.9, 1.1, 0.9, 1.1)	With programming error, $\boldsymbol{x_0}$ = (0.9, 1.1, 0.9, 1.1, 0.9)
Average error of f_o (% compared to the average of true f_o)	-	0.00658 (164.9%)	0.00505 (126.6%)
Average number of function evaluation	199	209	187

Table 8.3: Fits of the Weibull model to the error from PORT optimization of the parameterized Rosenbrock function.

Case 1 and Case 2 use different initial designs. $\hat{m}_{fit}$ and $\hat{s}_{fit}$ are estimates from the fit of the Weibull distribution, while $\hat{m}_{data}$ and $\hat{s}_{data}$ are estimates from the data using Eq. 8.5. The estimates of mean, m, from the fit are in good agreement for both Cases 1 and 2. The estimates of the standard deviation, s, is also reasonable for Case 2. The p-value of the c^2 test indicates the fit is particularly good for Case 2.

	Case 1 $\boldsymbol{x_0}$ = (1.1, 0.9, 1.1, 0.9, 1.1)	Case 2 $\boldsymbol{x_0}$ = (0.9, 1.1, 0.9, 1.1, 0.9)
$\hat{m}_{data}$	0.00658	0.00505
$\hat{m}_{fit}$ (discrepancy w.r.t $\hat{m}_{data}$)	0.00692 (5.2 %)	0.00496 (-1.8 %)
$\hat{s}_{data}$	0.00752	0.0110
$\hat{s}_{fit}$ (discrepancy w.r.t $\hat{s}_{data}$)	0.0102 (35.6%)	0.0102 (-7.3 %)
a (shape parameter)	0.6941	0.5297
b (scale parameter)	0.005421	0.002744
c^2 statistic	14.76	4.68
p-value	0.0392	0.6989

Table 8.4: Results of the indirect fit for the optimization error of PORT. The *p*-value of the c^2test indicates that the fit is acceptable.

Case 1	a	0.8507
	b	0.006214
Case 2	a	0.5134
	b	0.002698
c^2 statistic		4.84
p-value		0.4357

Table 8.5: Comparison of the estimates of mean ($\hat{m}_{fit}$) and the estimates of standard deviation ($\hat{s}_{fit}$) from indirect fit with $\hat{m}_{data}$ and $\hat{s}_{data}$ (see Eq. 8.5).
The indirect fit gave good estimates of mean error for both Case 1 and Case 2.

Cases	Case 1	Case 2
$\hat{m}_{data}$	0.00658	0.00505
$\hat{m}_{fit}$ from indirect fit (discrepancy w.r.t $\hat{m}_{data}$)	0.00676 (2.7%)	0.00515 (2.0%)
$\hat{s}_{data}$	0.00752	0.0110
$\hat{s}_{fit}$ from indirect fit (discrepancy w.r.t $\hat{s}_{data}$)	0.00798 (6.1%)	0.0111 (0.9 %)

Table 8.6: Results of outlier repair for the parameterized five dimensional Rosenbrock function.

	B	Number of outliers *a*/*b*/*c*[*]	Mean of repair on outliers[†]	Mean of repair on inliers[‡]	Ratio of mean repair on OL to IL	RMSE (% to the mean f_o)	mean f_o	R^2
Before repair	NA	NA	NA	NA	NA	0.00748 (54.3%)	0.0138	0.6800
IRLS repair	1.0	9/7/20	0.0124	0.0065	1.91	0.00439 (45.5%)	0.0096	0.8342
NIRLS repair	1.0	8/8/20	0.0213	0.0030	7.02	0.00222 (29.7%)	0.0075	0.8658
Full repair[§]	NA	NA	NA	NA	NA	0.00023 (4.3%)	0.0053	0.9970

[*]: *a* ~ Number of detected outliers
b ~ Number of big outliers detected (estimated error is greater than 10%)
c ~ Total number of big outliers out of the 27 data points (estimated error is greater than 10%)
[†]: (Sum of f_o repair on outliers)/*a*
[‡]: (Sum of f_o repair on data points other than outliers)/(Total number of points - *a*)
[§]: All 27 points repaired

Table 8.7: Results of optimization of $f_o(b_1, b_2, b_3)$ from the parameterized Rosenbrock function using RS approximations before and after outlier repair.

	Without repair (Optimum *O*)	IRLS repair (Optimum *I*)	NIRLS repair (Optimum *N*)	Full repair (Optimum *F*)	Exact
b_1^*	0.9583	0.9922	1.0014	1.0057	1.0
b_2^*	1.1000	1.0591	0.9877	1.0072	1.0
b_3^*	0.9000	0.9965	1.0378	1.0060	1.0
$f_o(b_1^*, b_2^*, b_3^*)$ predicted by RS	0.00066	-0.00175	-0.00018	-0.00007	-
$f_o(b_1^*, b_2^*, b_3^*)$ True	0.00303	0.00082	0.00028	0.00005	0.0

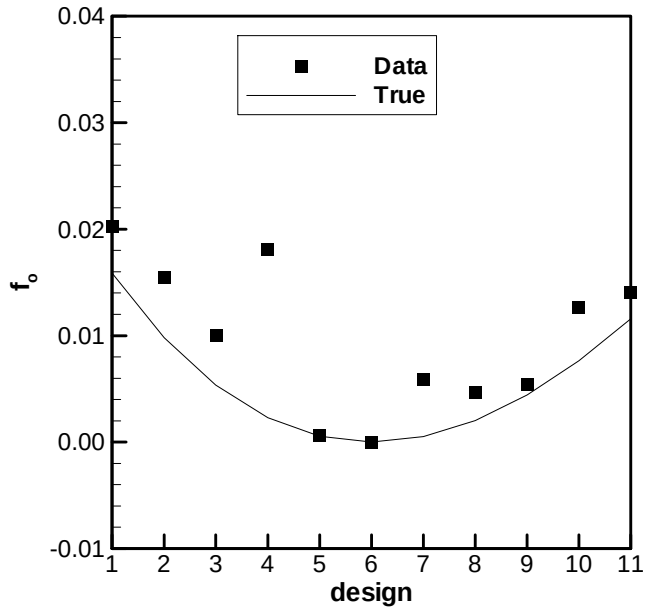

Figure 8.1: Design line plot of the optimal values (f_o) for the parameterized Rosenbrock function. Design 1 corresponds to b_k's at their lower limits and design 11 corresponds to b_k's at their upper limits. Noisy data are the results of PORT with a programming error, and the solid line is the true optima.

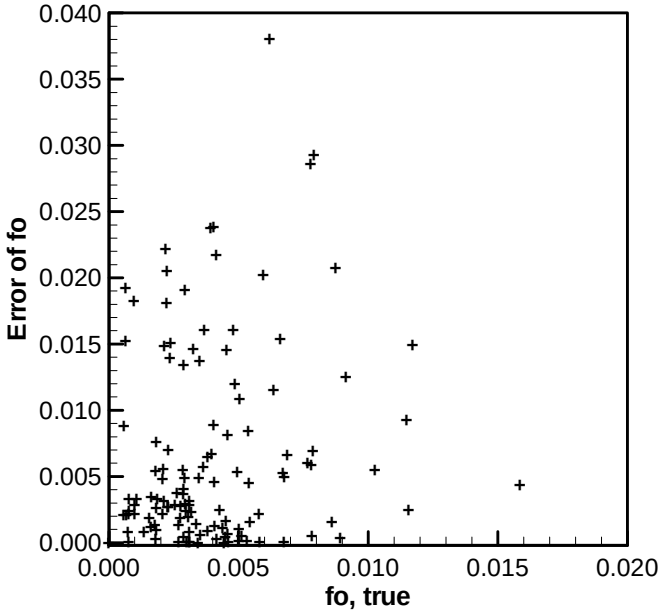

(a) Case 1 (correlation = 0.1635)

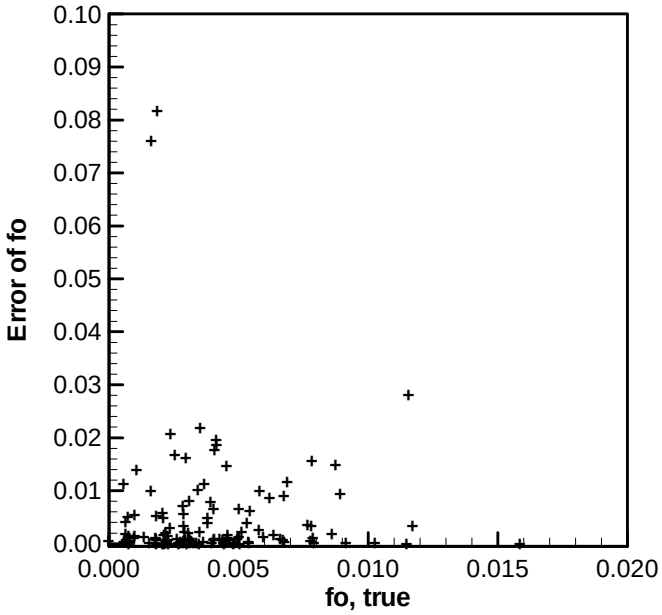

(b) Case 2 (correlation = -0.0264)

Figure 8.2: Plots of optimization error versus estimated true f_o.

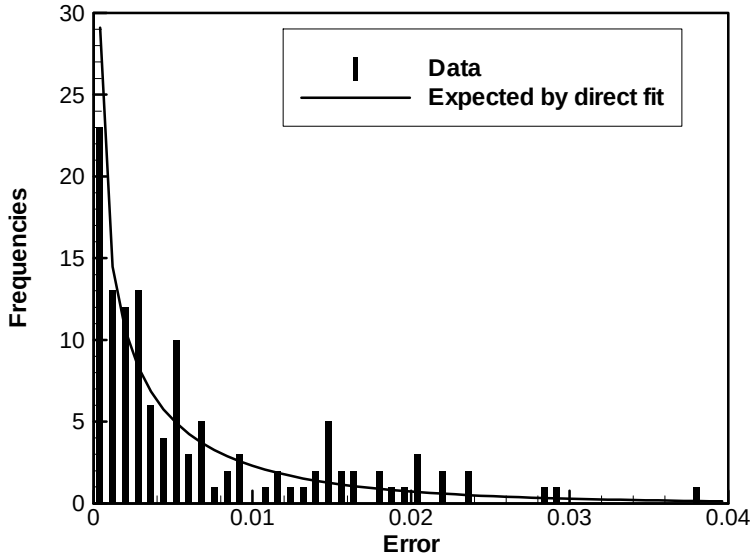

(a) Case 1.

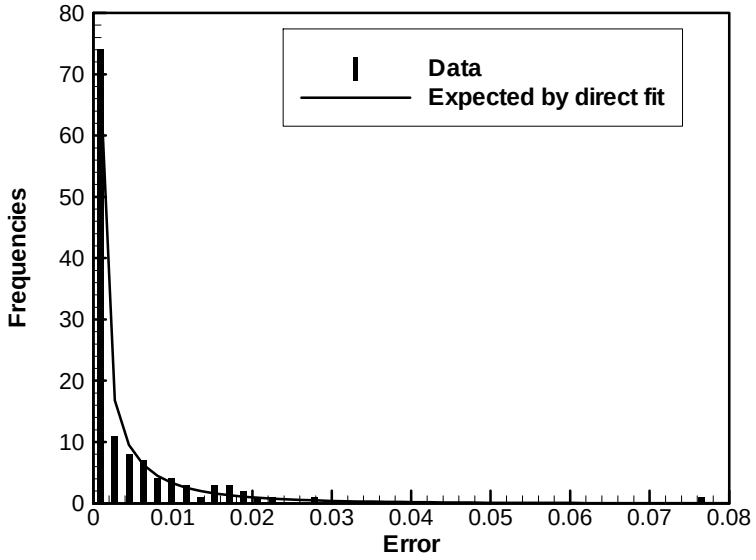

(b) Case 2.

Figure 8.3: Comparison of histograms between data and direct fits of Weibull model.

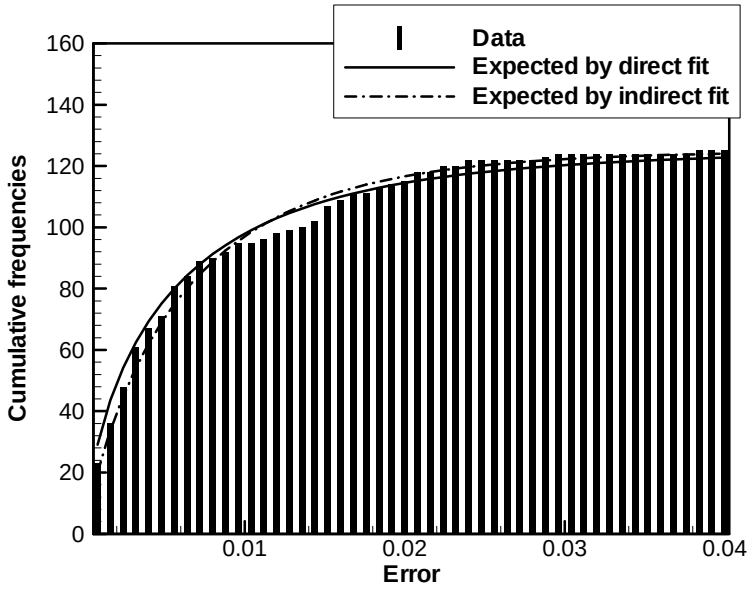

(a) Case 1.

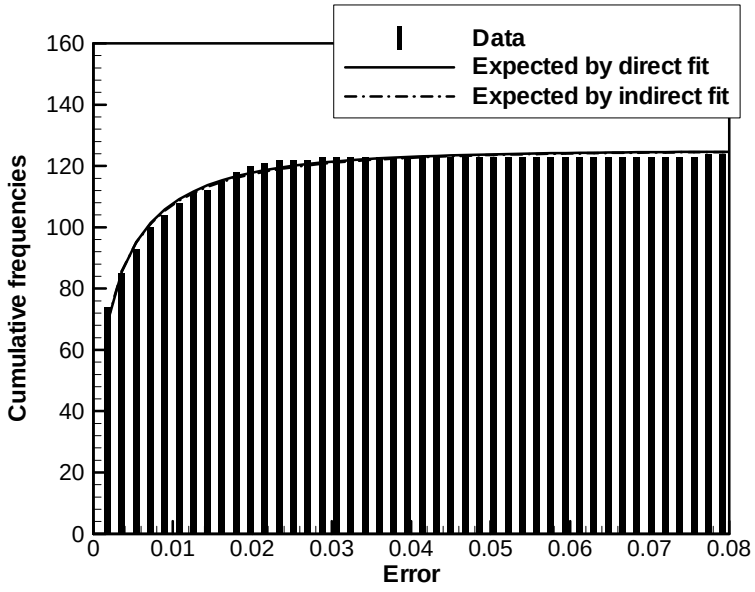

(b) Case 2.

Figure 8.4: Comparison of cumulative frequencies between direct fit and indirect (difference) fit of Weibull model.

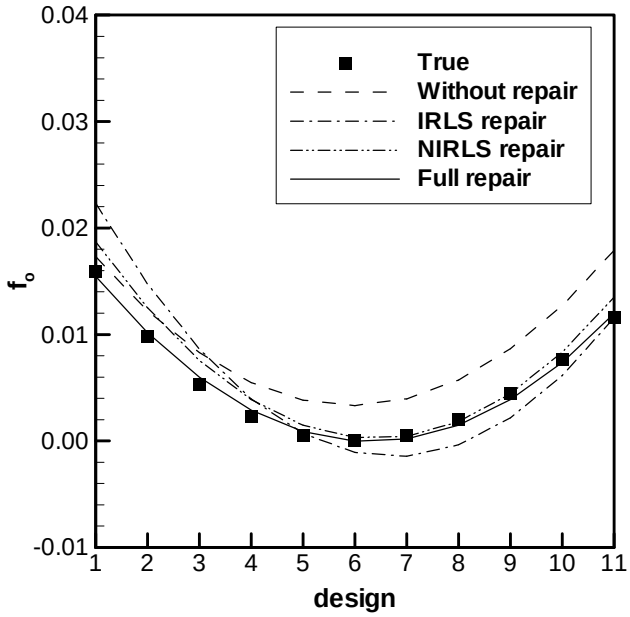

Figure 8.5: Design line plot of optimal values (f_o) for the parameterized Rosenbrock function predicted by quadratic RS approximations before and after outlier repair.
(The true minimum of f_o is located at design 6.)

Chapter 9 Estimation of Error from Structural Optimization

The error from structural optimization of the HSCT resulted in unreliable estimates of the wing structural weight. The source of the error was investigated by using various convergence parameters. Convergence difficulties in optimization procedures would produce one-sided noise error. A probabilistic approach is used to model the noise error from structural optimization. The Weibull model successfully used for the Rosenbrock test problem will be applied.

9.1 Effects of Convergence Control Parameters on the Optimization Error

We found that the error of structural optimization depends on the convergence criteria, which are called control parameters in GENESIS. The noise in the optimum structural wing weight (W_s) of an HSCT was greatly reduced by adjusting the GENESIS settings. Control parameters in GENESIS can be categorized into move limit parameters, convergence criteria, and inner optimization control parameters. Since we are dealing with a convergence problem of optimization, it will be helpful to understand the program structure of GENESIS. There are two loops in GENESIS (Figure 9.1). In the outer loop, an approximation for the optimization problem is generated and this approximate problem is passed to the inner loop of a gradient based optimization. We used the modified method of feasible direction (MMFD) for the inner loop optimization. After convergence of the approximate problem, a new approximation is constructed at the optimum of the approximate problem. The approximation and optimization is continued until no further change of design variables, called soft convergence, or no further change of the objective function, called hard convergence, occurs. The optimization parameters affect the performance of optimization, error in the optimization results, and the computational cost.

To study the error in the optimal structural weight calculation of the HSCT, we used a mixed experimental design [45] designed to permit fitting quadratic or cubic polynomial models using the five HSCT configuration design variables. The experimental design has 126 points that consist of a face centered central composite design (FCCC) at levels of ±1 (43 points), another FCCC at levels of ±0.75 (42 points), a *D*-optimal design from a 6 level design (27 points), and an orthogonal array design [91] (14 points).

GENESIS structural optimizations using six different sets of parameters were performed on each of the 126 points. Table 9.1 lists the description of the parameters and the actual values used in this study. Case A2 employs the default parameters provided by GENESIS. Case A3 and Case A5 are the same as Case A2 except that the parameter ITRMOP was increased to 3 and 5, respectively. ITRMOP controls the convergence of the inner optimization. For the approximate optimization to converge, the inner loop convergence criterion for change in the objective function must be satisfied ITRMOP consecutive times. The default value of ITRMOP is 2, and by increasing it, the inner iteration is forced to iterate further. In turn, this may force the outer loop to continue, because the so called soft convergence criteria –the change of design variables– are not met, which may have been satisfied if ITRMOP had been 2. This may result in significant improvement in the final design.

After extensive experimentation with the optimization parameters and help from the developers of GENESIS, we found that ITRMOP was the most important for improving the accuracy of the optimization for our problem. Case B2 employs tighter move limits and convergence criteria than Case A2. It reflects our first attempt to improve the optimization results. Case B3 and Case B5 are the same as Case B2 except that ITRMOP is 3 and 5, respectively. The values of all the control parameters for the six cases are given in Table 9.1. The data of W_s of the six convergence settings on the 126 data points are listed in Appendix D.

In order to visualize the behavior of the errors, Figures 9.2(a) and (b) show the W_s response for 21 HSCT designs generated by linear interpolation between two extreme points in the five variable HSCT problem. It is the same design line used for Figure 3.4 and design 1 corresponds to (1, -1, 1, -1, 1) and design 21 corresponds to (-1, 1, -1, 1, -1) in a coded form of the HSCT configuration variables. It is clear from the figures that Case A2 and Case B2 produced many runs with large errors, which were mostly positive. GENESIS seeks optimal design within feasible region because we use MMFD algorithm. There was no run for which

GENESIS failed to find a feasible design, and all of the erroneous optima were feasible. Therefore, the one-sided error in W_s calculated from GENESIS is attributed to convergence problem. By increasing ITRMOP, the noise in W_s was substantially reduced and the gain with ITRMOP = 5 over ITRMOP = 3 was small. To calculate the error for each case, we need to know the true W_s, which, strictly speaking, cannot be known due to the iterative procedure inherent in the optimization. Here we estimate the true W_s by taking the best of the six GENESIS runs we already did using different parameters.

Table 9.2 shows the performance of each set of GENESIS parameters for all 126 design points. The optimization error was calculated by comparing W_s to the best of the six W_s's available. Table 9.2 shows how many times each case produced the lowest weight, the best among the six W_s's for 126 points. Case A2 and Case B2 never found the best results. With ITRMOP = 5, Case A5 and Case B5 achieved the best W_s 58 and 52 times respectively, almost half of the data each, and together nearly 90 % of the data. Sometimes Case A3 and Case B3 came up with the best results, for 12 and 4 times, respectively.

For the default GENESIS parameter (Case A2), the mean error was 4.86 %. It is seen that tightening the convergence criteria for ITRMOP = 2 (Case B2) actually had a detrimental effect since the mean error increased to 5.63 %. By using ITRMOP = 3 (Case A3 and Case B3), the mean errors were reduced to 0.546 % and 0.762 % respectively, about a tenth of the levels of the low-fidelity errors. With Case A5 and Case B5, the mean error was very small, less than 0.2%. In terms of computational cost, the high-fidelity optimization using ITRMOP = 5 required more than twice the CPU time of the low-fidelity optimization, ITRMOP = 2.

In fact, the estimate of the true optimum by taking the best of six runs turned out to be very accurate, mostly thanks to the high-fidelity of Case A5 and Case B5. This was tested by doing nine additional GENESIS runs on 30 randomly selected HSCT configurations using Case B5 from different initial design variables. For these 30 configurations an average of 0.011% improvement was obtained. Therefore, we will denote the best of six W_s's as 'the estimate of true W_s', and accordingly the error of W_s with respect to this value will be denoted as 'estimated error', e_t, of optimization. Our concern about uncertainly will be mainly for the low (ITRMOP = 2) and mid-fidelity (ITRMOP = 3) cases. For the high-fidelity cases (ITRMOP = 5), the error appears to be negligible.

9.2 Estimation of Statistical Distribution

9.2.1 Homogeneity of Error

Our approach is to fit a model function to optimization error of various optimization convergence setups. A basic assumption behind the MLE fit is that the data is independently and identically distributed. For the optimization data at hand, there should be no problem concerning the independence of data, because the sampling was done by an experimental design without replicates. To check whether the error distribution is identical at different points, the estimated errors, e_t, were plotted against the estimated true W_s in Figure 9.3 for the absolute error (*lb*.) and in Figure 9.4 for the relative error (%). For example, with the absolute error of Case A2 in Figure 9.3(a), the mean and variance of error appears to increase as W_s increases. A relatively high correlation coefficient of 0.5685 indicates the trend. Scaling the error by W_s may help to stabilize the increasing mean and variance along W_s. For the relative error of Case A2 in Figure 9.4(a), the distribution became more even, and the correlation coefficient was reduced to 0.3210. One may observe similar effects of relative error over absolute error for other cases. The figures lead us to expect that if the structural optimization process ends with premature convergence, the absolute error would tend to be larger for heavy designs.

However, considering that highly influential points, such as the two outliers seen in Figure 9.3(b), tend to exaggerate the correlation coefficients, the assumption of homogeneous distribution may not be a bad assumption even for the absolute error. If the variation of distribution is important, the change of distribution may be modeled by the generalized linear model (GLM) [92]. In GLM the mean of the distribution is related to the regressor variables via a linear model, while the fit in our approach assumes the mean of the distribution is the same for different data points, which is a special case of GLM. Nonetheless, with the four distributions in Figure 9.3, the fit of a distribution should provide useful information about the overall behavior of the error. So we fitted model distributions to both absolute and relative errors.

9.2.2 Direct Fit of Estimated Error

In Chapter 8 the Weibull model was successfully fit to the optimization error of the Rosenbrock function. Again, the Weibull model is selected to fit the estimated error e_t, from the structural optimization of the HSCT. The results of the direct fit are summarized in Table 9.3 for the absolute error, and in Table 9.4 for the relative error. A Weibull model fit routine, *weibfit*, from the statistical toolbox of MATLAB was used. See Appendix E for an example of the MATLAB code for the direct fit. For the absolute error, the *p*-values of the c^2 test indicate that the fits are reasonable for Cases A2, B2, and B3 with 5% significance level. For Case A3, the fit was marginally rejected. For Case A5 and Case B5, the high-fidelity cases with ITRMOP = 5, the fits were not satisfactory at all. In fact, for those high-fidelity errors, almost half of the e_t's were zero, and the errors may be negligible. The Weibull fit of the relative error was not as good as the fit for the absolute error. For instance, the *p*-value of the fit to the relative error of Case B2 was only 0.0327 compared to 0.8327 for the fit to the absolute error. This is unexpected since we observed that the distribution appears to be more homogeneous with relative error than with absolute error.

Recalling that the standard deviation is the same as the mean for the exponential distribution (when a = 1 in Weibull), $\hat{s}_{fit}$ greater than $\hat{m}_{fit}$ in Table 9.3 indicates that the errors from the structural optimization have greater scatter than the exponential model. From the fits, overall characteristics of the error can be estimated in terms of the mean ($\hat{m}_{fit}$), and standard deviation ($\hat{s}_{fit}$) of the distribution. On the other hand, the mean and standard deviation can be estimated from e_t without fit by

$$\hat{m}_{data} = \bar{e}_t, \quad \hat{s}_{data} = \sqrt{\frac{\sum_{i=1}^{n}((e_t)_i - \bar{e}_t)^2}{n-1}}. \tag{9.1}$$

In Table 9.3, $\hat{m}_{fit}$ and $\hat{s}_{fit}$ were compared with $\hat{m}_{data}$ and $\hat{s}_{data}$, and the agreement is good for low-fidelity errors and is reasonable for the mid-fidelity errors except for $\hat{s}_{fit}$ of Case B3.

Table 9.3 and Table 9.4 are obtained from 126 data points. We expect that fewer points are required for a reasonable fit to estimate the mean and standard deviation of the error distribution. For a given sample size ranging from 10 to 150, we calculated $\hat{m}_{fit}$ and $\hat{s}_{fit}$ for 50 sets of random numbers generated from a Weibull distribution with a = 0.7682 and b = 3915, which is the fitted value for e_t of Case B2. The mean (m) and standard deviation (s) of the distribution are 4572 *lb*. and 6023 *lb*., respectively. The mean and standard deviation of $\hat{m}_{fit}$ are drawn in Figure 9.5(a) as dash-dot lines. Similarly the mean and standard deviation of $\hat{s}_{fit}$ are shown in Figure 9.5(b). It appears that we need at least 50 points to get a good fit with reasonable accuracy. Also, Figure 9.5(a) shows that the mean and scatter of $\hat{m}_{data}$ are very close to those of $\hat{m}_{fit}$, but Figure 9.5(b) shows that $\hat{s}_{fit}$ has a smaller scatter than $\hat{s}_{data}$ in terms of the standard deviation.

The probability plot is a graphical tool to show the goodness of fit of distribution. We used the quantile-quantile plots, or so-called Q-Q plot (see Section 5.5). In the Q-Q plot, the percentiles of the data are plotted against the expected percentiles from the fit. If the fit is good, the scatter plot should appear as a straight line passing the origin with unit slope. Figure 9.6 shows the Q-Q plots for the Weibull fit for e_t of the low and mid-fidelity optimizations. They show that the MLE resulted in a good fit for the majority of the data, while more or less ignoring the large error data. Figure 9.6(c) indicates a particularly good fit, which is in agreement with the results of the c^2 test. The histograms in Figure 9.7 compare the shape of the error distribution to the Weibull fit. The optimization error here is by definition nonnegative and the probability for large error decreases rapidly to zero. One can see that the fits match well with the data for the low-fidelity errors, Case A2 and Case B2, and the fits are reasonable for the mid-fidelity error cases, even for Case A3, although the fit was rejected by the c^2 test. This fact implies that the Weibull fit may be useful for Case A3 as well if we are mainly interested in the behavior of large error.

Again, it should be noted that the above discussions about the results of c^2 tests and the corresponding *p*-values are not rigorous probability statements, since the sample size n may not be large enough for the asymptotic c^2 approximation to be accurate. However, the Weibull distribution was able to model the errors of two different optimization problems, the Rosenbrock

function and the structural optimization of an HSCT. That may be an indication that there are some common error processes in the optimization errors.

9.2.3 Results of Indirect Fit of the Optimization Error

In our data, Case A3 and Case B2 represent our efforts to reduce the error in Case A2 by tightening the inner loop convergence criterion or outer loop criteria. If either optimization results by Case A3 or Case B2 are available along with Case A2, we can estimate the error distributions from the differences. Note that we use two sets of different convergence criteria, while we used two cases of different initial designs for the Rosenbrock example. Similarly to what was done for the Rosenbrock problem, the probability density of the difference, $f(x)$ in Eq. 5.12, was numerically integrated using the Gaussian quadrature (see Appendix C for the details of the integration). Table 9.5 contains the correlation of e_t between the low and mid-fidelity optimizations, Cases A2, A3, B2, and B3. The correlation coefficient between Cases A2 and A3 (0.2004), and Cases A2 and B2 (0.1983), indicate that it may be reasonable to treat them as independent.

The difference fit was performed on the pair of (A2, A3), and then on the pair of (A2, B2). See Appendix F for an example of MATLAB code for indirect fit. In the previous section, the direct fit of the Weibull model showed better fits for the absolute error (W_s error in *lb*.) than for the relative error (W_s error in percentage). Therefore, W_s data in *lb*. was used for indirect fit and the results were compared to the direct fit to the absolute error. The first pair consists of a low-fidelity and a mid-fidelity optimization while the second one engages two low-fidelity results. The results of the difference fit using the Weibull model are summarized in Table 9.6. According to the c^2 test, the fit was rejected for the pair of (A2, B3), but was reasonable for the pair of (A2, B2). From the difference fit using the Weibull model, we found the distribution parameters, a and b, for both cases in a pair simultaneously.

As results of the indirect fit, we can estimate the mean and standard deviation of the optimization error of each of the two cases involved, and one can compare them with the e_t data. In Table 9.7, the results from the difference fit were compared to e_t data. The estimates by the indirect fit for Case A2 were in a reasonable range, -9.7% and -2.1% of discrepancies for $\hat{m}_{fit}$ and

$\hat{s}_{fit}$ with respect to the $\hat{m}_{data}$ and $\hat{s}_{data}$ based on e_t. However, the estimates for Case A3 were in disagreement with the e_t data, -72.1% discrepancy for $\hat{m}_{fit}$ and –71.1% discrepancy for $\hat{s}_{fit}$. For the first pair, the inaccurate estimates for Case A3 may have been expected because the fit on the difference itself was poor. Figure 9.8 compares the direct and difference fits for the first pair in terms of cumulative frequencies. The difference fit for Case A2 is close to that of the direct fit as seen in Figure 9.8(a), although for Case A3 the difference fit does not match the direct fit well. Also, it would be meaningful to compare $\hat{m}_{fit}$ and $\hat{s}_{fit}$ from the difference fit with the estimates using the data used in the fit. For example, for the pair of Cases A2 and A3, we can calculate an 'approximate true W_s' as the best of W_s(A2) and W_s(A3). Accordingly the 'approximate error (e_a)' can be calculated with respect to the approximate true W_s, and then $\hat{m}_{data}$ and $\hat{s}_{data}$ are calculated by applying Eq. 9.1 to e_a. It turned out, as noted from Table 9.7, that $\hat{m}_{fit}$ and $\hat{s}_{fit}$ are better than $\hat{m}_{data}$ and $\hat{s}_{data}$ based on e_a for both Case A2 and Case A3. However, the estimates for Case A3 have big discrepancies with respect to $\hat{m}_{data}$ and $\hat{s}_{data}$ based on e_t. The results for the pair (A2, A3) indicate that when more accurate optimization results are available, the utility of the statistical model may be limited.

For the second pair, Cases A2 and B2, the indirect fit gives much better estimates of mean and standard deviation than $\hat{m}_{data}$ and $\hat{s}_{data}$ based on e_a, because e_a is far from the true error because it is based entirely on the low-fidelity data of Cases A2 and B2. For example, the $\hat{m}_{data}$ based on e_a has a –44.1% discrepancy compared to –13.7 % of $\hat{m}_{fit}$ for Case A2. Figure 9.9 shows the prediction by indirect fit is in a reasonable match with the direct fits for the second pair. If we compare the indirect fit for Case A2 between the first and the second pair, the first pair gives a little bit better fit than the second pair as seen in Figure 9.8(a) and Figure 9.9(a). However, it should be pointed out that the pair of (A2, B2) is computationally cheaper than the pair of (A2, A3), because it involves another low-fidelity optimization, Case B2, instead of the mid-fidelity optimization of Case A3. Overall we find that the Weibull model allows us to estimate well the mean and standard deviation of the error from two sets of low-fidelity optimizations.

To find how many points are required for the difference fit, we performed difference fits for the pair of (A2, B2) for various sample sizes. Samples were randomly generated from the 126 points with replacement, and the process was repeated 50 times for each sample size ranging

from 30 to 130. Figure 9.10(a) shows the mean and standard deviation of $\hat{m}_{fit}$ for Cases A2 and B2, and Figure 9.10(b) is the mean and standard deviation of $\hat{s}_{fit}$ for various sample sizes. Figure 9.10 implies that at least 70 points are required for reliable fits. The required sample size is a bit larger than the direct fit presented in Figure 9.5, where samples were generated from a known Weibull distribution. That may be attributed to that the number of distribution parameters estimated is doubled in the difference fit since we are fitting two low-fidelity errors simultaneously.

Table 9.1: Sets of optimization control parameters in GENESIS.

Category	Name of Parameter	Description	**Case A2**	**Case A3**	**Case A5**	**Case B2**	**Case B3**	**Case B5**
Move Limits	DELP	Fractional change allowed for properties	0.5			0.5		
	DPMIN	Minimum move limit for properties	0.1			0.00001		
	DELX	Fractional change allowed for design variables	0.5			0.5		
	DXMIN	Minimum move limit for design variables	0.1			0.00001		
	REDUC1	To multiply all the move limits by this number if internal approximate problem is NOT doing well	0.5			0.5		
	REDUC2	To divide all the move limits by this number if internal approximate problem is doing well	0.75			0.75		
Outer loop convergence on objective function (Hard convergence)	CONV1	Relative convergence criteria on objective function	0.001			0.0001		
	CONV2	Absolute convergence criteria on objective function	0.001			0.0001		
	GMAX	Maximum constraint violation allowed at optimum	0.0001			0.0001		
Outer loop convergence on design variables (Soft convergence)	CONVCN	Relative criteria for change in design variables	0.001			0.00001		
	CONVDV	Relative criteria for change in properties	0.001			0.00001		
	CONVPR	Allowable change in the maximum constraint	0.001			0.00001		
Inner loop convergence	ITRMOP	Number of consecutive iterations that must satisfy the relative or absolute convergence criteria before optimization is terminated in the approximate optimization problem	2	3	5	2	3	5

Table 9.2: Performance of structural optimization for various GENESIS parameter settings. Structural optimizations were performed for each of the 126 HSCT configurations using six different convergence settings. For each HSCT configuration, the best optimal structural weight, W_s, out of the six GENESIS runs was taken as the true optimum, and the optimization error was calculated with respect to the true optima.

	Case A2	**Case A3**	**Case A5**	**Case B2**	**Case B3**	**Case B5**
Number of points for which the best W_s was achieved	0	12	58	0	4	52
Mean of the estimated error, e_t (Percentage to the mean W_s)	3931.0 *lb*. (4.860%)	441.4 *lb*. (0.546%)	161.8 *lb*. (0.200%)	4552.8 *lb*. (5.629%)	616.2 *lb*. (0.762%)	32.7 *lb*. (0.040%)
CPU time per GENESIS run on a SGI Origin workstation (seconds)	78.1	117.6	156.7	61.4	109.0	143.3

Table 9.3: Quality of the fit of the Weibull model to the optimization error, e_t, for various convergence settings defined in Table 9.1.

The comparisons of the mean, m, of the fit and data indicate good agreement except for the most stringent convergence criteria, B5. The agreement is also good for the standard deviation, s, for the less stringent convergence cases, A2, A3, and B2. The p-value based on the c^2 test implies good fit when it is close to one, and cases A3, A5, and B5 clearly fit poorly.

	Error A2	Error A3	Error A5	Error B2	Error B3	Error B5
$\hat{m}_{data}$ for e_t, *lb*.	3931	441.4	161.8	4553	616.2	32.7
$\hat{m}_{fit}$, *lb*. (discrepancy w.r.t $\hat{m}_{data}$ for e_t)	3850 (-2.1 %)	462.3 (4.7 %)	147.2 (-9.0 %)	4572 (0.4 %)	689.2 (11.8 %)	146.3 (347.4 %)
$\hat{s}_{data}$ for e_t, *lb*.	7071	1408	966.6	5991	1086	73.8
$\hat{s}_{fit}$, *lb*. (discrepancy w.r.t $\hat{s}_{data}$ for e_t)	6894 (-2.5%)	1270 (-9.8 %)	1674 (73.2 %)	6023 (0.5 %)	1682 (54.9 %)	1695 (2197 %)
a (shape parameter)	0.5912	0.4348	0.2228	0.7682	0.4703	0.2214
b (scale parameter)	2510	172.2	2.870	3915	305.8	2.724
c^2 statistic	12.25	14.79	224.3	3.524	9.397	190.0
p-value	0.0925	0.0387	0.0000	0.8327	0.2254	0.0000

Table 9.4: Quality of fit of the Weibull model to the relative optimization error scaled with respect to W_s.

The estimates of the mean and standard deviation are good for less stringent cases A2, B2, and B3. The fits are not as good as the absolute error results in Table 9.3 particularly for Case B2, which was rejected by the c^2 test.

	Error A2	Error A3	Error A5	Error B2	Error B3	Error B5
$\hat{m}_{data}$ for e_t, %	3.99	0.394	0.098	6.08	0.733	0.046
$\hat{m}_{fit}$, % (discrepancy w.r.t $\hat{m}_{data}$ for e_t)	3.96 (-0.8 %)	0.468 (18.8 %)	0.173 (76.5 %)	6.10 (0.3 %)	0.768 (4.8%)	0.222 (382.6 %)
$\hat{s}_{data}$ for e_t, %	6.21	0.805	0.505	7.84	1.61	0.092
$\hat{s}_{fit}$, % (discrepancy w.r.t $\hat{s}_{data}$ for e_t)	6.07 (-2.3 %)	1.13 (40.4%)	2.11 (317.8 %)	8.09 (3.2 %)	1.74 (8.1 %)	2.60 (2726 %)
a (shape parameter)	0.6726	0.4730	0.2175	0.7636	0.4949	0.2209
b (scale parameter)	3.007	0.2102	0.0028	5.1977	0.3767	0.0041
c^2 statistic	16.06	24.63	228.6	15.27	9.2381	200.5
p-value	0.0245	0.0009	0.0000	0.0327	0.2360	0.0000

Table 9.5: Correlation coefficients of the estimated errors (e_t, *lb*.) between different GENESIS parameter settings.

	Case A2	Case A3	Case B2	Case B3
Case A2	1	0.2004	0.1983	0.1559
Case A3		1	0.0361	0.3967
Case B2			1	0.1811
Case B3				1

Table 9.6: Results of the difference fits for the pair of (A2, A3) and the pair of (A2, B2). The (A2, A3) pair consists of a low-fidelity convergence setting (A2) and a mid-fidelity setting (A3), while the pair (A2, B2) consists of two low-fidelity settings. The *p*-value of the c^2 test indicates that the fit to the optimization difference was not good for the pair of (A2, A3), while the fit was acceptable for the pair of (A2, B2).

		Tightening inner loop convergence criterion	Tightening outer loop convergence criteria
Difference of W_s in the pair		$W_s(A2)$-$W_s(A3)$	$W_s(A2)$-$W_s(B2)$
Parameters of distribution of optimization error for default convergence criteria	*a*	0.553	0.509
	b	2105	1756
Parameters of distribution of optimization error for tightened convergence criteria	*a*	0.389	0.710
	b	34.3	3187
c^2 statistic		25.1	7.33
p-value		0.0001	0.1970

Table 9.7: Comparison of the estimates of mean ($\hat{m}_{fit}$) and the estimates of standard deviation ($\hat{s}_{fit}$) from indirect fit with the estimates from data ($\hat{m}_{data}$ and $\hat{s}_{data}$, see Eq. 9.1).

$\hat{m}_{fit}$ and $\hat{s}_{fit}$ are compared with $\hat{m}_{data}$ and $\hat{s}_{data}$ from estimated error (e_t) based on the six optimization runs using various convergence settings. For the pair of (A2, A3), the difference fit gave good estimates of mean and standard deviation of the low-fidelity error (A2), but the estimates were not accurate for the mid-fidelity error (A3). For the pair of two low-fidelity optimizations, (A2, B2), the difference fit gave reasonable estimates of error for both A2 and B2. The estimates from approximate error (e_a) based on the two optimization runs involved in the difference fit gave poor estimates of error compared to the difference fit because e_a is not accurate with only two low-fidelity optimization results.

	Tightening inner loop convergence criterion		Tightening outer loop convergence criteria	
Cases	Error A2	Error A3	Error A2	Error B2
$\hat{m}_{data}$ for e_t, *lb*.	3931	441.4	3931	4553
$\hat{m}_{fit}$ from difference fit, *lb*. (discrepancy w.r.t $\hat{m}_{data}$ for e_t)	3550 (-9.7%)	123.3 (-72.1%)	3394 (-13.7%)	3981 (-12.6%)
$\hat{m}_{data}$ for e_a, best of two, *lb*. (discrepancy w.r.t $\hat{m}_{data}$ for e_t)	3535 (-10.1%)	46.1 (-89.6%)	2199 (-44.1%)	2821 (-38.0%)
$\hat{s}_{data}$ for e_t, *lb*.	7071.3	1407.8	7071.3	5991.0
$\hat{s}_{fit}$ from difference fit, *lb*. (discrepancy w.r.t $\hat{s}_{data}$ for e_t)	6922 (-2.1%)	406.2 (-71.1 %)	7393 (4.5%)	5729 (-4.4%)
$\hat{s}_{data}$ for e_a, best of two, *lb*. (discrepancy w.r.t $\hat{s}_{data}$ for e_t)	6895 (-2.5%)	349.6 (-75.2%)	5545 (-21.6%)	5082.9 (-15.2%)

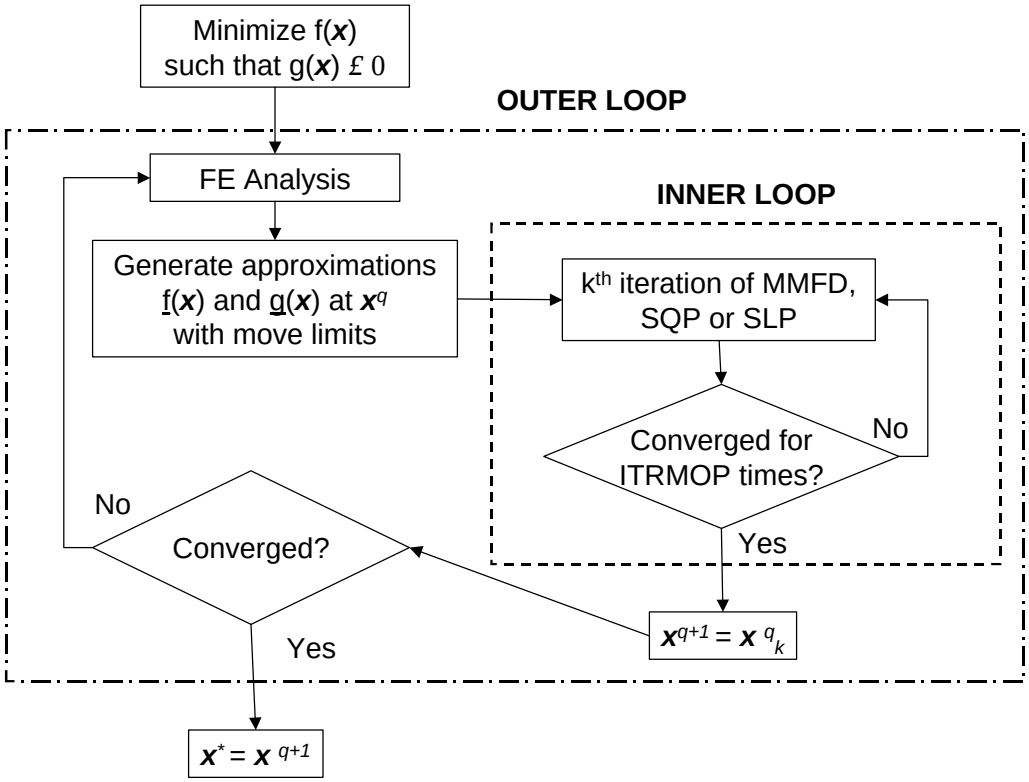

Figure 9.1: Flow chart of GENESIS structural optimization software.

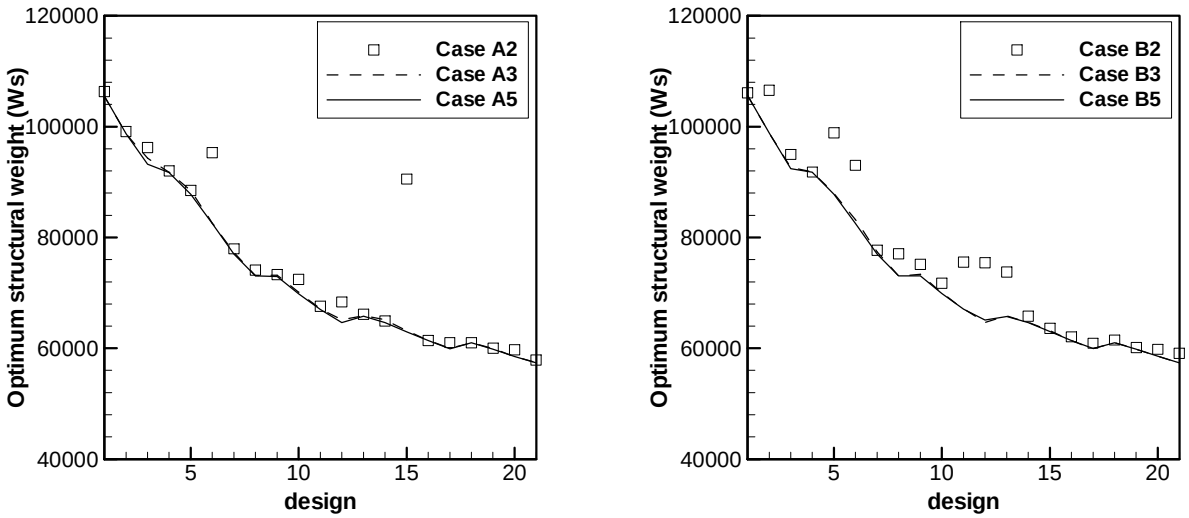

(a) (b)

Figure 9.2: Optimum structural weight response along a design line for different GENESIS parameters, (a) Case A2, A3, and A5, (b) Case B2, B3, and B5.

Structural optimizations are performed for 21 HSCT configurations generated by linear interpolation between two extreme points in the five variable HSCT problem. Design 1 corresponds to (1, -1, 1, -1, 1) and design 21 corresponds to (-1, 1, -1, 1, -1) in a coded form of the HSCT configuration variables. The structural optimization resulted in two runs of large error with the default convergence parameters (A2). Tightening the outer loop convergence criteria (B2) from the default did not improve the structural optimization and resulted in a very noisy response of the optimum wing structural weight. By tightening the inner loop convergence criterion (A3, A5, B3 or B5), the structural optimizations are much more consistent and much less noisy.

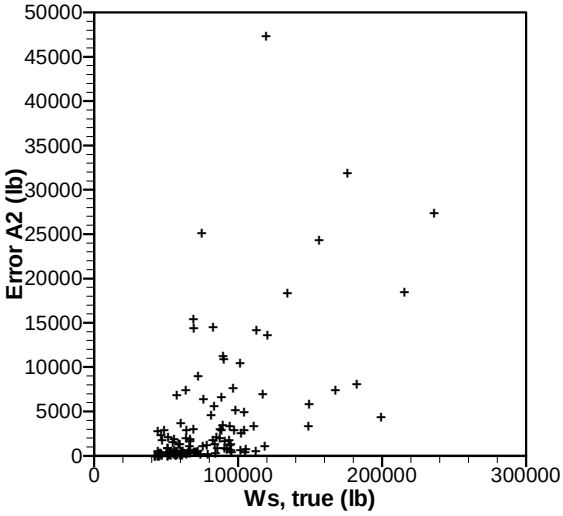

(a) Case A2 (correlation = 0.5685).

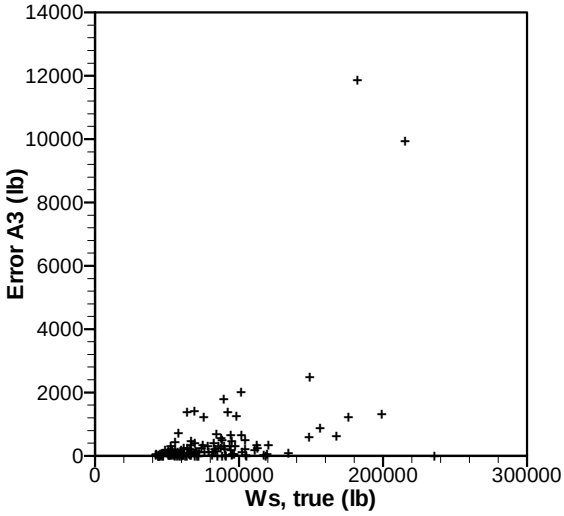

(b) Case A3 (correlation = 0.5089).

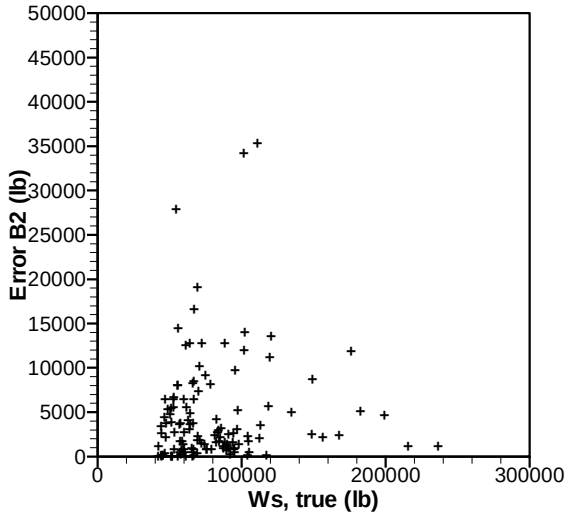

(c) Case B2 (correlation =0.0844).

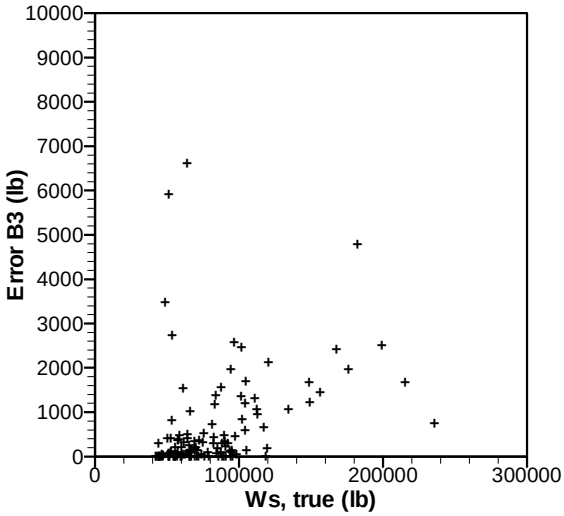

(d) Case B3 (correlation = 0.3588).

Figure 9.3: Plots of estimated error, e_t, versus estimated true W_s (absolute error).

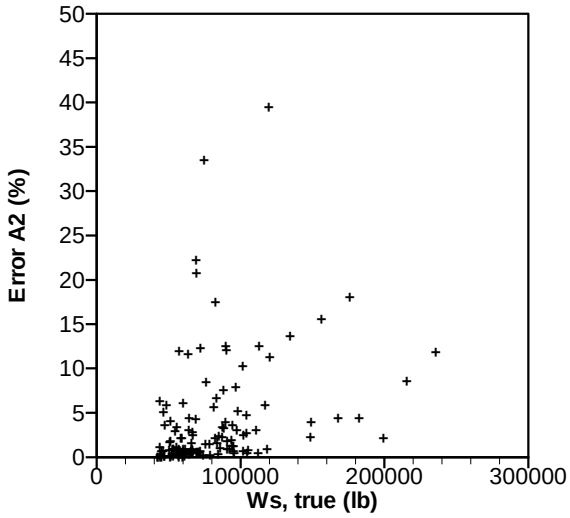

(a) Case A2 (correlation = 0.3210).

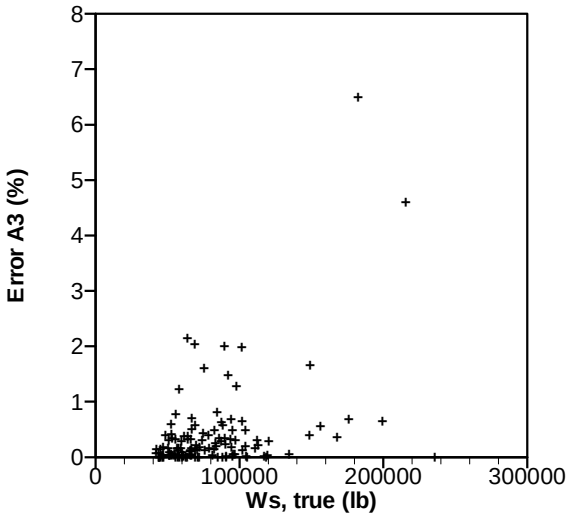

(b) Case A3 (correlation = 0.4326).

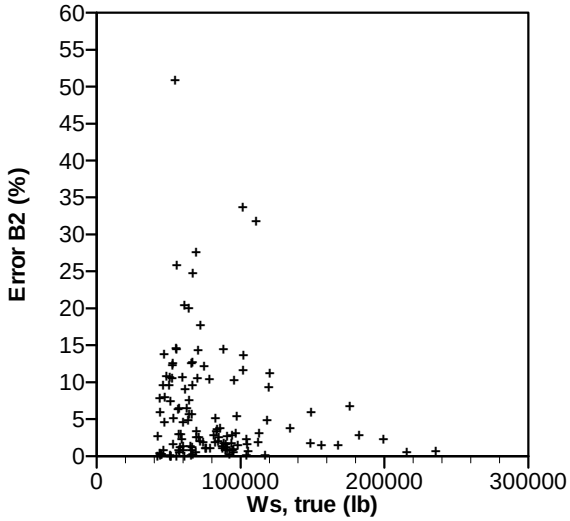

(c) Case B2 (correlation = -0.1321).

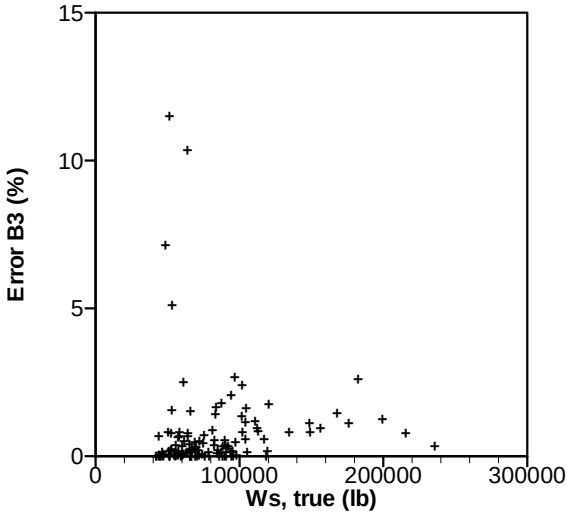

(d) Case B3 (correlation = 0.0412).

Figure 9.4: Plots of estimated error, e_t, versus estimated true W_s (relative error).

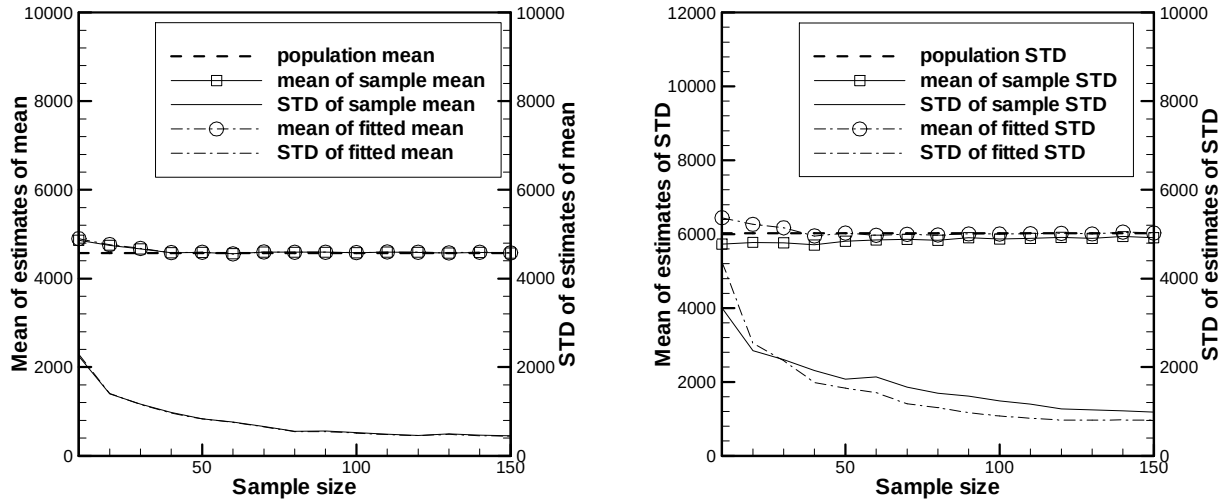

(a) $\hat{m}$. (b) $\hat{s}$.

Figure 9.5: Comparison of $\hat{m}$ and $\hat{s}$ between Weibull fits and estimates from data according to the sample size.

For a given sample size ranging from 10 to 150, 50 sets of pseudo random numbers were generated from a Weibull distribution (a = 0.7682, b = 3915). The Weibull distribution has a population mean m = 4572 *lb.* and standard deviation s = 6023 *lb.*, denoted as dashed lines. Then, m and s were estimated for each of the 50 sets by the two methods: estimates ($\hat{m}_{data}$ and $\hat{s}_{data}$) using Eq. 9.1 and fitting the Weibull model ($\hat{m}_{fit}$ and $\hat{s}_{fit}$). The two methods were compared (solid lines correspond to the estimates using Eq. 9.1 and dash-dot lines correspond to the Weibull fit method) in terms of the mean and scatter of the estimates.

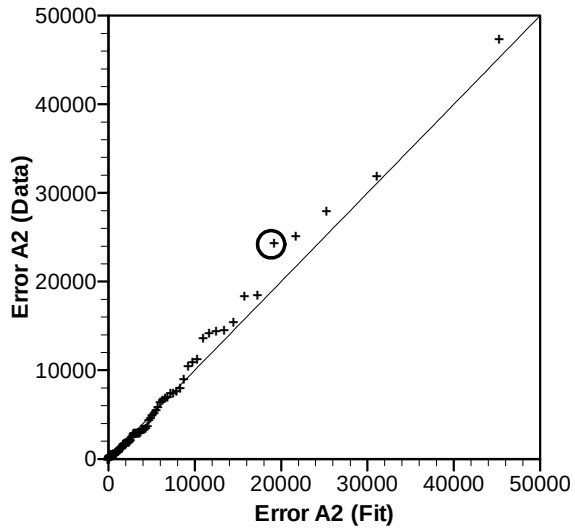

(a) Case A2.

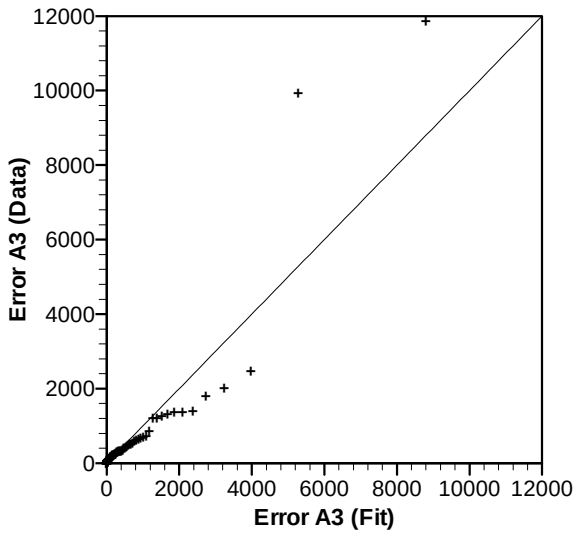

(b) Case A3.

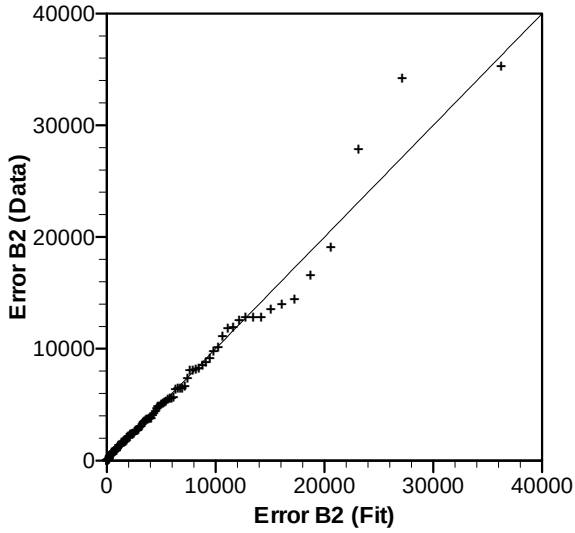

(c) Case B2.

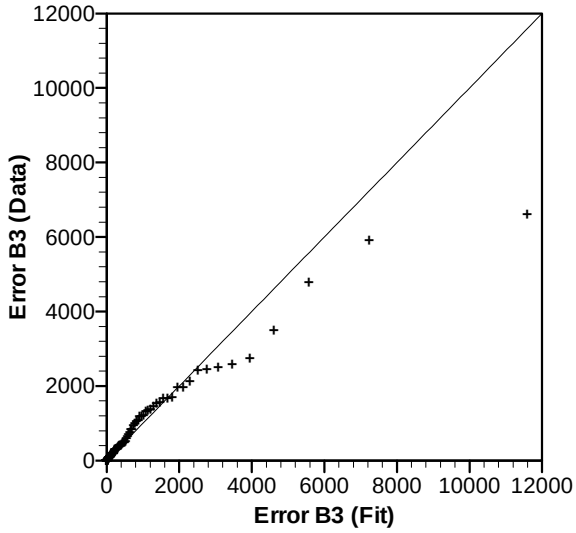

(d) Case B3.

Figure 9.6: Q-Q plots of Weibull fit for distribution of the estimated error.
Points above the line indicate that the data is from a distribution with a heavier tail than the fit. For example, the point circled in Case A2 indicates that the probability of having an error greater than 20000 *lb*. in the fitted distribution is equal to the probability of exceeding an error of 24000 *lb*. in the data.

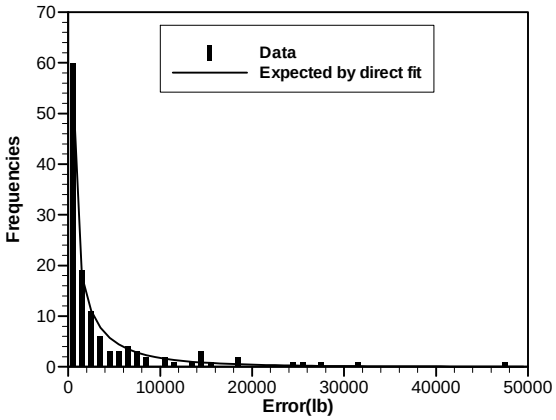

(a) Case A2.

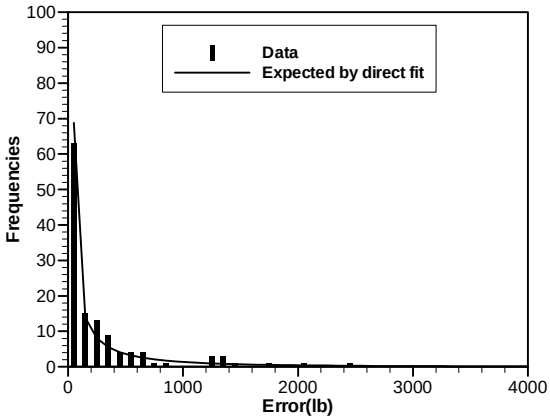

(b) Case A3.

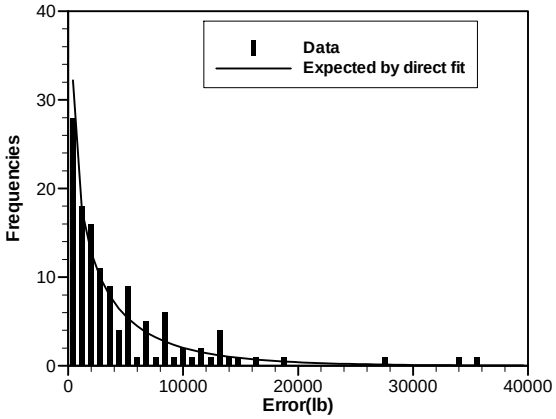

(c) Case B2.

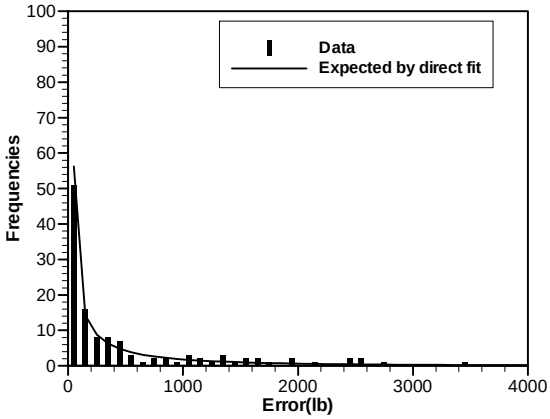

(d) Case B3.

Figure 9.7: Comparison of histograms of e_t and direct fits of Weibull model.

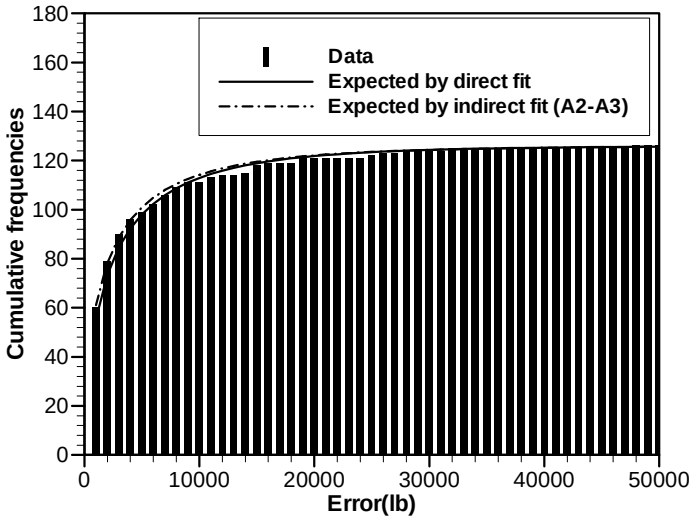

(a) Case A2.

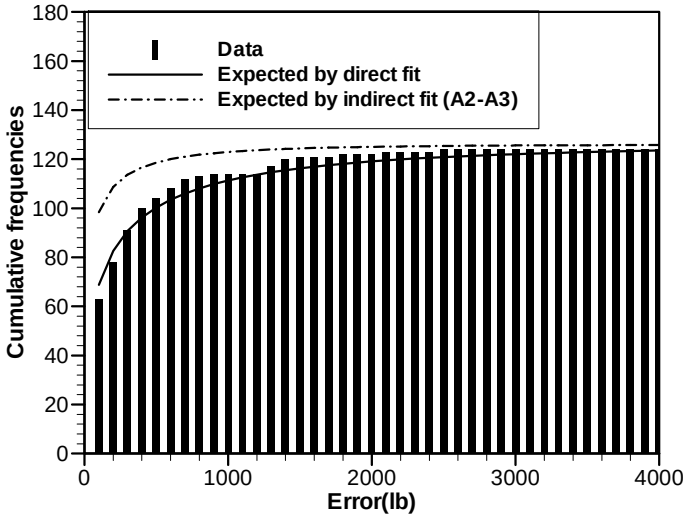

(b) Case A3.

Figure 9.8: Comparison of cumulative frequencies between direct fit and indirect (difference) fit of Weibull model (pair of Cases A2 and A3).

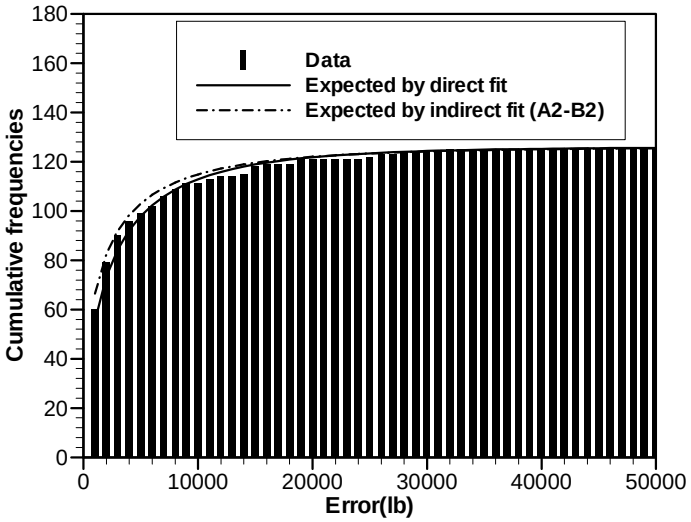

(a) Case A2.

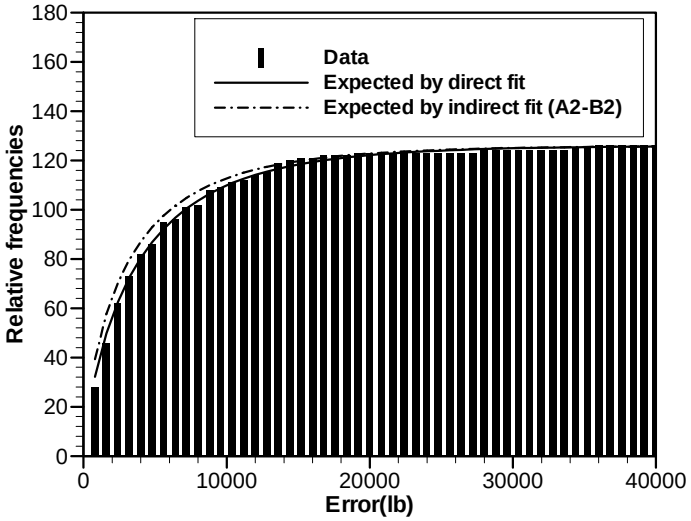

(b) Case B2.

Figure 9.9: Comparison of cumulative frequencies between direct fit and indirect (difference) fit of Weibull model (pair of Cases A2 and B2).

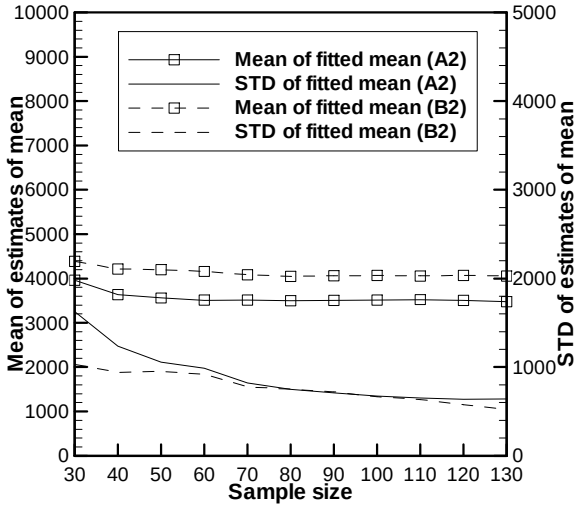

(a) $\hat{m}$.

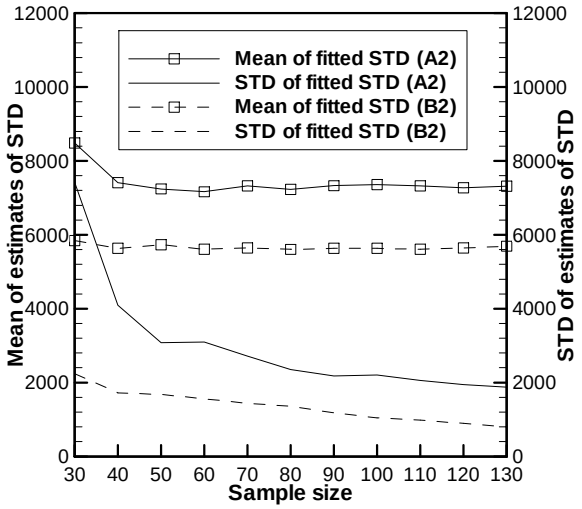

(b) $\hat{s}$.

Figure 9.10: $\hat{m}$ and $\hat{s}$ of the difference fit for the pair of (A2, B2) for various sample sizes. For each given sample size ranging from 30 to 130, 50 sets of data were generated from the 126 data with replacement. One can observe that $\hat{m}$ and $\hat{s}$ have large scatter at small sample sizes particularly for A2, and stabilize as the sample size increases.

Chapter 10 Detection and Repair of Poorly Converged Structural Optimization Runs

In the previous chapter we used probabilistic models to estimate the average error from structural optimization of the HSCT. In this chapter we will address the problem of structural optimizations with large error, *outliers*. In Chapter 8, robust regression techniques were used to identify outliers in optimization runs for the Rosenbrock test function, and we showed that outlier repair greatly improved the quality of the optimum of the response surface (RS) model based on the optimization data.

The structural optimization was performed to build a response surface approximation for the wing bending material weight of an HSCT. If we use low-fidelity data contaminated with outliers such as Case A2 of Section 9.1, the RS fit can be inaccurate because the least squares fit is not robust, and eventually it may increase uncertainty in the system level design of the HSCT. One obvious solution is to use high-fidelity data, such as Case A5 of Section 9.1, to get an accurate fit. However, high-fidelity optimizations may be much more expensive than low-fidelity cases. We noted that high-fidelity structural optimization requires more than twice the CPU time than low-fidelity cases. Moreover, it is possible that the high-fidelity simulation is not available because we do not know how to improve the low-fidelity simulation. Hence, it may be more efficient to repair only the identified outliers by high-fidelity simulations rather than doing high-fidelity simulations from the beginning, when high-fidelity runs are much more expensive than lower fidelity runs.

10.1 IRLS Procedures for the Optimization Error: Symmetric and Non-symmetric Weighting Functions

The IRLS procedure to identify poor optimizations was applied to the lower-fidelity HSCT structural optimization data, Case A2 and Case B2 (see Section 9.1). The SAS [90] statistical software was used to do the IRLS fit. See Appendix G for an example of the SAS input file for IRLS. A full quadratic polynomial model of a five dimensional design space was used for

the RS fit. The one-sidedness of the optimization error due to incomplete convergence led us to the nonsymmetric IRLS (NIRLS) using a nonsymmetic weighting function, which was compared to regular IRLS. The IRLS results depend on the shape of the weighting function. The tuning constant *B* acts like a threshold for outlier detection (see Table 6.1). A smaller *B* leads to a more aggressive outlier search; the allowable region around the RS for good points becomes narrower, and more points will be declared outliers. Two different values of the tuning constant *B* were tried. *B* = 1.0, the same value as for the Rosenbrock test function in Section 8.4, corresponds to an aggressive outlier search, while *B* = 1.9 corresponds to a moderate outlier search. For NIRLS, the tuning constant *H* controlling the weighting function for negative residuals was kept at 1.0, while *B* that controls the weighting function for the positive residuals was changed (see Table 6.1).

For the detected outlier points that have a weighting of less than 0.01, we corrected them by the estimated true W_s, which was calculated by taking the best of the two high-fidelity Cases (A5 and B5) and two low-fidelity cases (A2 and B2). The contribution from the mid-fidelity data (B3 and A3) to estimating true W_s would be small. The averages of the estimated errors are shown in Table 10.1, which shows almost the same magnitude compared to the results of Table 9.2 that utilized all of the six cases.

10.2 Results of Outlier Detection and Repair

Table 10.2 presents a summary of the outlier detection and correction results for Case A2 with IRLS and NIRLS. In the RS fit, we removed 11 points of extraordinarily heavy designs (W_s greater than 150000 *lb*., which is about triple the usual optimum designs) from 126 data points and used only 115 points, because we did not want to consider unreasonable designs. This approach of excluding design points with unreasonable results is known as the *reasonable design space approach* [8]. The identified outliers were repaired by the estimated true W_s. To assess the success in detection, all 115 points were also repaired, and the results are shown in the last row in Table 10.2.

With a tuning constant *B* = 1.9, IRLS and NIRLS identified two different sets of 21 data points as outliers. Twelve out of the 21 points were common. The error in the outliers is calculated by comparing W_s(A2) to the repaired value. For comparison, we also repaired points

not flagged as outliers. For IRLS, the average correction was 7391 *lb*. for outliers compared to 1516 *lb*. for inliers. NIRLS did a better job in finding outliers; the average correction was 8627 *lb*. for outliers and 1240 *lb*. for inliers. The ratio between the average corrections of W_s for outliers and inliers can be considered as a measure of the success of outlier detection. For NIRLS the ratio was 6.96 compared to 4.88 of IRLS.

Figure 10.1 shows the estimated error (*i.e.*, W_s repair) of both of the detected outliers and inliers versus *w*, the weighting in IRLS. Big outliers are of particular concern. We defined big outliers as those showing 10% or greater error. Eleven out of 115 points satisfy this criterion, and ten out of these were detected by all approaches listed in Table 10.2. Figure 10.1(a) shows that IRLS left many moderate outliers undetected. By more aggressive detection with B = 1.0, IRLS declared 40 points as outliers, and Figure 10.1(b) shows that more of the moderate outliers were detected by decreasing *B*. Again, NIRLS was more effective in discriminating outliers from inliers with a ratio of errors of 5.87 compared to 4.27 for IRLS. The aggressive outlier search with B = 1.0 does find more outliers. However, it declares more points as outliers and the computational advantage of repairing only outliers may be reduced. For example, the number of outliers declared by NIRLS increased from 21 with B = 1.9 to 41 with B = 1.0. Taking the mean CPU hour of Case A2 as a single unit, our efforts to repair Case A2, requiring GENESIS runs of Cases A5, B2, and B5, costs about extra 4.6 units of CPU hour. Compared to obtaining accurate W_s for all data points using Cases A2, A5, B2, and B5, NIRLS repair costs about 33% and 47% CPU hours for B = 1.9 and B = 1.0, respectively.

Table 10.3 and Figure 10.2 show results for Case B2. Again, nine data points of excessively heavy designs were excluded from the experimental design. There were 22 big outliers in the remaining 117 data points, indicating a higher level of noise than Case A2. The advantage of NIRLS over IRLS is clearly demonstrated by comparing the results when B = 1.0. NIRLS successfully detected all of the 22 big outliers and many moderate ones, while IRLS missed six of the big outliers. With more noise, the ratio of correction of W_s for outliers and inliers is 5.97 for NIRLS compared to 2.67 for IRLS with B = 1.0, indicating that NIRLS is more successful in homing in on points with large errors. Again, the aggressive outlier search detects more outliers but there is increased computational cost. Taking the mean CPU hour of Case B2 as a single unit, our efforts to repair Case B2, requiring GENESIS runs of Cases A2, A5, and B5, costs about six extra units of CPU hour. Compared to obtaining accurate W_s for all data points

using Cases A2, A5, B2, and B5, NIRLS repair costs about 36% and 52% of CPU hour for B = 1.9 and B = 1.0, respectively.

Taken together, the results of Case A and Case B indicate that the IRLS procedures are useful for detecting points with large optimization errors, and that the NIRLS procedures are more reliable in this task, especially under conditions of greater noise.

10.3 Advantage of Outlier Repair over Exclusion

The IRLS procedure in itself achieves a better fit than the least squares by down-weighting outlier points and excluding them from the fit. However, removing the outliers can result in a poor approximation in the region where these outliers are located [45]. Repairing these outliers, on the other hand, does not suffer from this problem. Figure 10.3 compares the W_s prediction by RS approximations along a design line connecting two detected outliers. It shows that the least squares results based on repaired data are better than IRLS without repair because the latter excluded those outliers from the fit. Therefore, it was decided to use the least squares fit to the repaired data to obtain improved RS approximations.

10.4 Improvement of Wing Structural Weight RS Approximations Using Repaired Data

A full quadratic RS model was fit to the original and repaired data of Case A2 using the least squares fit, and the accuracy measures are shown in the last two columns of Table 10.2. Before repair, the root mean square error (RMSE) was 6.0% of the mean W_s, and this was reduced to 3.2% by IRLS repair. Although more of the moderate outliers were repaired by NIRLS than IRLS, further improvement of the fit by NIRLS was small; the RMSE was 3.1%. It implies that the gain of outlier repair in terms of fit is saturated with IRLS. In fact the RMSE was slightly increased to 3.3% with full repair. That is because IRLS/NIRLS procedure identifies only offending data points against the fit, while full repair may move away non-offending points from the fit. Besides, this problem of the full repair may be attributed to that the repaired W_s response is not perfectly smooth as seen in Figure 3.4. Overall, about the half of the RMSE

before outlier repair is due to the error from incomplete convergence, and the rest may be attributed to the modeling deficiency of the quadratic model.

For Case B2 in Table 10.3, the RMSE of the quadratic RS fits on W_s(B2) was reduced from 8.7% to 4.1% by IRLS repair, and reduced further to 3.2% by NIRLS repair. Note that six additional big outliers were repaired with NIRLS. Figure 10.4 compares the RS approximations before and after repair along the same HSCT designs used in Figure 9.2. The RS fit based on the uncorrected W_s (B2) over-predicted the response in the middle of the plot. For B = 1.9, as shown in Figure 10.4(a), the RS approximation based on data repaired by IRLS improved. Note that the RS approximation from NIRLS repair lies almost on top of that of IRLS. However, Figure 10.4(b) indicates that NIRLS repair was slightly better than IRLS with B = 1.0 at the right region of the plot. These observations are in agreement with the results of RMSE of Table 10.3. In terms of accuracy of W_s RS fits, outlier repair by IRLS improved the RS approximations substantially, and further gain by NIRLS repair was relatively small.

10.5 HSCT Configuration Optimization Using Improved W_b RS Approximations

We performed HSCT configuration optimizations using the quadratic W_b RS fits obtained in the previous section. The effects of improvements of RS approximations by outlier repair on optimum HSCT designs were investigated. Note that W_b RS approximations were obtained by multiplying the W_s response surface approximations by a factor of 0.7 because we assumed that W_b was 70% of W_s. Table 10.4 contains the initial and optimal designs according to the RS models used. The initial design point was the center of the design box except that the fuel weight was increased to 430000 *lb*. to satisfy the range constraint at the beginning of the configuration optimization. The RS fit based on Case B2 data without outlier repair was first used to find the optimal HSCT configuration, called optimum *O*. Then, configuration optimizations starting from optimum *O* are performed using RS fits based on repaired data: IRLS repair with B = 1.9 (RS_I), NIRLS repair with B = 1.9 (RS_N), and full repair (RS_F). The corresponding optimal HSCT designs were labeled as optimum *I*, *N*, and *F*, respectively. At the initial design, the estimated true W_b was 48633 *lb*. but the RS approximation without outlier repair, RS_O, over-predicted W_b

with 12.0% error. By repairing outliers, the error was reduced to 7.4%, 5.1%, and 1.8% for RS_I, RS_N, and RS_F, respectively.

Comparing the RS prediction for a given optimum design (column), we observe that the predicted W_b's decrease along RS_O, RS_I, RS_N, and RS_F. It is seen that the original RS approximation, RS_O, has positive errors while RS fits with repair tend to have negative errors, which increase in magnitude along RS_I, RS_N, and RS_F. For example, at optimum *O*, RS_O has a positive error of 9.1%, but the errors became more negative along RS_I, RS_N, and RS_F with –4.9%, -6.8%, and –7.3% errors, respectively. The same trend is observed for optima *I*, *N*, and *F*. This may be attributed to *over-optimism of the optimizer*; optimizers tend to exploit regions where the fits are erroneously optimistic, and converge to designs for which the RS approximations under-predict the response. By intensive outlier repair such as NIRLS or full repair, W_b estimates by the RS fits are lowered, and then any exploitation of weakness of the RS approximations by the optimizer is fully experienced at the optimum.

Therefore, a moderate outlier search such as IRLS may be conservative in the terms of the configuration optimization. It has a protective margin against *over-optimism of the optimizer* because the moderately corrected RS fit would slightly over-predict the structural weight over much of the design space. The errors of the RS approximation at optima support this conjecture. For optimum *O*, RS_O over-predicted W_b with 9.1% error. For optimum *I* of IRLS repair, the error of RS_I was only 0.4%, although RS_I cannot be expected to show such accuracy in general because for other optima, RS_I has errors around –5%. For optimum *N* of NIRLS repair, RS_N under-predicted the W_b with –3.2% error. Furthermore, for optimum *F* of full repair, RS_F has –7.5% error. The take-off gross weight of the optima decreases as W_b predicted by RS approximations decreases with more outliers repaired.

Table 10.4 contains the configuration variables at the optima, and the shape of the planform and airfoil are compared in Figure 10.5 for initial and optimal designs. Comparing optimum *O*, *I*, *N*, and *F*, they are very similar with the only significance being the fuel weight (v_5), which decreases as a compensation of the decrease in predicted W_b. Accordingly, the objective function, W_{TOGW}, decreases along optimum *O*, *I*, *N*, and *F*, and the range constraint was active for all the optima.

Table 10.1: Performance of structural optimization for various GENESIS parameter settings.

	Case A2	**Case A5**	**Case B2**	**Case B5**
Number of points for which the best W_s was achieved out of 126 points	0	65	0	61
Mean of the estimated errors by taking the best of four runs as true W_s (percentage of mean W_s)	3925 *lb*. (4.85%)	155.8 *lb*. (0.193%)	4547 *lb*. (5.62%)	26.8 *lb*. (0.033%)

Table 10.2: Results of outlier repair for Case A2.

	B	Number of outliers *a*/*b*/*c*[*]	Mean of repair on outliers(lb)[†]	Mean of repair on inliers(lb)[‡]	Ratio of mean repair on OL to IL	mean W_s	R^2	RMSE in *lb*. (% to the mean W_s)
Before repair	NA	NA	NA	NA	NA	74795	0.9652	4520 (6.0%)
IRLS repair	1.9	21/10/11	7391	1516	4.88	73445	0.9836	2944 (4.0%)
NIRLS repair	1.9	21/10/11	8627	1240	6.96	73220	0.9878	2484 (3.4%)
IRLS repair	1.0	40/10/11	5172	1211	4.27	72996	0.9891	2367 (3.2%)
NIRLS repair	1.0	41/10/11	5555	946	5.87	72815	0.9900	2252 (3.1%)
Full repair[§]	NA	NA	NA	NA	NA	72206	0.9885	2388 (3.3%)

[*]: *a* ~ Number of detected outliers
b ~ Number of big outliers detected (estimated error is greater than 10%)
c ~ Total number of big outliers out of the 115 data points (estimated error is greater than 10%)
[†]: (Sum of W_s repair on outliers)/*a*
[‡]: (Sum of W_s repair on data points other than outliers)/(Total number of points - *a*)
[§]: All 115 points repaired

Table 10.3: Results of outlier repair for Case B2.

	B	Number of outliers *a*/*b*/*c* [*]	Mean of repair on outliers(lb) [†]	Mean of repair on inliers(lb) [‡]	Ratio of mean repair on OL to IL	mean W_s	R^2	RMSE in *lb*. (% to the mean W_s)
Before repair	NA	NA	NA	NA	NA	77701	0.9297	6755 (8.7%)
IRLS repair	1.9	27/11/22	8694	3314	2.62	75695	0.9769	3527 (4.7%)
NIRLS repair	1.9	29/19/22	11379	2307	4.93	74881	0.9824	3042 (4.1%)
IRLS repair	1.0	49/16/22	7158	2680	2.67	74703	0.9828	3052 (4.1%)
NIRLS repair	1.0	52/22/22	8476	1419	5.97	73934	0.9902	2335 (3.2%)
Full repair [§]	NA	NA	NA	NA	NA	73146	0.9879	2578 (3.5%)

[*]: *a* ~ Number of detected outliers
b ~ Number of big outliers detected (estimated error is greater than 10%)
c ~ Total number of big outliers out of the 117 data points (estimated error is greater than 10%)
[†]: (Sum of W_s repair on outliers)/*a*
[‡]: (Sum of W_s repair on data points other than outliers)/(Total number of points - *a*)
[§]: All 117 points repaired

Table 10.4: Results of five variable configuration optimizations using W_b RS before and after outlier repair (Based on data of Case B2).

		Initial design	Optima using W_b RS approximations			
			Without repair (Optimum *O*)	IRLS repair (Optimum *I*)	NIRLS repair (Optimum *N*)	Full repair (Optimum *F*)
W_{TOGW} (*lb.*)		784923	788157	779512	775931	771693
W_b (*lb.*)	RS_o, Without repair	54492 (Error* = 12.0%)	**39912** (Error = 9.1%)	39941 (Error = 9.5%)	39873 (Error = 9.6%)	39900 (Error = 9.6%)
	RS_I, with IRLS repair	52222 (Error = 7.4%)	34792 (Error = -4.9%)	**36601** (Error = 0.4%)	36442 (Error = 0.1%)	34695 (Error = -4.7%)
	RS_N, with NIRLS repair	51124 (Error = 5.1%)	34088 (Error = -6.8%)	34071 (Error = -6.6%)	**35235** (Error = -3.2%)	33892 (Error = -7.0%)
	RS_F, With full repair	49499 (Error = 1.8%)	33895 (Error = -7.3%)	33859 (Error = -7.2%)	33678 (Error = -7.5%)	**33686** (Error = -7.5%)
	best of four GENESIS runs	**48633**	**36574**	**36473**	**36397**	**36414**
$0.01 \times (v_1, ft.)$		1.7	1.82000	1.81619	1.81382	1.81081
$0.1 \times (v_2, ft.)$		1.0	1.01932	1.01929	1.01913	1.01910
$1.0 \times (v_3$, deg.)		71.5	67.4904	67.5588	67.4791	67.5157
$100 \times (v_4$, %)		2.1	2.12321	2.12528	2.12585	2.12664
$0.00001 \times (v_5, lb.)$		4.3	4.14019	4.09583	4.07589	4.05421

*: percentage error in W_b prediction by RS with respect to the best of four GENESIS runs.
v_i, (i = 1,…,5): configuration design variables at the calculated optima of the HSCT.

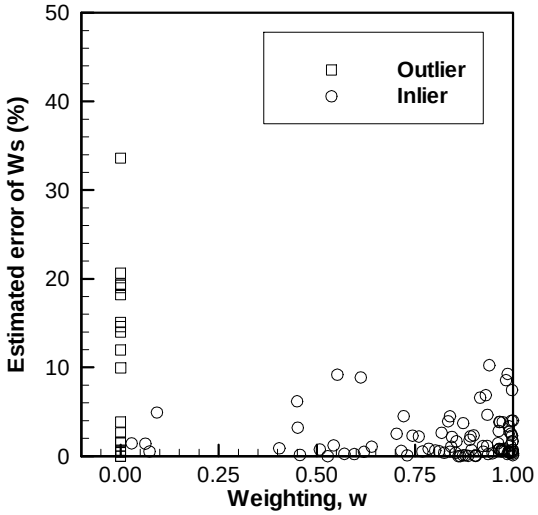

(a) IRLS, B = 1.9.

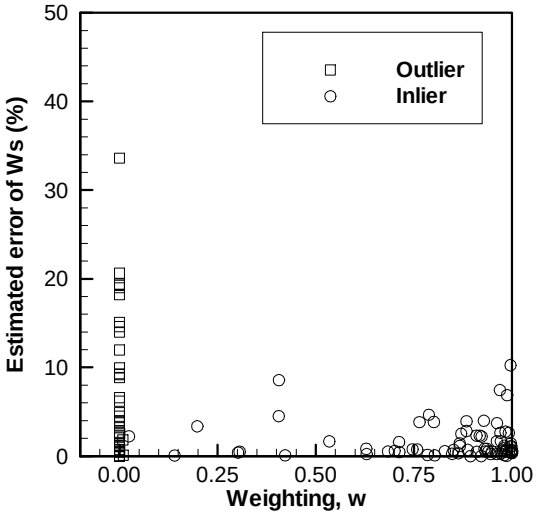

(b) IRLS, B = 1.0.

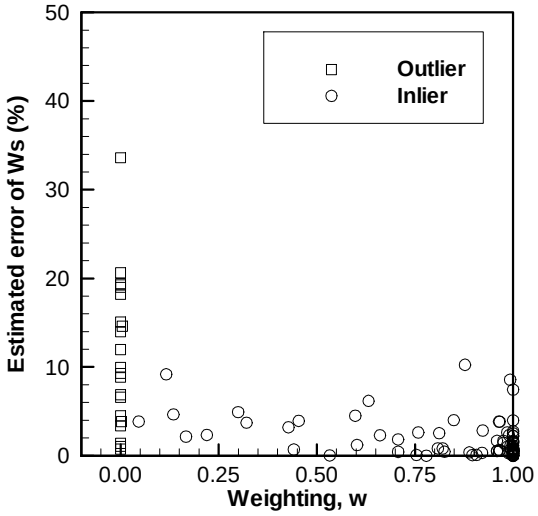

(c) NIRLS, B = 1.9.

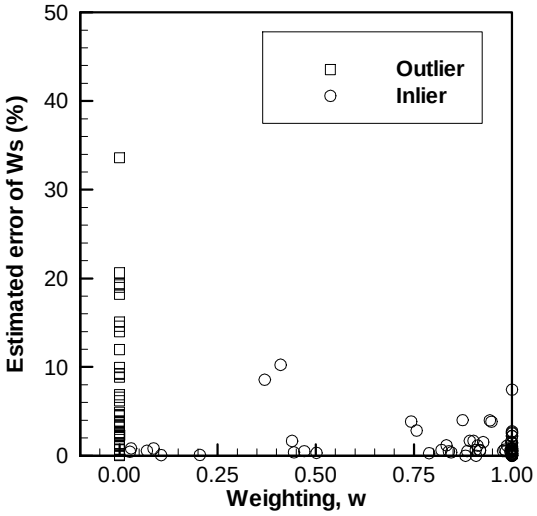

(d) NIRLS, B = 1.0.

Figure 10.1: Estimated error for the detected outliers and inliers for Case A2.

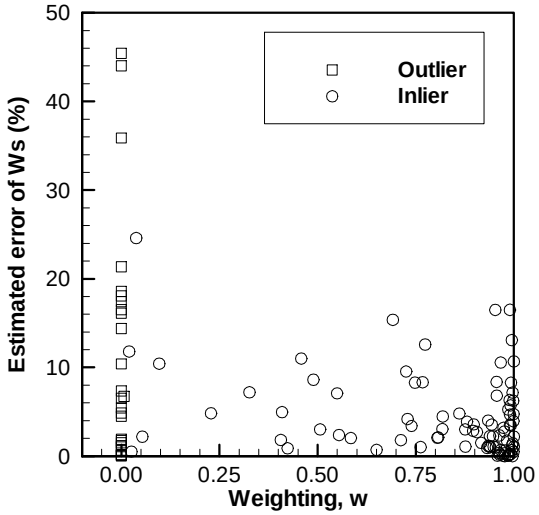

(a) IRLS, $B = 1.9$.

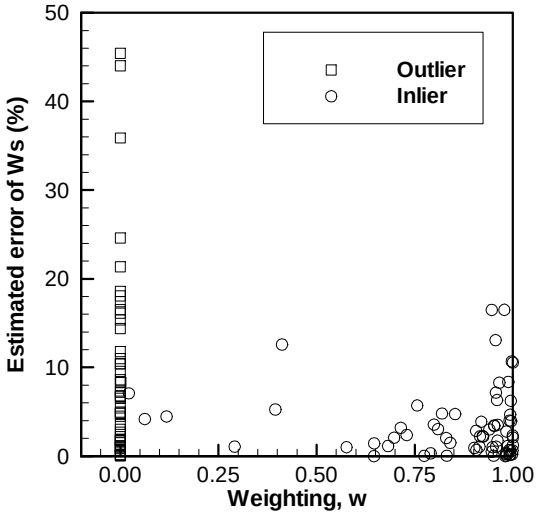

(b) IRLS, $B = 1.0$.

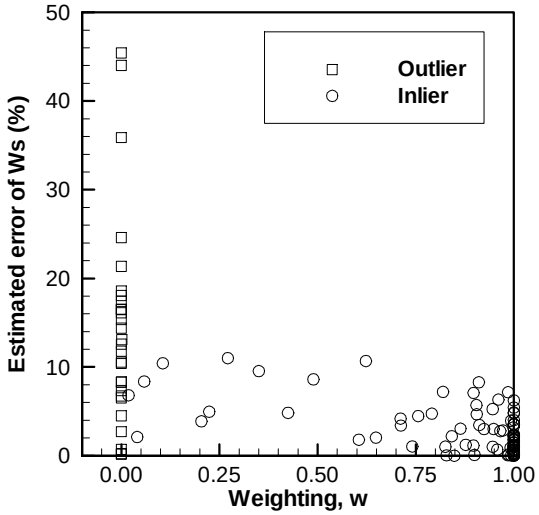

(c) NIRLS, $B = 1.9$.

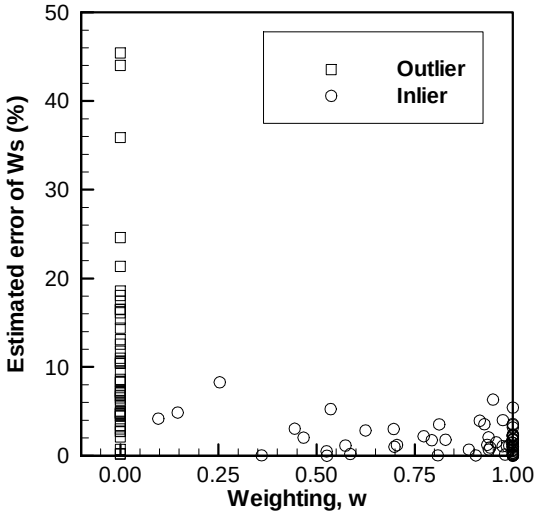

(d) NIRLS, $B = 1.0$.

Figure 10.2: Estimated error for the detected outliers and inliers for Case B2.

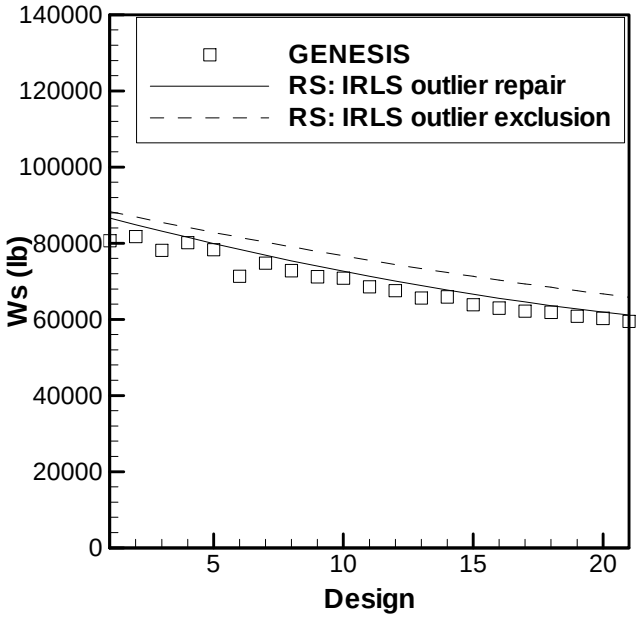

Figure 10.3: Comparison of RS approximations between outlier repair and outlier exclusion on a design line connecting two identified outliers by IRLS.

IRLS removes outliers from the fit by downweighting them (IRLS outlier exclusion). Alternatively, the identified outliers may be repaired and least squares fit can be used to the repaired data (IRLS repair). Accurate W_s data from GENESIS runs are plotted for the 21 HSCT configurations generated by linear interpolation between the two identified outliers (design 1 and 21). The plot indicates RS with outlier repair is more accurate than RS with outlier exclusion in the region where the outliers are located.

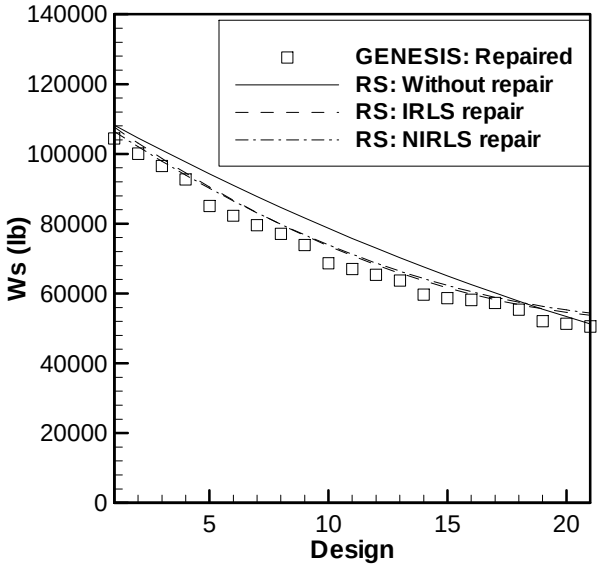

(a) Case B2, B = 1.9.

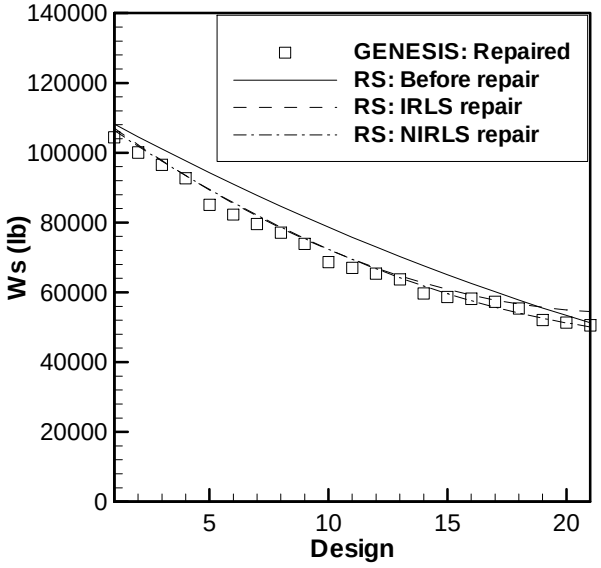

(b) Case B2, B = 1.0.

Figure 10.4: Effects of outlier repair on the W_s RS approximations.

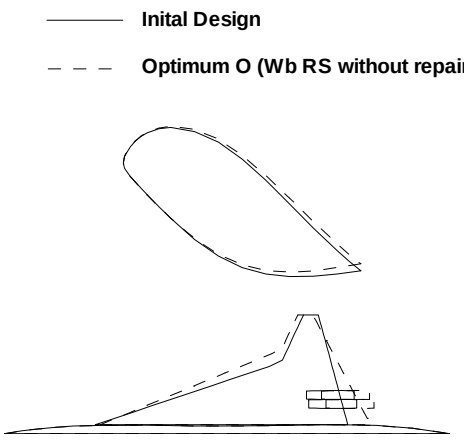

(a) Initial design and original optimum

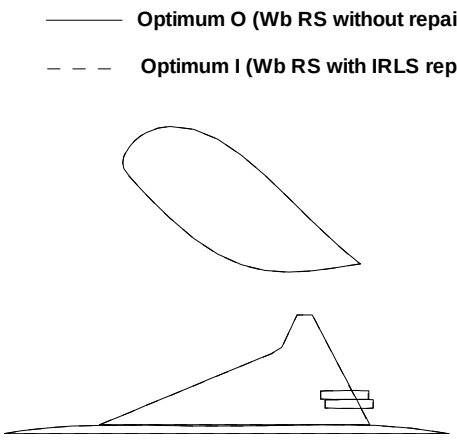

(b) IRLS repair.

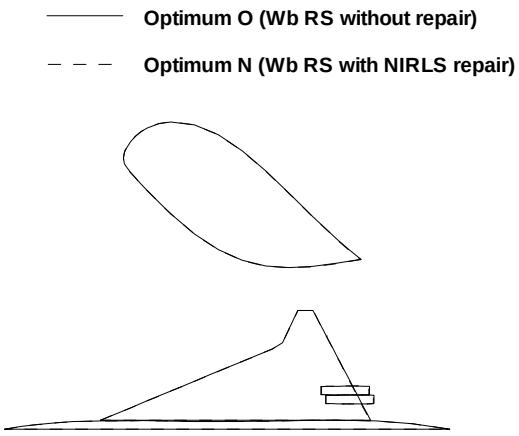

(c) NIRLS repair.

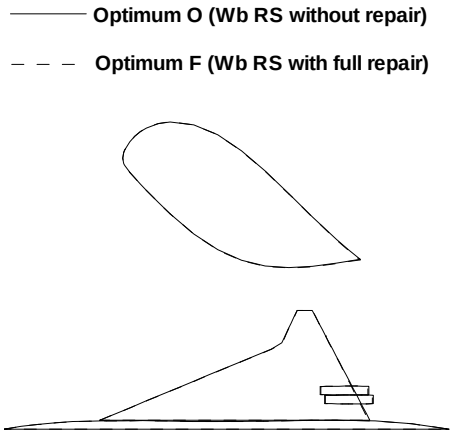

(d) Full repair.

Figure 10.5: Comparison of optimum designs using W_b RS approximations without and with outlier repair (based on data of Case B2).

Chapter 11 Conclusions

The goal of this work was to apply statistical techniques to estimate and reduce errors of the computational simulations used in the design of an HSCT. First, discretization error from a supersonic panel method, WINGDES, was considered. Second, errors in wing structural weight calculated from a structural optimization procedure using GENESIS were analyzed along with the Rosenbrock test problem. The noisy optimization errors were modeled via probability distributions. A robust regression technique, IRLS, was used to identify optimization runs with large errors and to improve the RS fit on the optimization data.

A grid convergence study showed that C_L calculated from WINGDES was subject to discretization error that converged like $h^{0.5}$. Richardson extrapolation was not accurate because it magnified the noise in C_L data. A RS model using several mesh sizes reduced the noise problem associated with the Richardson extrapolation. In addition, the RS approach was compared to *posterior* response surface fit to Richardson extrapolation, and was shown to be efficient in estimating the discretization error by using carefully selected experimental designs.

Probabilistic models were applied to optimization errors due to incomplete convergence. The Weibull model was successfully fit to the optimization errors for the Rosenbrock test function and structural optimization of the HSCT. The minimum sample size for a reliable estimate of average error was around 50. An indirect approach using differences between two optimization results was proposed. The indirect fit enabled us to estimate the average errors of low-fidelity optimizations without performing high-fidelity optimizations that can be expensive. The results demonstrated the usefulness of the probabilistic model of the optimization error. As a result, we obtained a data-driven probability model of the simulation errors, which can be easily utilized in robust design studies.

A robust regression technique, *M*-estimation implemented by the IRLS algorithm, was applied to the Rosenbrock problem to identify optimization runs with large errors, *outliers*. We elected to repair the outliers by performing higher fidelity optimization runs, because excluding data points may reduce the accuracy of the RS model. For the Rosenbrock problem, outlier repair efforts substantially improved the quality of the optimum of the RS model. Then we devised nonsymmetric IRLS (NIRLS) with a nonsymmetric weighting function, to utilize the tendency of

one-sidedness of the optimization errors. It was shown that NIRLS was more reliable than IRLS in identifying outliers from optimization results.

Structural optimization data with large errors resulted in inaccurate RS models of the wing bending material weight (W_b). The IRLS/NIRLS procedure was also applied to identify and repair the outliers. Again, NIRLS was more effective than IRLS in identifying outliers. In terms of RS fit, IRLS repair substantially improved the accuracy of the RS model, while further improvements by NIRLS were relatively small. HSCT configuration optimizations were performed using W_b RS models before and after outlier repair. The results indicated that the system optimizer exploited the modeling error of the RS model, and the moderate outlier repair of IRLS was a conservative choice compared to NIRLS repair in the HSCT design problem.

Bibliography

[1] Sobieszczanski-Sobieski, J., "Multidisciplinary Design Optimization (MDO) methods: their synergy with computer technology in the design process," *Aeronautical Journal*, Vol. 103, No. 1026, 1999, pp. 373-382.

[2] Mavris, D. N., DeLaurentis, D. A., Bandte, O., and Hale, M. A., "A Stochastic Approach to Multi-disciplinary Aircraft Analysis and Design," AIAA Paper 98-0912, 36th Aerospace Science Meeting & Exhibit, Reno, NV, January, 1998.

[3] Sobieszczanski-Sobieski, J. and Haftka, R. T., "Multidisciplinary Aerospace Design Optimization: Survey of Recent Developments," *Structural Optimization*, Vol. 14, No. 1, 1997, pp. 1-23.

[4] Knill, D. L., Giunta, A. A., Baker, C. A., Grossman, B., Mason, W. H., Haftka, R. T., and Watson, L. T., "Response Surface Models Combining Linear and Euler Aerodynamics for Supersonic Transport Design," *Journal of Aircraft*, Vol. 36, No. 1, 1999, pp. 75-86.

[5] Raveh, D. E., Levy, Y., and Karpel, M., "Aircraft Aeroelastic Analysis and Design Using CFD-Based Unsteady Loads," AIAA Paper 2000-1325, 41st AIAA/ASME/ASCE/AHS/ASC Structures, Structural Dynamics, & Materials Conference, Atlanta, GA, April, 2000.

[6] Sobieszczanski-Sobieski, J., Kodiyalam, S., and Yang, R., "Optimization of Car Body under Constraints of Noise, Vibration, and Harness (HVN), and Crash," AIAA Paper 2000-1521, 41st AIAA/ASME/ASCE/AHS/ASC Structures, Structural Dynamics, & Materials Conference, Atlanta, GA, April, 2000.

[7] Balabanov, V., Kaufman, M., Knill, D. L., Haim, D., Golovidov, O., Giunta, A., A., Haftka, R. T., Grossman, B., Mason, W. H., and Watson, L. T., "Dependence of Optimal Structural Weight on Aerodynamic Shape for a High Speed Civil Transport," AIAA Paper 1996-4046, 6th AIAA/NASA/ISSMO Symposium on Multidisciplinary Analysis and Optimization, Bellevue, WA, September, 1996.

[8] Balabanov, V., Giunta, A. A., Golovidov, O., Grossman, B., Mason, W. H., Watson, L. T., and Haftka, R. T., "Reasonable Design Space Approach to Response Surface Approximation," *Journal of Aircraft*, Vol. 36, 1999, pp. 308-315.

[9] Roache, P. J., *Verification and Validation in Computational Science and Engineering*, Hermosa Publishers, Albuquerque, NM, 1998.

[10] Giunta, A. A., Dudley, J. M., Narducci, R., Grossman, B., Haftka, R. T., Mason, W. H., and Watson, L. T., "Noisy Aerodynamics Response and Smooth Approximations in HSCT Design," AIAA Paper 94-4376, 5th AIAA/USAF/NASA/ISSMO Symposium on Multidisciplinary Analysis and Optimization, Panama City, FL, September, 1994.

[11] Venter, G., Haftka, R. T., and Starnes, J. H., "Construction of Response Surfaces for Design Optimization Applications," AIAA Paper 96-4040, 6th AIAA/NASA/ISSMO Symposium on Multidisciplinary Analysis and Optimization, Bellevue, WA, September, 1996.

[12] Mehta, U. B., "Guide to Credible Computer Simulations of Fluid Flows," *Journal of Propulsion and Power*, Vol. 12, No. 5, 1996, pp. 940-948.

[13] Chen, W., Allen, J. K., Mistree, F., and Tsui, K. L., "A Procedure for Robust Design: Minimizing Variations Caused by Noise Factors and Control Factors," *Journal of Mechanical Design*, Vol. 118, No. 4, 1996, pp. 478-485.

[14] Mavris, D. N., Bandte, O., and Schrage, D. P., "Application of Probabilistic Methods for the Determination of Probabilistic Methods for the Determination of an Economically Robust HSCT Configuration," AIAA Paper 96-4090, 6th AIAA/NASA/ISSMO, Symposium on Multidisciplinary Analysis and Optimization, Bellevue, WA, September, 1996.

[15] Gantois, K. and Morris, A. J., "Incorporation of Manufacturing Information into an MDO environment," *Aeronautical Journal*, Vol. 103, No. 1026, 1999, pp. 383-388.

[16] Mavris, D. N., Bandte, O., and DeLaurentis, D. A., "Robust Design Simulation: A Probabilistic Approach to Multidisciplinary Design," *Journal of Aircraft*, Vol. 36, No. 1, 1999, pp. 298-307.

[17] Venter, G. and Haftka, R. T., "Using Response Surface Approximations in Fuzzy Set Based Design Optimization," *Structural Optimization*, Vol. 18, No. 4, 1999, pp. 218-227.

[18] Chen, S., Nikolaidis, E., Cudney, H. H., Rosca, R., and Haftka. R.T., "Comparison of Probabilistic and Fuzzy Set Methods for Designing under Uncertainty," AIAA Paper 99-1579, 40th AIAA/ASME/ASCE/AHS/ASC Structures, Structural Dynamics, & Materials Conference, St. Louis, MO, April, 1999.

[19] Lombardi, M. and Haftka, R. T., "Anti-Optimization Technique for Structural Design under Uncertainties," *Computer Methods in Applied Mechanics and Engineering*, Vol. 157, No. 1, 1998, pp. 19-31.

[20] Chen, R. and Ward, A. C., "The RANGE Family of Propagation Operations for Intervals on Simultaneous Linear Equations," *Artificial Intelligence for Engineering Design, Analysis and Manufacturing*, Vol. 9, No. 3, 1995, pp. 183-196.

[21] Hoover, S. V. and Perry, R. F., *Simulation: A Problem-Solving Approach*, Addison Wesley Longman, Reading, MA, 1989.

[22] Stein, M., "Large Sample Properties of Simulations Using Latin Hypercube Sampling," *Technometrics*, Vol. 29, No. 2, 1987, pp. 143-151.

[23] Phadke, M. S., *Quality Engineering using Robust Design*, Prentice-Hall, Englewood Cliffs, NJ, 1989.

[24] Southwest Research Institute, *FPI User's and Theoretical Manual*, San Antonio, TX, 1995.

[25] Mavris, D. N. and Bandte, O., "A Probabilistic Approach to Multivariate Constrained Robust Design Simulation," AIAA Paper 97-5508, AIAA and SAE 1997 World Aviation Congress, Anaheim, CA, October, 1997.

[26] Celik, I. and Zhang, W., "Calculation of Numerical Uncertainty Using Richardson Extrapolation: Application to Some Simple Turbulent Flow Calculations," *Journal of Fluids Engineering, Transactions of ASME*, Vol. 117, No. 3, 1995, pp. 439-435.

[27] Coleman, H. W. and Stern, F., "Uncertainties and CFD Code Validation," *Journal of Fluids Engineering*, Vol. 119, No. 4, 1997, pp. 795-803.

[28] Anderson, E. L. and Hattis, D., "Uncertainty and Variability," *Risk Analysis*, Vol. 19, No. 1, 1999, pp. 47-49.

[29] Antonsson, E. K. and Otto, K. N., "Imprecision in Engineering Design," *ASME Journal of Mechanical Engineering*, Vol. 117B, 1995, pp. 25-32.

[30] French, S., "Uncertainty and Imprecision: Modelling and Analysis," *Journal of the Operational Research Society*, Vol. 46, No. 1, 1995, pp. 70-79.

[31] Coleman, H. W. and Steele, W. G., Jr., *Experimentation and Uncertainty Analysis for Engineers*, 1st Ed., John Wiley & Sons, New York, 1989.

[32] Gu, X., Renaud, J. E., and Batill, S. M., "An Investigation of Multidisciplinary Design Subject to Uncertainty," AIAA Paper 98-4747, 7th AIAA/NASA/USAF/ISSMO Symposium on Multidisciplinary Analysis and Optimization, St. Louis, MO, September, 1998.

[33] Oberkampf, W. L., DeLand, S. M., Rutherford, B. M., Diefert, K. V., and Alvin, D. F., "A New Methodology for the Estimation of Total Uncertainty in Computational Simulation," AIAA Paper 99-1612, 40th AIAA/ASME/ASCE/AHS/ASC Structures, Structural Dynamics, and Materials Conference, St. Louis, MO, April, 1999.

[34] Oberkampf, W. L., DeLand, S. M., Rutherford, B. M., Diefert, K. V., and Alvin, D. F., "Estimation of Total Uncertainties in Modeling and Simulation," Sandia Report SAND2000-0824, Sandia National Laboratories, Albuquerque, NM, April, 2000.

[35] Batill, S. M., Renaud, J. E., and Gu, X., "Modeling and Simulation Uncertainty in Multidisciplinary Design Optimization," AIAA Paper 2000-4803, 8th AIAA/USAF/NASA/ISSMO Symposium on Multidisciplinary Analysis and Optimization, Long Beach, CA, September, 2000.

[36] Roache, P. J., *Computational Fluid Dynamics*, Hermosa Publishers, Albuquerque, NM, 1972.

[37] Alvin, K. F., "A Method for Treating Discretization Error in Nondeterministic Analysis," AIAA Paper 1999-1611, 40th AIAA/ASME/ASCE/AHS/ASC Structures, Structural Dynamics, and Materials Conference, St. Louis, MO, April, 1999.

[38] Kammer, D. C., Alvin, K. F., and Malkus, D. S., "Combining Metamodels with Rational Function Representations of Discretization Error for Uncertainty Quantification," a manuscript prepared for journal submission, 2000.

[39] DeLaurantis, D. A. and Mavris, D. N., "Uncertainty Modeling and Management in Multidisciplinary Analysis and Synthesis," AIAA Paper 2000-0422, 38th Aerospace Sciences Meeting & Exhibit, Reno, NV, January, 2000.

[40] Papila, M. and Haftka, R. T., "Uncertainty and Response Surface Approximations," AIAA Paper 2001-1680, 42th AIAA/ASME/ASCE/AHS/ASC Structures, Structural Dynamics, and Material Conference, Seattle, WA, April, 2001.

[41] Myers, R. H. and Montgomery, D. C., *Response Surface Methodology: Process and Product Optimization Using Designed Experiments*, John Wiley and Sons, New York, N. Y., 1995.

[42] Beckman, R. J. and Cook, R. D., "Outlier…….s," *Technometrics*, Vol. 25, No. 2, 1983, pp. 119-149.

[43] Rousseuw, P. J. and Leroy, A. M., *Robust Regression and Outlier Detection*, Wiley, NY., 1987.

[44] Holland, P. H. and Welsch, R. E., "Robust Regression Using Iteratively Reweighted Least Squares," *Communications in Statistics: Theory and Methods*, Vol. 6, 1977, pp. 813-827.

[45] Papila, M. and Haftka, R. T., "Uncertainty and Wing Structural Weight Approximations," AIAA Paper 99-1312, 40th AIAA/ASME/ASCE/ASC Structures, Structural Dynamics, and Material Conference, St. Louis, MO, April, 1999.

[46] Papila, M. and Haftka, R. T., "Response Surface Approximations: Noise, Error Repair, and Modeling Errors," *AIAA Journal*, Vol. 38, No. 12, 2000, pp. 2336-2343.

[47] Kim, H., Papila, M., Mason, W. H., Haftka, R. T., Watson, L. T, and Grossman, B., "Detection and Correction of Poorly Converged Optimizations by Iteratively Reweighted Least Squares," AIAA 2000-1525, 41st AIAA/ASME/ASCE/AHS/ASC Structures, Structural Dynamics, and Materials Conference, Atlanta, GA, April, 2000.

[48] Giunta, A. A., Balabanov, V., Burgee, S., Grossman, B., Haftka, R. T., Mason, W. H., and Watson, L. T., "Multidisciplinary Optimisation of a Supersonic Transport Using Design of Experiments Theory and Response Surface Modelling," *Aeronautical Journal*, Vol. 101, No. 1008, 1997, pp. 347-356.

[49] Burgee, S., Giunta, A. A., Balabanov, V., Grossman, B., Mason, W. H., Narducci, R., Haftka, R. T., and Watson, L. T., "A Coarse-Grained Parallel Variable-Complexity Multidisciplinary Optimization Paradigm," *International Journal of Supercomputing Applications and High Performance Computing*, Vol. 10, No. 4, 1996, pp. 269-299.

[50] Kaufman, M., Balabanov, V., Burgee, S. L., Giunta, A. A., Grossman, B., Haftka, R. T., Mason, W. H., and Watson, L. T., "Variable Complexity Response Surface Approximations for Wing Structural Weight in HSCT Design," *Computational Mechanics*, Vol. 18, No. 2, 1996, pp. 112-126.

[51] McCullers, L. A., *Flight Optimization System*, Release 5.92, NASA Langley Research Center, 1997.

[52] VMA Engineering, *GENESIS User Manual*, Version 5.0, Colorado Springs, CO, 1998.

[53] Carlson, H. W. and Walkley, K. B., "Numerical Methods and a Computer Program for Subsonic and Supersonic Aerodynamic Design and Analysis of Wings with Attainable Thrust Considerations," NASA CR 3808, 1984.

[54] Carlson, H. W. and Miller, D. S., "Numerical Methods for the Design and Analysis of Wings at Supersonic Speeds," NASA TN D-7713, 1974.

[55] Balabanov, V. O., *Development of Approximations for HSCT Wing Bending Material Weight Using Response Surface Methodology*, Ph. D dissertation, Virginia Polytechnic Institute and State University, Blacksburg, VA, 1997.

[56] Hutchison, M. G., *Multidisciplinary Optimization of High-Speed Civil Transport Configurations Using Variable-Complexity Modeling*, Ph. D dissertation, Virginia Polytechnic Institute and State University, Blacksburg, VA, 1993.

[57] Burden, R. L. and Faires, J. D., *Numerical Analysis*, 6th Ed., Brooks/Cole Publishing Company, Pacific Grove, CA, 1997.

[58] Schittkowski, K., *More Test Problems for Nonlinear Programming Codes, Lecture Notes in Economics and Mathematical Systems*, Vol. 282, Springer-Verlag, Berlin, 1987, pp. 118-123.

[59] Kim, H., Haftka, R. T., Mason, W. H., Watson, L. T, and Grossman, B., "A Study of the Statistical Description of Errors from Structural Optimization," AIAA 2000-4840, 8th AIAA/USAF/NASA/ISSMO Symposium on Multidisciplinary Analysis and Optimization, Long Beach, CA, September, 2000.

[60] Montgomery, D. C., *Design and Analysis of Experiments*, John Wiley, New York, 1991.

[61] Law, A. M. and Kelton, W. D., *Simulation Modeling and Analysis*, McGraw Hill, New York, 1982.

[62] Hahn, G. J. and Shapiro, S. S., *Statistical Models in Engineering*, John Wiley and Sons, Inc., New York, 1994.

[63] Bury, K. V., *Statistical Distributions in Engineering*, Cambridge University Press, New York, 1999.

[64] Huber, P. J., *Robust Statistics*, Wiley, New York, 1981.

[65] Birch, J. B., *Applied Contemporary Statistics: An Exploratory and Robust Data Analysis Approach*, Class Note, University Printing Services, Virginia Polytechnic Institute and State University, Blacksburg, VA, 2000.

[66] Beaton, A. E. and Tukey, J. W., "The Fitting of Power Series, Meaning Polynomials, Illustrated on Band-Spectroscopic Data," *Technometrics*, Vol. 16, 1974, pp. 147-185.

[67] Giunta, A. A., *Aircraft Multidisciplinary Design Optimization Using Design of Experiments Theory and Response Surface Modeling Methods*, Ph. D dissertation, Virginia Polytechnic Institute and State University, Blacksburg, VA, 1997.

[68] Eminton, E., "On the Numerical Evaluation of the Drag Integral," ARC Reports and Memoranda No. 3341, 1961.

[69] Harris, R. V., Jr., "An Analysis and Correlation of Aircraft Wave Drag," NASA TM X-947, 1964.

[70] Cohen, D. and Friedman, M. D., "Theoretical Investigations of the Supersonic Lift and Drag of Thin, Sweptback Wings with Increased Sweep Near the Root," NACA TN 2959, 1953.

[71] Hopkins, E. J. and Inouye, M., "An Evaluation of Theories for Predicting Turbulent Skin Friction and Heat Transfer on Flat Plates at Supersonic and Hypersonic Mach Numbers," *AIAA Journal*, Vol. 9, No. 6, 1971, pp. 993-1003.

[72] Mason, W. H., *Aerodynamic Calculation Methods for Programmable Calculators and Personal Computers, Pak #4 ¾ Boundary layer Analysis Methods*, Aerocal, Huntington, NY, 1981.

[73] Huang, X., Haftka, R. T., Grossman, B., and Mason, W. H., "Comparison of Statistical-based Weight Equations with Structural Optimization for Supersonic Transport Wings," AIAA Paper 94-4379, 1994.

[74] Lomax, H., Heaslet, M. A., and Fuller, F. B., "Integrals and Integral Equations in Linearized Wing Theory," NACA Report 1054, 1951.

[75] Hildebrand, F. B., *Advanced Calculus for Application*, 2nd Ed., Prentice Hall, 1976.

[76] Myers, R. H., *Classical and Modern Regression with Applications*, PWS-KENT, Boston, 1990, pp. 351-356.

[77] Zink, P. S., Raveh, D. E., and Mavris, D. N., "Robust Structural Design for Active Aeroelastic Wing with Aerodynamic Uncertainties," AIAA 2000-1439, 41st AIAA/ASME/ASCE/AHS/ASC Structures, Structural Dynamics, and Materials Conference, Atlanta, GA, April, 2000.

[78] Weiss, N. A. and Hassett, M. J., *Introductory Statistics*, 3rd Ed., Addison-Wesley, Reading, MA, 1991.

[79] Solomon, F., *Probability and Stochastic Processes*, Prentice-Hall, New Jersey, 1987.

[80] Huber, P. J., "Robust Estimation of a Location Parameter," *Annals of Mathematical Statistics*, Vol. 35, 1964, pp. 73-101.

[81] Birch, J. B., "Some Convergence Properties of Iteratively Reweighted Least Squares in the Location Model," *Communications in Statistics: Simulation and Computation*, Vol. 9, 1980, pp. 359-369.

[82] Papila, M. and Haftka, R. T., "Response Surfaces for Optimal Weight of Cracked Composite Panels: Noise and Accuracy," AIAA Paper 2000-4755, 8th AIAA/USAF/NASA/ISSMO Symposium on Multidisciplinary Analysis and Optimization, Long Beach, CA, September, 2000.

[83] Letcher, J. S., Jr., "Convergence of Lift and Drag predictions by a Morino Panel Method (VSAERO)," *AIAA Journal*, Vol. 27, No. 8, 1989, pp. 1019-1020.

[84] Margason, R. J., Kjelgaard, S. O., Sellers, W. L., III., Morris, C. E. K., Jr., Walkley, K. B., and Shields, E. W., "Subsonic Panel Methods – A Comparison of Several Production Codes," AIAA Paper 85-0280, 1985.

[85] Vanderplaats Research & Development, Inc., *DOT Design Optimization Tools Users Manual*, Colorado Springs, CO, 1995.

[86] Math Works, Inc., *Matlab Optimization Toolbox Users Guide*, Version 5, Natick, MA, 1997.

[87] Gay, D. M., "Subroutines for Unconstrained Minimization Using a Model/Thrust-Region Approach," *ACM Transactions on Mathematical Software*, Vol. 9, No. 4, December, 1983, pp.503-512, see also http://www.bell-labs.com/projects /PORT.

[88] Dennis, J. E., Jr. and Schnabel, R. B., *Numerical Methods for Unconstrained Optimization and Nonlinear Equations*, Prentice Hall, Englewood Cliffs, NJ, 1983, pp. 129-147.

[89] Math Works, Inc., *Matlab Statistics Toolbox Users Guide*, Version 2, Natick, MA, 1999.

[90] SAS Institutes, Inc., *SAS Users Guide*, Version 6, 4th Ed., 1990.

[91] Owen, A., "Lattice Sampling Revisited: Monte Carlo Variance of Means over Randomized Orthogonal Arrays," *Annals of Statistics*, Vol. 22, No. 2, 1994, pp. 930-945.

[92] McCullough, P. and Nelder, J. A., *Generalized Linear Models*, 2nd Ed., Chapman and Hall, New York, NY, 1989.

[93] Box, M. J. and Draper, N. R., "Factorial Designs, the | X^TX | criterion, and Some Related Matters," *Technometrics*, Vol. 13, No. 4, 1971, pp. 731-742.

[94] Squire, W., *Integration for Engineers and Scientists*, American Elsevier Publishing Company, Inc., New York, 1970.

Appendix A Design of Experiments

A.1 Full Factorial Design

For experimental design, allowable range of each independent variable is defined by lower and upper bounds. In full factorial designs, equally spaced levels of each variable are combined to generate enough data points to create a response surface model (Ref. [41], pp. 79-123). Figure A.1 shows the three level full factorial (FF) design in three dimensional design space, which is sufficient for a quadratic polynomial model. In an *m*-dimensional design space, *l*-level full factorial design requires l^m data points. When a three level FF design is used, the largest possible number of design variables would not be greater than ten because $3^{10} = 59049$, unless the experiments (computational simulations) are very cheap.

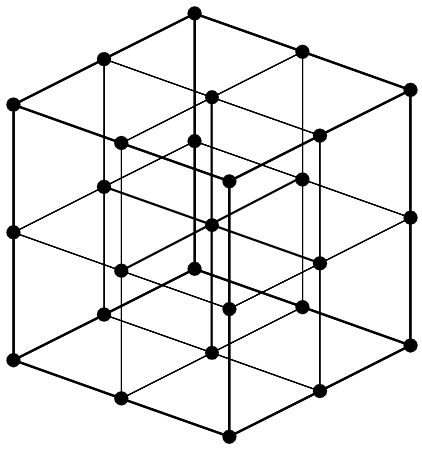

Figure A.1: Three level full factorial design of three dimensions.

A.2 Centered Composite Design (CCD)

To fit a quadratic model with a reasonable number of design points, central composite design (CCD) can be used (Ref. [41], pp. 297-340). The CCD consists of two level full factorial design, a center point, and *star* points located in the direction of each face of the hypercube. Face

centered central composite design (FCCC) is a special case of CCD, for which the star points are located on the center of each face of the hypercube. Figure A.2 shows a FCCC in three dimensional design space. The CCD model can be used to fit a quadratic model and requires $2^m + 2m + 1$ experiments. For example, 1045 experiments (computational simulations) are needed in a ten dimensional design space compared to 59049 for the FF design.

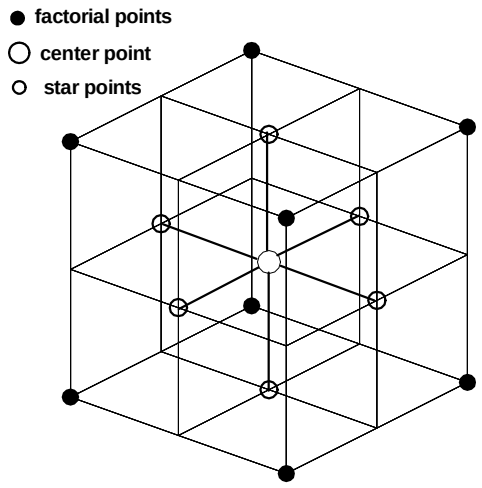

Figure A.2: Face centered central composite design of three dimensions.

A.3 *D*-optimal Design

For a higher dimensional problem, FCCC still requires too many experiments. *D*-optimal design (Ref. [41], pp. 363-393) provides a systematic way to select a subset of design points from a pool of design points such as FF or FCCC. A *D*-optimal experimental design is a collection of design points in a design space that minimizes the variance of the estimated regression coefficients. There are several desirable properties of *D*-optimal designs [93].

- The variance in the estimated coefficients is minimized.
- The maximum variance of any predicted value, $\hat{y}$, is minimized.
- $|X^T X|$ is invariant to the scaling of $\boldsymbol{x}$.

Typically, optimization methods are used to select design points from a pool of data points.

Appendix B Failure Rate of the Weibull Distribution

In the context of failure test problems such as measuring the lifetime of light bulbs, it is useful to consider a function that gives the probability of failure during a very small time increment, assuming that no failure occurred before this time. This function known as the failure rate [62], or conditional failure function, is expressed as

$$f(t) = \frac{f(t)}{1 - F(t)}, \tag{B.1}$$

where $f(t)$ and $F(t)$ are the probability density and cumulative distribution functions for the time to failure. Consequently, $f(t)dt$ can be interpreted as the conditional probability that failure will occur during the period between t and $(t+dt)$, on condition that there was no failure until time t.

For the Weibull distribution, the failure rate becomes

$$f(t) = a b^{-a} t^{a-1}. \tag{B.2}$$

Figure 5.2 shows the Weibull density functions with b =1 and various values of a. The corresponding failure rates are shown in Figure B.1. Note that when a = 1, the failure rate is constant, and the Weibull model is reduced to the exponential distribution. For a < 1, the failure rate decreases asymptotically to zero along t, but with a > 1, the failure rate increases to infinity from zero. For example, a manufacturer of light bulbs may want to know the expected lifetime of their products by measuring the time to failure. Increasing failure rate implies that old light bulbs have greater chance of failure than newer ones, whereas decreasing failure rate indicates that old light bulbs are more unlikely to fail maybe because most of the problems occur at the beginning of the lifetime of light bulbs. Constant failure rate indicates that the probability of failure does not depend on how long the light bulbs have been in use.

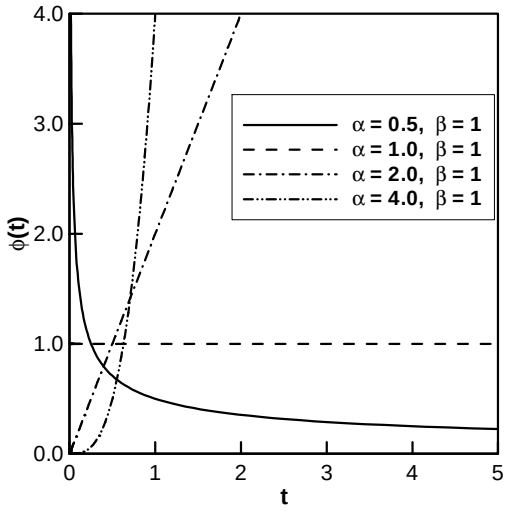

Figure B.1: Failure rate for Weibull distribution with b = 1 and various a.

Appendix C Numerical Integration of Joint Probability Distribution of the Weibull Models

For the indirect approach using differences between two simulation results, the probability density function (PDF) of the difference is obtained via integration of Eq. 5.12. The integration has a closed form solution for exponential models. However, for Weibull models, there is no closed form solution and numerical integration is required. If random variables *s* and *t* are modeled as Weibull,

$$\begin{aligned} s \quad &\sim \quad g(s) = a_1 b_1^{-a_1} s^{a_1 - 1} \exp\left(-\left(\frac{s}{b_1} \right)^{a_1} \right) \\ t \quad &\sim \quad h(t) = a_2 b_2^{-a_2} t^{a_2 - 1} \exp\left(-\left(\frac{t}{b_2} \right)^{a_2} \right). \end{aligned} \tag{C.1}$$

Now, Eq. 5.12 is written as

$$\int_0^\infty a_1 a_2 b_1^{-a_1} b_2^{-a_2} s^{a_1 - 1} (s - x)^{a_2 - 1} \exp\left(-\left(\frac{s}{b_1} \right)^{a_1} - \left(\frac{s - x}{b_2} \right)^{a_2} \right) ds \quad \text{if} \quad x < 0, \tag{C.2}$$

and

$$\int_x^\infty a_1 a_2 b_1^{-a_1} b_2^{-a_2} s^{a_1 - 1} (s - x)^{a_2 - 1} \exp\left(-\left(\frac{s}{b_1} \right)^{a_1} - \left(\frac{s - x}{b_2} \right)^{a_2} \right) ds \quad \text{if} \quad x > 0. \tag{C.3}$$

Note that the integrand of Eq. C.2 or Eq. C.3 has a singularity at the lower bound of the integration, when $a_1 < 1$ for Eq. C2 or $a_2 < 1$ for Eq. C3. A technique of change of variable

(Ref. [94], p. 163) was utilized to remove the singularities. For Eq. C.2, we change the variable of integration, *s*, by introducing *x* such that

$$s \equiv x^{\frac{1}{1+(a_1-1)}} = x^{\frac{1}{a_1}}. \tag{C.4}$$

Now, Eq. C.2 is rewritten as

$$a_2 b_1^{-a_1} b_2^{-a_2} \int_0^{\infty} \left(x^{1/a_1} - x\right)^{a_2-1} \exp\left(-\frac{x}{b_1^{a_1}} - \left(\frac{x^{1/a_1} - x}{b_2}\right)^{a_2}\right) dx \quad \text{if} \quad x < 0. \tag{C.5}$$

Similarly, by introducing

$$s - x \equiv x^{\frac{1}{1+(a_2-1)}} = x^{\frac{1}{a_2}}, \tag{C.6}$$

Eq. C3 is rewritten as

$$a_1 b_1^{-a_1} b_2^{-a_2} \int_0^{\infty} \left(x + x^{1/a_2}\right)^{a_1-1} \exp\left(-\left(\frac{x + x^{1/a_2}}{b_1}\right)^{a_1} - \frac{x}{b_2^{a_2}}\right) dx \quad \text{if} \quad x > 0. \tag{C.7}$$

Since the singularities are removed, Eqs. C.5 and C.7 can be numerically integrated. Eqs. C.5 and C.7 are improper integrals due to the infinite range. In numerical integration, the upper bound of integration is set to be sufficiently large to guarantee that the contribution of the range cut off is negligible. Gaussian quadrature of degree of precision three was performed on 100 subintervals logarithmically distributed. The MATLAB source codes for numerical integration are included in Appendix F.

Appendix D Experimental Design of HSCT and W_s Data

This table contains observation numbers (ID), HSCT configuration design variables (v_i) in a coded form, and W_s data according to convergence settings of GENESIS (see Table 9.1).

ID	v_1	v_2	v_3	v_4	v_5	W_s(A2)	W_s(A3)	W_s(A5)	W_s(B2)	W_s(B3)	W_s(B5)
1	-1.0000	-1.0000	-1.0000	-1.0000	-1.0000	106332.40	105457.10	105545.20	106094.60	105608.50	105607.50
2	-1.0000	-1.0000	-1.0000	-1.0000	1.0000	167000.50	119731.40	119708.40	130862.10	119878.90	119689.30
3	-1.0000	-1.0000	-1.0000	1.0000	-1.0000	52039.14	51355.46	51194.86	56694.88	51272.82	51244.04
4	-1.0000	-1.0000	-1.0000	1.0000	1.0000	58139.32	57835.40	57739.08	58019.96	57846.68	57796.78
5	-1.0000	-1.0000	1.0000	-1.0000	-1.0000	190725.50	194565.80	191812.00	187808.40	187481.30	182697.10
6	-1.0000	-1.0000	1.0000	-1.0000	1.0000	234341.00	225817.00	220917.00	217070.40	217563.60	215875.20
7	-1.0000	-1.0000	1.0000	1.0000	-1.0000	89058.14	83702.04	83488.70	86268.12	84671.00	83487.62
8	-1.0000	-1.0000	1.0000	1.0000	1.0000	104526.00	96904.66	97306.20	99919.14	99438.82	96857.64
9	-1.0000	1.0000	-1.0000	-1.0000	-1.0000	109287.30	104564.60	104378.00	104537.90	105553.90	104354.80
10	-1.0000	1.0000	-1.0000	-1.0000	1.0000	124378.50	117463.50	117577.90	117568.80	118104.40	117437.50
11	-1.0000	1.0000	-1.0000	1.0000	-1.0000	50933.34	50631.46	50548.68	55400.02	50961.22	50643.84
12	-1.0000	1.0000	-1.0000	1.0000	1.0000	57014.02	57004.92	56915.02	60542.10	56972.50	56956.66
13	-1.0000	1.0000	1.0000	-1.0000	-1.0000	203871.00	200829.80	199567.60	204194.80	202037.20	199517.60
14	-1.0000	1.0000	1.0000	-1.0000	1.0000	263923.40	235927.40	239247.20	237663.40	236686.40	236512.20
15	-1.0000	1.0000	1.0000	1.0000	-1.0000	90722.86	88296.52	87747.98	88677.62	89304.80	87748.90
16	-1.0000	1.0000	1.0000	1.0000	1.0000	102593.50	102595.10	101940.70	113878.40	104394.80	101935.30
17	1.0000	-1.0000	-1.0000	-1.0000	-1.0000	66092.94	65497.42	64124.26	76944.06	70750.98	64139.26
18	1.0000	-1.0000	-1.0000	-1.0000	1.0000	84773.64	69416.90	69334.50	88443.62	69527.42	69560.20
19	1.0000	-1.0000	-1.0000	1.0000	-1.0000	42375.82	42402.96	42374.24	42388.44	42374.74	42374.58
20	1.0000	-1.0000	-1.0000	1.0000	1.0000	45668.54	45442.28	45380.18	45489.02	45386.28	45383.38
21	1.0000	-1.0000	1.0000	-1.0000	-1.0000	101277.90	90567.38	90351.54	91465.70	90695.50	90350.30
22	1.0000	-1.0000	1.0000	-1.0000	1.0000	107276.10	104907.00	104411.00	106736.90	104990.00	104396.60
23	1.0000	-1.0000	1.0000	1.0000	-1.0000	53731.12	51620.70	51606.92	51609.00	51609.52	51606.86
24	1.0000	-1.0000	1.0000	1.0000	1.0000	57268.46	57245.26	57245.22	57747.56	57291.00	57292.04
25	1.0000	1.0000	-1.0000	-1.0000	-1.0000	64612.34	64646.06	64398.98	68080.40	64823.10	64472.42
26	1.0000	1.0000	-1.0000	-1.0000	1.0000	69940.16	69555.72	69643.38	71897.14	69554.16	69556.54
27	1.0000	1.0000	-1.0000	1.0000	-1.0000	42600.66	42660.40	42605.82	43756.36	42600.38	42599.40
28	1.0000	1.0000	-1.0000	1.0000	1.0000	45416.66	45415.04	45414.14	45517.78	45414.72	45414.42
29	1.0000	1.0000	1.0000	-1.0000	-1.0000	92567.38	90904.04	90944.52	93378.46	90906.52	90900.94
30	1.0000	1.0000	1.0000	-1.0000	1.0000	105474.50	105018.40	105026.50	106700.90	106700.70	104996.00
31	1.0000	1.0000	1.0000	1.0000	-1.0000	51865.88	51857.66	51838.60	51839.62	51839.62	51839.34
32	1.0000	1.0000	1.0000	1.0000	1.0000	57868.72	57414.40	57346.32	59077.90	57358.88	57358.88
33	-1.0000	0.0000	0.0000	0.0000	0.0000	100422.00	97777.18	97486.42	102726.90	97947.46	97650.86
34	1.0000	0.0000	0.0000	0.0000	0.0000	58412.00	58954.34	58237.34	58960.66	58627.98	58238.38
35	0.0000	-1.0000	0.0000	0.0000	0.0000	68891.74	67021.44	67182.54	73427.40	67001.24	66999.18
36	0.0000	1.0000	0.0000	0.0000	0.0000	67398.60	66410.72	66321.44	74623.80	67338.62	66394.38
37	0.0000	0.0000	-1.0000	0.0000	0.0000	56398.60	54806.26	54798.16	82663.16	54797.66	54789.08
38	0.0000	0.0000	1.0000	0.0000	0.0000	84875.72	85243.72	84569.36	86252.76	84629.40	84549.32
39	0.0000	0.0000	0.0000	-1.0000	0.0000	104841.30	102452.50	102327.70	116375.90	103165.70	102473.20
40	0.0000	0.0000	0.0000	1.0000	0.0000	53490.94	53236.12	53012.44	59706.26	53137.94	53026.66
41	0.0000	0.0000	0.0000	0.0000	-1.0000	63148.18	62883.12	62889.78	66971.08	62946.30	62932.60
42	0.0000	0.0000	0.0000	0.0000	1.0000	71660.06	71236.48	71281.12	73086.04	71376.78	71242.36
43	0.0000	0.0000	0.0000	0.0000	0.0000	67567.28	67117.62	67008.62	75559.64	67101.84	67087.56
44	-0.7500	-0.7500	-0.7500	-0.7500	-0.7500	93122.32	91426.56	90098.18	90326.06	89649.82	89638.34
45	-0.7500	-0.7500	-0.7500	-0.7500	0.7500	103405.40	99527.36	98378.68	99656.72	98307.74	98261.22
46	-0.7500	-0.7500	-0.7500	0.7500	-0.7500	54127.98	53811.36	53621.48	56364.98	56364.98	53718.84
47	-0.7500	-0.7500	-0.7500	0.7500	0.7500	59951.34	58687.28	58705.32	60451.38	59168.76	58779.54
48	-0.7500	-0.7500	0.7500	-0.7500	-0.7500	152378.30	149592.70	149010.70	151503.80	150682.90	149006.10
49	-0.7500	-0.7500	0.7500	-0.7500	0.7500	175400.80	168567.80	167960.10	170373.30	170373.30	167953.10
50	-0.7500	-0.7500	0.7500	0.7500	-0.7500	86149.28	81560.16	81528.08	83889.06	82245.40	81527.18
51	-0.7500	-0.7500	0.7500	0.7500	0.7500	91730.22	90886.52	90885.88	91762.94	91110.40	90875.34
52	-0.7500	0.7500	-0.7500	-0.7500	-0.7500	89483.68	87773.00	87520.34	88694.28	87622.78	87521.72
53	-0.7500	0.7500	-0.7500	-0.7500	0.7500	96136.06	95762.24	95717.68	105490.30	95715.74	95714.08
54	-0.7500	0.7500	-0.7500	0.7500	-0.7500	52828.56	52662.04	52636.42	58204.50	52739.58	52725.52
55	-0.7500	0.7500	-0.7500	0.7500	0.7500	64513.44	57656.02	57649.02	61382.40	58022.62	57704.88
56	-0.7500	0.7500	0.7500	-0.7500	-0.7500	180922.10	157423.40	156556.00	158775.90	158007.80	156558.60
57	-0.7500	0.7500	0.7500	-0.7500	0.7500	208151.40	177464.30	176256.30	188143.40	178224.70	176258.80
58	-0.7500	0.7500	0.7500	0.7500	-0.7500	85471.04	84258.78	84104.64	87108.06	85489.78	84098.20
59	-0.7500	0.7500	0.7500	0.7500	0.7500	95735.40	94282.86	93990.80	95629.72	94109.74	93986.40

-----(Continued from the previous page)-----

ID	v_1	v_2	v_3	v_4	v_5	W_s(A2)	W_s(A3)	W_s(A5)	W_s(B2)	W_s(B3)	W_s(B5)
60	0.7500	-0.7500	-0.7500	-0.7500	-0.7500	62413.66	62078.72	61842.98	67439.00	62158.70	61843.70
61	0.7500	-0.7500	-0.7500	-0.7500	0.7500	67047.74	66642.68	66430.50	70209.74	66436.14	66426.16
62	0.7500	-0.7500	-0.7500	0.7500	-0.7500	44480.96	44403.68	44415.34	47057.78	44416.18	44425.62
63	0.7500	-0.7500	-0.7500	0.7500	0.7500	47030.40	46991.16	46975.52	53448.40	46974.30	46975.50
64	0.7500	-0.7500	0.7500	-0.7500	-0.7500	87257.58	85202.66	85240.18	87409.90	85379.06	85199.60
65	0.7500	-0.7500	0.7500	-0.7500	0.7500	98044.42	94847.48	94718.80	95492.50	94678.42	94672.36
66	0.7500	-0.7500	0.7500	0.7500	-0.7500	55973.40	55718.84	55806.66	63814.12	55735.12	55734.90
67	0.7500	-0.7500	0.7500	0.7500	0.7500	63992.06	60334.24	60316.98	61096.46	60326.70	60319.04
68	0.7500	0.7500	-0.7500	-0.7500	-0.7500	61445.64	61396.06	61377.12	73911.84	62919.34	61584.66
69	0.7500	0.7500	-0.7500	-0.7500	0.7500	66449.28	66070.32	66001.70	66068.68	66011.22	66024.14
70	0.7500	0.7500	-0.7500	0.7500	-0.7500	47023.24	44236.30	44239.04	44387.22	44532.00	44524.82
71	0.7500	0.7500	-0.7500	0.7500	0.7500	49123.68	46727.26	46723.76	47105.62	46732.30	46728.84
72	0.7500	0.7500	0.7500	-0.7500	-0.7500	86786.86	86215.90	85996.76	89165.36	85910.22	85913.18
73	0.7500	0.7500	0.7500	-0.7500	0.7500	95913.28	95324.88	95313.70	95837.00	95444.32	95300.98
74	0.7500	0.7500	0.7500	0.7500	-0.7500	56456.18	56010.02	55832.82	55866.54	55836.78	55834.66
75	0.7500	0.7500	0.7500	0.7500	0.7500	60827.32	60442.10	60446.26	60973.76	60475.74	60467.64
76	-0.7500	0.0000	0.0000	0.0000	0.0000	95116.86	88482.68	88496.44	101316.00	88489.30	88485.76
77	0.7500	0.0000	0.0000	0.0000	0.0000	60894.46	59749.10	59712.32	61006.82	59651.90	59649.92
78	0.0000	-0.7500	0.0000	0.0000	0.0000	68762.20	67580.68	67166.50	83693.58	67259.34	67108.56
79	0.0000	0.7500	0.0000	0.0000	0.0000	67001.22	66686.32	66616.24	67430.96	66716.48	66706.32
80	0.0000	0.0000	-0.7500	0.0000	0.0000	57878.92	56412.22	55995.08	70424.04	56188.30	55980.74
81	0.0000	0.0000	0.7500	0.0000	0.0000	84318.34	82705.72	82589.88	84198.34	82884.04	82615.84
82	0.0000	0.0000	0.0000	-0.7500	0.0000	101273.90	90302.30	89994.74	91405.06	90484.88	90035.28
83	0.0000	0.0000	0.0000	0.7500	0.0000	56016.32	55669.00	55641.38	63745.34	55655.14	55654.54
84	0.0000	0.0000	0.0000	0.0000	-0.7500	71287.36	63859.12	63854.64	66971.44	63937.82	63935.66
85	0.0000	0.0000	0.0000	0.0000	0.7500	70524.50	70319.58	70166.34	77578.64	70367.88	70169.70
86	-0.7500	-1.0000	0.2500	0.7500	-1.0000	83912.78	69910.44	69654.36	71329.58	69683.68	69514.26
87	-0.7500	-1.0000	0.7500	-0.2500	-1.0000	127326.70	113382.60	113127.80	116613.50	114088.70	113135.40
88	-0.7500	1.0000	-0.7500	-0.2500	1.0000	79769.12	78895.88	78581.62	86779.58	78673.74	78673.74
89	-0.7500	1.0000	-0.2500	-0.7500	1.0000	134293.90	121008.00	120670.30	134204.90	122791.90	120677.50
90	-0.7500	1.0000	-0.2500	0.7500	1.0000	72148.34	70558.14	69147.70	69543.38	69484.20	69434.86
91	-0.7500	1.0000	0.7500	0.2500	1.0000	113048.50	112831.60	112490.50	114591.00	113543.30	112483.90
92	-0.2500	-1.0000	-0.7500	-0.7500	-1.0000	74372.02	74427.08	74196.26	75564.12	74243.74	74242.86
93	-0.2500	-1.0000	0.7500	0.7500	1.0000	100128.20	75321.84	75007.96	84158.12	75311.36	74991.76
94	-0.2500	1.0000	-0.7500	0.7500	-1.0000	46772.84	46453.24	46439.08	50876.72	46495.58	46480.02
95	0.2500	-1.0000	-0.7500	0.7500	1.0000	51762.92	49085.12	48892.30	54190.26	52377.96	48956.14
96	0.2500	1.0000	-0.7500	-0.7500	1.0000	71309.64	70984.56	70967.40	81046.04	70883.30	70884.74
97	0.2500	1.0000	0.7500	-0.7500	1.0000	114528.00	111356.10	111184.80	146473.30	112490.60	111168.80
98	0.7500	-1.0000	-0.7500	-0.2500	-1.0000	53192.74	53088.46	52775.20	59274.66	53180.18	52853.12
99	0.7500	-1.0000	0.2500	0.7500	-1.0000	51244.04	51262.88	51248.44	51275.88	51253.02	51243.96
100	0.7500	-1.0000	0.7500	-0.2500	1.0000	79352.56	79305.70	79184.68	80004.84	79178.26	79174.36
101	0.7500	1.0000	0.2500	-0.7500	-1.0000	76918.50	77045.24	75830.92	76616.84	76349.94	75828.30
102	0.7500	1.0000	0.7500	0.2500	-1.0000	61628.70	61363.60	61358.84	61376.60	61396.96	61350.48
103	-0.7500	-1.0000	-0.7500	0.2500	-1.0000	60927.40	60408.52	60352.74	63110.08	60563.26	60383.58
104	-0.2500	-1.0000	0.7500	-0.7500	1.0000	152999.00	134714.00	134651.30	139712.70	135717.50	134642.20
105	-0.2500	1.0000	-0.7500	-0.7500	-1.0000	72682.30	72190.86	72190.92	73671.94	72209.22	72196.98
106	-0.2500	1.0000	0.7500	-0.7500	-1.0000	119817.70	118773.40	118819.70	124480.20	118770.40	118769.70
107	-0.2500	1.0000	0.7500	0.7500	-1.0000	67422.86	67370.88	67029.92	67172.94	67164.80	67035.38
108	0.2500	-1.0000	-0.7500	-0.7500	1.0000	81461.52	72636.32	72504.52	85316.16	72880.92	72513.34
109	0.2500	-1.0000	0.7500	-0.7500	-1.0000	96498.06	95697.48	95243.94	96193.96	95356.12	95399.74
110	0.2500	1.0000	-0.7500	0.7500	-1.0000	44829.96	44345.86	44310.30	47788.98	44319.92	44311.96
111	0.2500	1.0000	0.7500	0.7500	1.0000	66612.16	66337.86	66322.34	66839.98	66318.64	66317.82
112	0.7500	1.0000	-0.7500	0.2500	1.0000	52368.60	51507.82	51464.46	55315.24	57378.02	51489.00
113	-1.0000	-0.3333	-0.3333	-0.3333	-0.3333	95690.64	95190.58	94566.34	97228.48	96506.76	94541.92
114	-1.0000	0.3333	0.3333	0.3333	0.3333	112135.90	103692.40	101670.90	135873.20	103035.90	101670.30
115	-0.3333	-1.0000	-0.3333	0.3333	1.0000	67204.94	64545.60	64337.98	69251.90	64847.40	64385.22
116	-0.3333	-0.3333	-1.0000	1.0000	0.3333	47391.50	47408.80	47323.92	49485.54	47354.52	47362.22
117	-0.3333	0.3333	1.0000	-1.0000	-0.3333	155274.80	151927.90	149467.40	158219.90	150680.00	149447.40
118	-0.3333	1.0000	0.3333	-0.3333	-1.0000	91446.70	89071.58	88563.30	90144.84	88873.14	88624.58
119	0.3333	-1.0000	0.3333	1.0000	-0.3333	53456.92	53397.88	53382.92	54215.84	54215.84	53387.88
120	0.3333	-0.3333	1.0000	0.3333	-1.0000	65997.12	65666.22	65641.32	66512.42	65883.84	65622.96
121	0.3333	0.3333	-1.0000	-0.3333	1.0000	60000.64	60147.52	59978.32	66422.10	59991.08	60001.44
122	0.3333	1.0000	-0.3333	-1.0000	0.3333	97324.00	83220.44	82868.60	87033.42	83250.00	82814.44
123	1.0000	-1.0000	1.0000	-0.3333	0.3333	82599.14	76292.38	76196.84	76983.96	76196.46	76194.60
124	1.0000	-0.3333	0.3333	-1.0000	1.0000	93147.72	93717.76	92378.96	92596.24	92647.28	92349.98
125	1.0000	0.3333	-0.3333	1.0000	-1.0000	44493.46	44494.92	44491.44	44535.08	44491.70	44491.62
126	1.0000	1.0000	-1.0000	0.3333	-0.3333	49267.06	47533.12	47641.70	51293.52	47555.22	47542.42

Appendix E MATLAB Code for Direct Fit of Weibull Model to Optimization Errors

This MATLAB source code is used to fit the Weibull model to the error of Case A2. It reads in data files of optimal wing structural weight (W_s). It calculates the error with respect to the best of the six runs from different GENESIS parameter settings. As an output, a QQ plot is generated. It also prints out histograms and cumulative frequencies to compare data and fit. The results of c^2 goodness-of-fit test are printed.

```
clear all;
%%%%%%%%%%%%%%%%%%%%%%%%%%%%%%%%%%%%%%%%%%%%%%%%
% read in Ws data stored in files
%%%%%%%%%%%%%%%%%%%%%%%%%%%%%%%%%%%%%%%%%%%%%%%%
%Case A2
fid=fopen('Ws.CaseA2.dat','r');
WsA2=fscanf(fid,'%g');
fclose(fid);
%Case A3
fid=fopen('Ws.CaseA3.dat','r');
WsA3=fscanf(fid,'%g');
fclose(fid);
%Case A5
fid=fopen('Ws.CaseA5.dat','r');
WsA5=fscanf(fid,'%g');
fclose(fid);
%Case B2
fid=fopen('Ws.CaseB2.dat','r');
WsB2=fscanf(fid,'%g');
fclose(fid);
%Case B3
fid=fopen('Ws.CaseB3.dat','r');
WsB3=fscanf(fid,'%g');
fclose(fid);
%Case B5
fid=fopen('Ws.CaseB5.dat','r');
WsB5=fscanf(fid,'%g');
fclose(fid);
% observation index
index=[1:length(WsA2)]';
%%%%%%%%%%%%%%%%%%%%%%%%%%%%%%%%%%%%%%%%%%%%%%%%%%%%%%%%%%%%%%%%%%%%%%%%%%%%
% estimate true Ws by taking the best of six cases
%%%%%%%%%%%%%%%%%%%%%%%%%%%%%%%%%%%%%%%%%%%%%%%%%%%%%%%%%%%%%%%%%%%%%%%%%%%%
Wst=(min([WsA2 WsA3 WsA5 WsB2 WsB3 WsB5]'))';
% calculate error of Case A2
X=(WsA2-Wst);
% sort the error data
X=sort(X);
% Find id numbers of data points of nonzero values
non0X=find(X);
```

```
% add offset to avoid singularity of X=0 for alpha < 1
if length(non0X) == length(X)
   os=0.;
else
   os=min( .00001*mean(X), X(non0X(1)) );
end
X=X+os;

%%%%%%%%%%%%%%%%%%%%%%%%%%%%%%%%%%%%%%%%%%%%%%%%%%%%%%%%%%%%%%%%%%%%%%%%%%%
%               Fitting Weibull model to the data
%
% weibfit from MATLAB statistics toolbox
% Use 5% confidence level
% Estimated parameters are returned to mu
% Confidence interval of mu are returned to muci
%%%%%%%%%%%%%%%%%%%%%%%%%%%%%%%%%%%%%%%%%%%%%%%%%%%%%%%%%%%%%%%%%%%%%%%%%%%
[mu muci]=weibfit(X,.05)
mu1=mu(1);
mu2=mu(2);
% MATLAB uses parameters in a different form. Convert them to alpha and beta.
alpha=mu(2);
beta=(1/mu1)^(1/mu2);
% Calculate Log likelihood function for the estimated parameters
ONES=ones(length(X),1);
LL=sum(  log(  weibpdf(X,mu1*ONES,mu2*ONES) )   )
%%%%%%%%%%%%%%%%%%%%%%%%%%%%%%%%%%%%%%%%%%%%%%%%%%%%%%%%%%%%%%%%%%%%%%%%%%%
%      Generating QQ plot between data and fit
%
% invX: expected location of X from fit
%%%%%%%%%%%%%%%%%%%%%%%%%%%%%%%%%%%%%%%%%%%%%%%%%%%%%%%%%%%%%%%%%%%%%%%%%%%
pX=( ([1:length(X)]-.5)./length(X) )';
invX=weibinv(pX,mu1,mu2);
maxX=max([max(invX) max(X)]);
XSCL=[1 10 100 1000 10000 100000];
ISCL=find( maxX./XSCL < 10 );
SCL=XSCL(ISCL(1));
xrange=SCL*round(max([max(invX) max(X)])/SCL+.5);
figure;
plot(invX,X,'r+',[0 xrange],[0 xrange],'b-');
%
axis equal
axis([0 xrange 0 xrange]);
set(gca,'xtick',[0:SCL:xrange]);
set(gca,'ytick',[0:SCL:xrange]);
set(gca,'XTickLabel',[0:SCL:xrange]);
set(gca,'YTickLabel',[0:SCL:xrange]);
set(gca,'FontSize',15);
xlabel('X Quantiles(Fit)','FontSize',15);
ylabel('Y Quantiles(Data)','FontSize',15);
fid=fopen('qqWEIBcaseA2.plt','w');
fprintf(fid,'%15.7e %15.7e %15.7e\n',…
[invX X (linspace(0,xrange,length(X)))' ]');
fclose(fid);
%%%%%%%%%%%%%%%%%%%%%%%%%%%%%%%%%%%%%%%%%%%%%%%%%%%%%%%%%%%%%%%%%%%%%%%%%%%
%       GENERATE data for histogram and cumulative frequency plot
%
% BND : subintervals
% XBND: center point of subintervals
% IBIN: frequencies of data
% SBIN: Cumulative frequencies of data
% RBIN: complementary cumulative frequencies, (Total # of data)-SBIN
% XFRQexp: expected frequencies from the fit
```

```
% CFRQexp: expected cumulative frequencies from the fit
%%%%%%%%%%%%%%%%%%%%%%%%%%%%%%%%%%%%%%%%%%%%%%%%%%%%%%%%%%%%%%%%%%%%%%%%%%%%%%%%
nbin=50;
MpctL=0;
%MpctU=xrange;
MpctU=SCL*round(max(X)/SCL+.5);
Mpct=MpctU-MpctL;
binsize=Mpct/nbin;
BND=[MpctL :binsize:MpctU]';
for n=1:nbin
   XBND(n,1)=.5*( BND(n)+BND(n+1) );
end
%
IBIN=zeros([nbin 1]);
SBIN=zeros([nbin 1]);
RBIN=zeros([nbin 1]);
for k=1:length(X)
     ibin=floor( (X(k)-MpctL)/binsize ) + 1 ;
     IBIN(ibin)=IBIN(ibin)+1;
end
%
SBIN(1)=IBIN(1);
for n=2:nbin
  SBIN(n)=SBIN(n-1)+IBIN(n);
end
%
for n=1:nbin
   RBIN(n)=length(X)-SBIN(n);
end
%
for i=1:nbin
    Xexp(i,1)=weibcdf(BND(i+1),mu1,mu2)-weibcdf(BND(i),mu1,mu2);
    XFRQexp(i,1)=length(X)*Xexp(i);
    CFRQexp(i,1)=length(X)*weibcdf(BND(i+1),mu1,mu2);
end
% print out histogram data as TECPLOT format
fid=fopen('WEIBcaseA2hist.plt','w');
fprintf(fid,'variables=XBND,IBIN,XFRQexp\n');
fprintf(fid,'%13.5e %13.5e %13.5e \n',[XBND IBIN XFRQexp ]');
fclose(fid);
% print out CDF data as TECPLOT format
fid=fopen('WEIBcaseA2cdf.plt','w');
fprintf(fid,'variables=BND,SBIN,CFRQexp\n');
fprintf(fid,'%13.5e %13.5e %13.5e \n',[BND(2:end) SBIN CFRQexp ]');
fclose(fid);
%return to original data
X=X-os;
%%%%%%%%%%%%%%%%%%%%%%%%%%%%%%%%%%%%%%%%%%%%%%%%%%%%%%%%%%%%%%%%%%%%%%%%%%%%%%%%
%          Chi-square goodness of fit TEST
%
% nb: # of intervals for Chi-square test
% ip: x-locations of the intervals having the same probability
% IX: prob( x < x_i), probability that x is less than the i-th observation
% IB: number of data points belong to each interval
%%%%%%%%%%%%%%%%%%%%%%%%%%%%%%%%%%%%%%%%%%%%%%%%%%%%%%%%%%%%%%%%%%%%%%%%%%%%%%%%
nb=10;
nbi=1./nb;
p=[0 : nbi : 1]
np=length(X)*nbi;
for i=1:length(p)-1
 ip(i,1)=weibinv(p(i),mu1,mu2);
end
```

```
ip(length(p),1)=Inf;
%
for i=1:length(X)
IX(i)=weibcdf(X(i),mu1,mu2);
end
IB=zeros([nb 1]);
for k=1:length(X)
     if IX(k) == 0
        IB(1)=IB(1)+1;
     elseif IX(k) ==1
        IB(end)=IB(end)+1;
     else
        ib=floor( (IX(k)-p(1))/nbi ) + 1 ;
        IB(ib)=IB(ib)+1;
     end
end
sum(IB)
%
fprintf('%3d %12.5e %12.5e %3d %12.5e %12.5e %12.5e\n', ...
[ [1:nb]' ip(1:end-1) ip(2:end) IB np*ones(nb,1) (IB-np) (IB-np).^2/np]');
X2=sum( (IB-np).^2 )/np;
%chi2cdf(X2,nb-1)
pvalue=1-chi2cdf(X2,nb-1-2);
fprintf('%15.4f %15.4f\n',[mu1 mu2]);
meanE=beta/alpha*gamma(1/alpha);
varE=beta^2/alpha*( 2*gamma(2/alpha)-1/alpha*(gamma(1/alpha))^2 );
stdE=sqrt(varE);
fprintf(' alpha=%15.4f\n beta=%15.4f\n meanE=%15.4f\n stdE=%15.4f\n',...
[alpha beta meanE stdE]);
fprintf(' X^2=%15.4f\n pvalue=%15.4f\n',[X2 pvalue]);
```

Appendix F MATLB Code for Indirect Fit of Weibull Model to Optimization Errors

INDIRECTFIT.m reads in W_s data files and performs the indirect fit of differences between Cases A2 and A3. A set of distribution parameters are sought to maximize the log likelihood function by using a constrained minimization routine, *fmincon*, from the optimization toolbox of MATLAB [86]. *LOGL.m* calculates the negative of the log likelihood function. *WJIM.m* and *WJIP.m* are integrands of convolution for $x < 0$ and $x > 0$, respectively (see Eqs. C.5 and C.7 in Appendix C). *COSLOGSPACE.m* is used to generate intervals for numerical integration. The outputs are the parameters of the Weibull models for Cases A2 and A3 and the c^2 test results for the fit on the differences.

INDIRECTFIT.m

```
clear all;
%%%%%%%%%%%%%%%%%%%%%%%%%%%%%%%%%%%%%%%%%%%%
% read in Ws data stored in files
%%%%%%%%%%%%%%%%%%%%%%%%%%%%%%%%%%%%%%%%%%%%
%Case A2
fid=fopen('Ws.CaseA2.dat','r');
WsA2=fscanf(fid,'%g');
fclose(fid);
%Case A3
fid=fopen('Ws.CaseA3.dat','r');
WsA3=fscanf(fid,'%g');
fclose(fid);
%Case A5
fid=fopen('Ws.CaseA5.dat','r');
WsA5=fscanf(fid,'%g');
fclose(fid);
%Case B2
fid=fopen('Ws.CaseB2.dat','r');
WsB2=fscanf(fid,'%g');
fclose(fid);
%Case B3
fid=fopen('Ws.CaseB3.dat','r');
WsB3=fscanf(fid,'%g');
fclose(fid);
%Case B5
fid=fopen('Ws.CaseB5.dat','r');
WsB5=fscanf(fid,'%g');
fclose(fid);
% observation index
index=[1:length(WsA2)]';
%%%%%% calculate differences between Case A2 and Case A3
X=(WsA2-WsA3);
```

```
% perturb data of x = 0
npt=length(X);
izero=find(X==0);
if length(izero) > 0
   X(izero)=0.5*( X(izero(1)-1) +X(izero(end)+1) );
end
%%%%%%%%%%%%%%%%%%%%%%%%%%%%%%%%%%%%%%%%%%%%%%%%%%%%%%%%%%%%%%%%%%%%%%%%%%%%%%%
%   Minimization of LOGL.m
%   using fmincon of optimization toolbox of MATLAB
%   LOGL.m : objective function, calculate -loglikelihood
%   beta's are scaled (multiplied by 0.001 ) to prevent
%   numerical difficulties during optimization
%%%%%%%%%%%%%%%%%%%%%%%%%%%%%%%%%%%%%%%%%%%%%%%%%%%%%%%%%%%%%%%%%%%%%%%%%%%%%%%
OPTIONS=optimset('Diagnostics',1,'Display','iter','MaxIter',30,'MaxFunEvals',1000);
[B,FVAL,EXITFLAG]= fmincon('LOGL',[0.7663 3.9012907 0.4703 0.3058443],...
[],[],[],[],[.3 2 .1 0.01],[.8 8 .6 1.],[],OPTIONS,X);

% Rescale beta's
B(2)=1000*B(2);
B(4)=1000*B(4);
%%%%%%%%%%%%%%%%%%%%%%%%%%%%%%%%%%%%%%%%%%%%%%%%%%%%%%%%%%%%%%%%%%%%%%%%%%%%%%%
%    Generate empirical CDF of differences
% mc: size of sample
% R1: weibull random numbers for Case A2
% R2: weibull random numbers for Case A3
% RDIFF: R1-R2, sorted
%%%%%%%%%%%%%%%%%%%%%%%%%%%%%%%%%%%%%%%%%%%%%%%%%%%%%%%%%%%%%%%%%%%%%%%%%%%%%%%
mc=100;
rand('state',0);
%
R1=weibrnd(B(2)^(-(B(1))),B(1),npt*mc,1);
R2=weibrnd(B(4)^(-(B(3))),B(3),npt*mc,1);
RDIFF=sort(R1-R2);
%%%%%%%%%%%%%%%%%%%%%%%%%%%%%%%%%%%%%%%%%%%%%%%%%%%%%%%%%%%%%%%%%%%%%%%%%%%%%%%
%  Chi-square goodness of fit TEST for the difference fit
%
% nb: # of intervals for Chi-square test
% ip: x-locations of the intervals having the same probability
% IB: number of data points belong to each interval
%%%%%%%%%%%%%%%%%%%%%%%%%%%%%%%%%%%%%%%%%%%%%%%%%%%%%%%%%%%%%%%%%%%%%%%%%%%%%%%
nb=10;
nbi=1./nb;
p=[0 : nbi : 1];
np=length(X)*nbi;
ip(1,1)=RDIFF(1);
for i=2:length(p)-1
    ip(i,1)=RDIFF( round( (length(RDIFF)*p(i)) ) );
end
ip(length(p),1)=RDIFF(end);
%
IB=zeros([nb 1]);
for i=1:length(X)
  if X(i) < ip(2)
     IB(1)=IB(1)+1;
  elseif X(i) >= ip(end-1)
     IB(end)=IB(end)+1;
  else
     j=2;
     while ~( ip(j) <=  X(i) & ip(j+1) >  X(i) )
        j=j+1;
     end
     IB(j)=IB(j)+1;
```

```
  end
end
sum(IB)
%
fprintf('%3d %12.5e %12.5e %3d %12.5e %12.5e %12.5e\n', ...
[ [1:nb]' ip(1:end-1) ip(2:end) IB np*ones(nb,1) (IB-np) (IB-np).^2/np]');
X2=sum( (IB-np).^2 )/np
%chi2cdf(X2,nb-1);
pvalue=1.-chi2cdf(X2,nb-4-1);
alpha1=B(1);
beta1=B(2);
alpha2=B(3);
beta2=B(4);
fprintf(' alpha1=%12.5e\n beta1=%12.5e\n alpha2=%12.5e\n beta2=%12.5e\n',...
alpha1,beta1,alpha2,beta2);
fprintf(' X^2=%12.5e\n pvalue=%12.5e\n',X2,pvalue);
```

LOGL.m

```
function R=LOGL(B,XS);
npt=length(XS);
id=[];
% return to original scale
B(2)=1000.*B(2);
B(4)=1000.*B(4);
% large enough upper bound of integration
Irange=100000;
%
fprintf(1,'B = %15.7e %15.7e %15.7e %15.7e\n',B);
for i=1:npt
  if XS(i) < 0
     s_0=0;
     s_1=s_0+Irange;
     s_0=s_0^B(1);
     s_1=s_1^B(1);
  elseif XS(i) > 0
     s_0=XS(i);
     s_1=s_0+Irange;
     s_0=(s_0-XS(i))^B(3);
     s_1=(s_1-XS(i))^B(3);
  else
     fprintf('x is zero, perturb it \n');
  end

%%%%%%%%%%%%%%%%%%%%%%%%%%%%%%%%%%%%%%%%%%%%%%%%%%%%%%%%%%%%%%%%%%%%%%%%%%%%
%          set subintervals for integration
% - use logarithmic distribution to use dense intervals near lower bound
% - use offset to prevent too dense s near zero
%%%%%%%%%%%%%%%%%%%%%%%%%%%%%%%%%%%%%%%%%%%%%%%%%%%%%%%%%%%%%%%%%%%%%%%%%%%%
  offset=0.1*s_1;
  s=COSLOGSPACE(log10(s_0+offset),log10(s_1+offset),101);
  s=s-offset;
  s(1)=s_0;

% Gaussian quadrature of third order accuracy
  n=length(s)-1;
  for j=1:n
    a=s(j);
    b=s(j+1);
    c1=1;
    c2=1;
```

```
    t1=-1/sqrt(3);
    t2= 1/sqrt(3);
    s1=.5*((b-a)*t1+a+b);
    s2=.5*((b-a)*t2+a+b);
% WJIM: integrand for x < 0
% WJIP: integrand for x > 0
    if XS(i) < 0
       fsum(j)=.5*(b-a)* (c1*WJIM(s1,XS(i),B)+c2*WJIM(s2,XS(i),B));
    else
       fsum(j)=.5*(b-a)* (c1*WJIP(s1,XS(i),B)+c2*WJIP(s2,XS(i),B));
    end
  end
  f(i)=sum(fsum);
end
% negative of loglikelihood for minimization
R=-sum( log(f) );
fprintf(1,'OBJ = %15.7e\n',R);
```

WJIM.m

```
function f=WJIM(s,x,B);

% integrand for x < 0
a1=B(1);
b1=B(2);
a2=B(3);
b2=B(4);
%
f=a2*b1^(-a1)*b2^(-a2)*(s.^(1/a1)-x).^(a2-1).*exp(-s./(b1.^a1)-((s.^(1/a1)-
x)./b2).^a2);
```

WJIP.m

```
function f=WJIP(s,x,B);

% integrand for x > 0
a1=B(1);
b1=B(2);
a2=B(3);
b2=B(4);
%
f=a1*b1^(-a1)*b2^(-a2)*(s.^(1/a2)+x).^(a1-1).*exp(-s./(b2.^a2)-
((s.^(1/a2)+x)./b1).^a1);
```

COSLOGSPACE.m

```
function y = COSLOGSPACE(d1, d2, n)

% generate highly stretched intervals between d1 and d2 by
% combining cosine and log
pw=d1+(d2-d1)*(1-cos(linspace(0,.5*pi,n))).^2;
y=10.^pw;
```

Appendix G SAS Input File for IRLS Procedure

The SAS input file performs the IRLS procedure on W_s data of Case A2 using a quadratic model. IRLS with Huber's weighting function is performed first to get initial regression coefficients. Then, IRLS with biweight function is performed to identify outliers.

```
options pagesize = 30000 nodate;
TITLE '--- IRLS FIT: QUADRATIC ----';
/* read in X data */
DATA WSTW;
   INFILE 'Hsct5B.dat';
   INPUT X01 X02 X03 X04 X05 ;
   RUN;
/* read in Ws data */
DATA WSTW;
   SET WSTW;
   INFILE 'Ws.caseA2.dat';
   INPUT Y;
   RUN;
/* remove unreasonable designs */
DATA WSTW;
   SET WSTW;
   IF Y GT 150000 THEN DELETE;
   RUN;
DATA WSTW;
   SET WSTW;
   Y=1.E-4*Y;
   X0101 = X01*X01; X0102 = X01*X02; X0103 = X01*X03; X0104 = X01*X04;
   X0105 = X01*X05; X0202 = X02*X02; X0203 = X02*X03; X0204 = X02*X04;
   X0205 = X02*X05; X0303 = X03*X03; X0304 = X03*X04; X0305 = X03*X05;
   X0404 = X04*X04; X0405 = X04*X05; X0505 = X05*X05;
   RUN;
/* least squares fit to get scale parameter s */
PROC REG DATA=WSTW OUTEST=ESTL;
     TITLE 'REG FIT TO GET INITIAL SIGMA';
     MODEL Y = X01 X02 X03 X04 X05 X0101 X0102 X0103 X0104 X0105 X0202
     X0203 X0204 X0205 X0303 X0304 X0305 X0404 X0405 X0505
     ;
     OUTPUT OUT=WSTW R=RL;
/* pass LS coefficients to IRLS with Huber */
DATA ESTL;
   SET ESTL;
   CALL SYMPUT('INTERCEP',INTERCEP); CALL SYMPUT('B01',X01); CALL SYMPUT('B02',X02);
   CALL SYMPUT('B03',X03); CALL SYMPUT('B04',X04); CALL SYMPUT('B05',X05);
   CALL SYMPUT('B0101',X0101); CALL SYMPUT('B0102',X0102); CALL SYMPUT('B0103',X0103);
   CALL SYMPUT('B0104',X0104); CALL SYMPUT('B0105',X0105); CALL SYMPUT('B0202',X0202);
   CALL SYMPUT('B0203',X0203); CALL SYMPUT('B0204',X0204); CALL SYMPUT('B0205',X0205);
   CALL SYMPUT('B0303',X0303); CALL SYMPUT('B0304',X0304); CALL SYMPUT('B0305',X0305);
   CALL SYMPUT('B0404',X0404); CALL SYMPUT('B0405',X0405); CALL SYMPUT('B0505',X0505);
PROC PRINT DATA=WSTW;
     VAR X01 X02 X03 X04 X05 RL;
     RUN;
PROC UNIVARIATE DATA=WSTW;
     VAR RL;
     OUTPUT OUT=MRL MEDIAN=MDN;
DATA MRL;
```

```
     SET MRL;
     CALL SYMPUT('MDN',MDN);
DATA WSTW;
     SET WSTW;
     MAD=ABS(RL-&MDN);
PROC UNIVARIATE DATA=WSTW;
     VAR MAD;
     OUTPUT OUT=MADSET MEDIAN=MMAD;
DATA MADSET;
     SET MADSET;
     CALL SYMPUT('MMAD',MMAD);

/* IRLS fit with Huber weighting function to get initial coeff */
PROC NLIN DATA=WSTW NOHALVE MAXITER=1000 OUTEST=ESTP;
     TITLE 'NONLINEAR REGRESSION TO GET IRLS INITIAL COEFF';
     PARMS
       INTERCEP = &INTERCEP
       B01 = &B01
       B02 = &B02
       B03 = &B03
       B04 = &B04
       B05 = &B05
       B0101 = &B0101
       B0102 = &B0102
       B0103 = &B0103
       B0104 = &B0104
       B0105 = &B0105
       B0202 = &B0202
       B0203 = &B0203
       B0204 = &B0204
       B0205 = &B0205
       B0303 = &B0303
       B0304 = &B0304
       B0305 = &B0305
       B0404 = &B0404
       B0405 = &B0405
       B0505 = &B0505
     ;
     MODEL Y = INTERCEP +B01*X01 +B02*X02 +B03*X03 +B04*X04 +B05*X05 +B0101*X0101
       +B0102*X0102 +B0103*X0103 +B0104*X0104 +B0105*X0105 +B0202*X0202 +B0203*X0203
       +B0204*X0204 +B0205*X0205 +B0303*X0303 +B0304*X0304 +B0305*X0305 +B0404*X0404
       +B0405*X0405 +B0505*X0505
     ;
  DER.INTERCEP = 1; DER.B01=X01; DER.B02=X02; DER.B03=X03; DER.B04=X04; DER.B05=X05;
  DER.B0101=X0101; DER.B0102=X0102; DER.B0103=X0103; DER.B0104=X0104; DER.B0105=X0105;
  DER.B0202=X0202; DER.B0203=X0203; DER.B0204=X0204; DER.B0205=X0205; DER.B0303=X0303;
  DER.B0304=X0304; DER.B0305=X0305; DER.B0404=X0404; DER.B0405=X0405; DER.B0505=X0505;

     R=Y-MODEL.Y;

     SIG=1.4826*&MMAD;
     H=1.;

     RPS=ABS(R/SIG);
     IF RPS <= H THEN _WEIGHT_=1.;
     ELSE _WEIGHT_= H/RPS;
     OUTPUT OUT=WSTW R=RP;
DATA WSTW;
   SET WSTW;
   SIG=1.4826*&MMAD;
   H=1.0;
   RPS=ABS(RP/SIG);
```

```
   IF RPS <= H THEN _WEIGHT_=1.;
   ELSE _WEIGHT_= H/RPS;
PROC PRINT DATA=WSTW;
     VAR X01 X02 X03 X04 X05 SIG RL RP RPS H  _WEIGHT_;
     RUN;

PROC UNIVARIATE DATA=WSTW;
     VAR RP;
     OUTPUT OUT=MRP MEDIAN=MDN2;
DATA MRP;
     SET MRP;
     CALL SYMPUT('MDN2',MDN2);
DATA WSTW;
     SET WSTW;
     MAD2=ABS(RP-&MDN2);
PROC UNIVARIATE DATA=WSTW;
     VAR MAD2;
     OUTPUT OUT=MADSET2 MEDIAN=MMAD2;
DATA MADSET2;
     SET MADSET2;
     CALL SYMPUT('MMAD2',MMAD2);

PROC PRINT DATA=ESTP;
     RUN;
DATA ESTP;
     SET ESTP;
     IF _TYPE_ ~= 'FINAL' THEN  DELETE;
PROC PRINT DATA=ESTP;
     RUN;
/* pass coefficients to IRLS with biweight */
DATA ESTP;
   SET ESTP;
   CALL SYMPUT('INTERCEP',INTERCEP); CALL SYMPUT('B01',B01); CALL SYMPUT('B02',B02);
   CALL SYMPUT('B03',B03); CALL SYMPUT('B04',B04); CALL SYMPUT('B05',B05);
   CALL SYMPUT('B0101',B0101); CALL SYMPUT('B0102',B0102); CALL SYMPUT('B0103',B0103);
   CALL SYMPUT('B0104',B0104); CALL SYMPUT('B0105',B0105); CALL SYMPUT('B0202',B0202);
   CALL SYMPUT('B0203',B0203); CALL SYMPUT('B0204',B0204); CALL SYMPUT('B0205',B0205);
   CALL SYMPUT('B0303',B0303); CALL SYMPUT('B0304',B0304); CALL SYMPUT('B0305',B0305);
   CALL SYMPUT('B0404',B0404); CALL SYMPUT('B0405',B0405); CALL SYMPUT('B0505',B0505);
/* IRLS with biweight */
PROC NLIN DATA=WSTW NOHALVE MAXITER=1000 ;
     TITLE 'NONLINEAR REGRESSION TO GET IRLS FIT';
     PARMS
       INTERCEP = &INTERCEP
       B01 = &B01
       B02 = &B02
       B03 = &B03
       B04 = &B04
       B05 = &B05
       B0101 = &B0101
       B0102 = &B0102
       B0103 = &B0103
       B0104 = &B0104
       B0105 = &B0105
       B0202 = &B0202
       B0203 = &B0203
       B0204 = &B0204
       B0205 = &B0205
       B0303 = &B0303
       B0304 = &B0304
       B0305 = &B0305
       B0404 = &B0404
```

```
      B0405 = &B0405
      B0505 = &B0505
    ;
    MODEL Y = INTERCEP +B01*X01 +B02*X02 +B03*X03 +B04*X04 +B05*X05 +B0101*X0101
      +B0102*X0102 +B0103*X0103 +B0104*X0104 +B0105*X0105 +B0202*X0202 +B0203*X0203
      +B0204*X0204 +B0205*X0205 +B0303*X0303 +B0304*X0304 +B0305*X0305 +B0404*X0404
      +B0405*X0405 +B0505*X0505
    ;

  DER.INTERCEP=1; DER.B01=X01; DER.B02=X02; DER.B03=X03; DER.B04=X04; DER.B05=X05;
  DER.B0101=X0101; DER.B0102=X0102; DER.B0103=X0103; DER.B0104=X0104; DER.B0105=X0105;
  DER.B0202=X0202; DER.B0203=X0203; DER.B0204=X0204; DER.B0205=X0205; DER.B0303=X0303;
  DER.B0304=X0304; DER.B0305=X0305; DER.B0404=X0404; DER.B0405=X0405; DER.B0505=X0505;

    R=Y-MODEL.Y;

    B=1.9;

    SIG2=1.4826*&MMAD2;
    RBS=ABS(R/SIG2);
    IF RBS <= B THEN _WEIGHT_=(1.-(RBS/B)**2)**2;
    ELSE _WEIGHT_=0.;
    OUTPUT OUT=WSTW R=RB;
    RUN;

DATA WSTW;
   SET WSTW;
   B=1.9;

   SIG2=1.4826*&MMAD2;
   RBS=ABS(RB/SIG2);
   IF RBS <= B THEN _WEIGHT_=(1.-(RBS/B)**2)**2;
   ELSE _WEIGHT_=0.;
/* print out results */
PROC PRINT DATA=WSTW;
    VAR X01 X02 X03 X04 X05 SIG SIG2 RL RP RPS RB RBS B  _WEIGHT_;
    RUN;
```

VITA

Hongman Kim was born on July 31, 1970 in Pusan, South Korea. In 1993, He graduated with his B.S. degree in Aerospace Engineering from Seoul National University in South Korea. After he earned his M.S. degree in Aerospace Engineering in 1995 from the same school, he worked as a staff scientist in the application of computational fluid dynamics at Systems Engineering Research Institute in Taejon, South Korea. In August 1997, he continued his study at Virginia Tech and earned his Ph.D. degree in Aerospace Engineering in June 2001. While working as a graduate research assistant at Virginia Tech, he joined a team of faculty and graduate students working on advanced techniques in multidisciplinary design and optimization of a high-speed civil transport.